THE UNIVERSITY OF
WAIKATO
Te Whare Wānanga o Waikato

THE UNIVERSITY OF WAIKATO
ENGEN594
ENGINEERING THESIS

THE INVESTIGATION OF MULTI-STORIED JAPANESE TIMBER PAGODAS DURING EARTHQUAKE EVENTS AND THE APPLICATION OF NON-LINEAR JOINTS WITHIN VIRTUAL MODELS

PHILIP ROUX
10/7/2022

SUPERVISOR : DR. YUSUKE MOCHIDA

ACKNOWLEDGEMENTS

Firstly, I would like to thank Dr. Yusuke Mochida for his advice and help during the completion of this thesis. Yusuke has been of major assistance during the research phase and especially during the writing and editing phase of the thesis. I would like to thank Dr. Yusuke for the time and expertise he has dedicated towards assisting me in my research over the past year.

Secondly, I would like to thank The University of Waikato for providing me the space and resources to carry out this research. I would also like to thank the University of Waikato library staff for their help during the covid lockdowns. Without them scanning resources and texts for me to access I would not have been able to finish this thesis.

Lastly, I would like to thank my family for supporting me over the last year. All the love and support has meant so much to me.

TABLE OF CONTENTS

EXECUTIVE SUMMARY

This paper investigates the structural mechanisms contributing to the excellent performance of Japanese pagodas during earthquake events and applies them to modern multi-storeyed timber structure models. Horyu-ji Pagoda was used as a basis for the modelling of the pagoda structure.

It was discovered that there were six major mechanisms, these were; base isolation joints, sliding friction joints, rocking column joints, nuki joints, a balancing toy effect and the presence of a central pillar (shin-bashira). The first four unique joints were chosen to investigate further for practicality reasons, and they were added to a generic three-storied timber model. These models had different earthquake time histories applied to them and output data was collected using non-linear time history (NLTH) analysis. They key output data that was analysed was the acceleration, displacement and storey drift at each level of the different models. The energy dissipation within the models were also investigated. It was found that each of the unique joints had a certain strength and weakness in decreasing the effects of the earthquake on the structure, however when all of them were used together the best results were seen.

The combined mechanisms model had an average decrease of 43% in peak acceleration, 50% in average acceleration, 31% in peak displacement, 37% in peak storey drift, 65% in maximum internal energy and 81% in residual energy. The model had a 13% increase in peak displacement when considering horizontal loading due to wind. These differences were observed when comparing the combined mechanisms model to a generic timber model with joints that were all linear and moment resisting.

1. INTRODUCTION

Japanese timber pagodas have been constructed in Japan from the 6th century AD up to the present and have a strong connection to the Buddhist religion dominating Japan. There are currently over 300 structures of this type all over the country.

Japanese timber pagodas are well known for being able to withstand strong earthquake motion. For example, there is no recorded event of a timber pagoda collapsing during an earthquake event in Japan. Even during the 1995 Hanshin-Awaji Earthquake, with an intensity of M 7.2, there was no major damage seen in any of the pagodas in the affected prefectures (Nakahara et al. 2000).

The aim of this study is to analyse the design of a Japanese timber pagoda in order to discover which internal mechanisms within the structure are the reason for the improved earthquake performance. These mechanisms will then be applied to modern day multi-storied timber structures in order to improve their earthquake performance. Focus will be put on two to four storied wooden structures.

The reason for this is that timber is a renewable and cost-effective resource compared to steel and concrete. Constructing earthquake resistant office buildings in the future out of this cost-effective and renewable resource can only be seen as beneficial. This practice is not currently widespread as multi-storied steel structures perform better during earthquake loading. If modern multi-storied timber structure performance can be improved then timber can be seen as an alternative to steel and concrete in earthquake prone zones in the future.

The five-storied pagoda of Horyu-ji is considered the oldest pagoda in Japan, having been constructed in 711 AD. Figure 1 below shows an image of this pagoda. Horyu-ji Pagoda will be focused on in this study as it has been investigated multiple times by different groups of engineers. Because of this there is more structural information relating to it available compared to that of other timber pagodas within Japan.

Figure 1: Image of Horyu-ji Pagoda (Reproduced from Ar Orientalis 2016).

A two-dimensional model of Horyu-ji Pagoda has been constructed within SAP2000. The identified mechanisms and construction techniques have been included within this model as separate unique links and joints. This model has had horizontal loading and displacements applied to it. If the performance of this virtual model matches the response of the real structure when similar loadings are applied to it then the virtual model will be validated. This means that the unique joints and links are accurately modelled. The two analyses run on this model are modal analysis and equivalent static analysis (also known as static pushover analysis) representing horizontal earthquake loading.

After this, a two-dimensional model of a three storeyed generic timber structure will be created. This structure has a square floor plan with two bays per frame. The total height of the structure is 9 m and the total width is 10 m. The unique joints and links created for use within Horyu-ji Pagoda are then placed within this generic timber model. Non-linear time history (NLTH) analysis is carried out on the model. The changes in accelerations, displacements and energy within the system will be investigated in order to gauge the benefits or drawbacks of these unique joints. Static pushover analysis is also carried out in order to observe the response of the model when wind loads are applied. These analyses will give a clear picture of how the unique joints operate and what the degree of benefit is. From this, conclusions can be drawn on the potential of their use in earthquake design.

2. LITERATURE REVIEW

Horyu-ji Pagoda is a 22.8 m tall five storeyed structure. The pagoda has a 9.8 m spire (known traditionally as a sorin) extending from the top of it, giving a total structure height of 32.6 m. This spire extends through the entire height of the structure and is situated in the centre of the pagoda. All five levels have a similar layout, the key difference is that each level is slightly smaller than the level below it. This gives the structure a staggered tiered look. Another key feature of the pagoda is the large overhang of the roof sections. The total width of the rooves are between two to three times the width of the floor at that level. When looking at the internal construction of traditional Japanese pagodas it is noted that there is no steel or iron used within the joints. All of the joints are made of timber only, with structural members being connected through the use of dowels and grooves slotted together.

Japanese pagodas have been a focus of many studies in the past. These studies have tried to pinpoint exactly what makes a pagoda so resilient to horizontal loading. A combination of micro-tremor excitation testing has been used alongside virtual modelling of the structure. These studies found that there were six major mechanisms that resisted horizontal loading (Nakahara et al. 2000; Hanazato et al. 2004):

1. Base isolation joints: These occur at the ground floor. The column bases are placed within a depression in the foundation and have a small leeway where horizontal motion is allowed.
2. Slip friction joints: These occur at the connection between the columns and the beams resting on top of them at each level. Here there is also a small leeway for horizontal motion.
3. Rocking column Joints: These occur at the base of every column except for the ground floor columns. The columns are effectively freestanding and are not connected to the floor they stand upon.
4. Nuki joints: These joints occur at the same location as the rocking column joints. A continuous horizontal beam penetrates the base of all of the columns in the frame at each level, excluding the ground level.
5. Balancing toy effect: Due to the large mass of the clay tile rooves and to the fact that the centre of mass of the roof sections extend out far from the structure the system acts like two pendulums resting upon a central spire. As this system rotates a moment resisting this rotation is created.
6. Tuned mass damper (TMD)/presence of a shin-bashira: The central column extends from the base of the structure up into the fifth-floor roof and continues as a spire above the roof. This continuous column is not fixed at the base of the structure so potentially acts as a tuned mass

damper. This member simultaneously facilitates the transfer of horizontal shear between the pagoda floor levels.

Figure 2 shows the locations of these unique joints and mechanisms within Horyu-ji Pagoda.

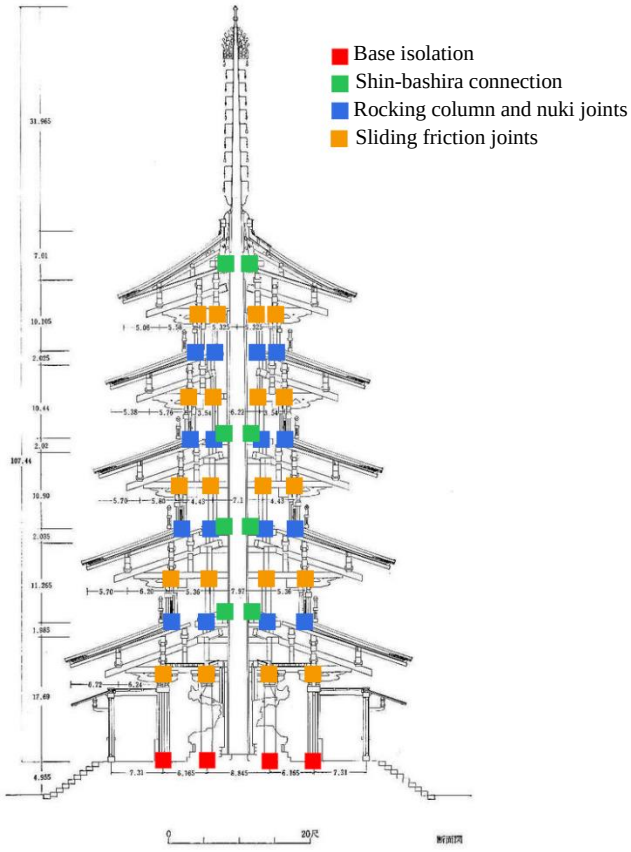

Figure 2: Location of the unique joints within Horyu-ji Pagoda. (Unedited image reproduced from Yasuhara et al. 2007).

Engineers have taken these finding and have applied them to large modern structures within Japan. The Tokyo Sky Tree is a 634 m high structure built in 2012. It uses a central column which is 375 m high, 8 m in diameter and 60 cm in thickness. This replicates the shin-bashira (central column) present in timber pagodas. The findings were that “40% of the response shear stress will be reduced compared with the case of no cylinder” (Konishi 2011). The Marubiru Office Building in Tokyo also uses the principle of a central column found in pagodas. This structure is 178.5 m high and has four structural shafts running the height of the structure. The presence of these four structural shafts decreases the maximum layer distortion by 60% (Ogawa 2006). As can be seen the central column mechanism can be very effective in earthquake design.

The first step is virtually modelling the Horyu-ji pagoda. A study was undertaken by Nakahara and focused on the Horyu-ji pagoda (Nakahara et al. 2000). This study used a simple 2-D model shown in Figure 3. A damping ratio of 4% was used. This model gave accurate results, giving a first mode period of 1.13 s compared to 1.11 s obtained from the micro-tremor test. The second and third mode periods obtained from the analysis were also considered accurate.

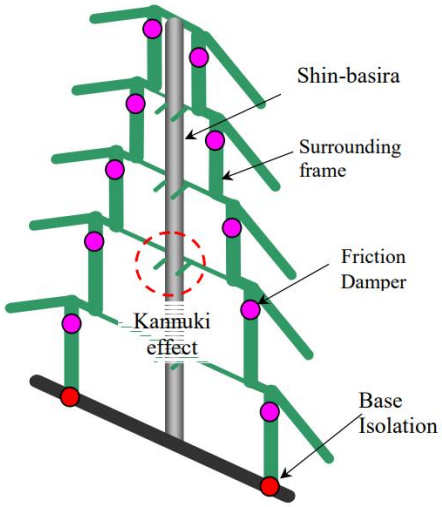

Figure 3: 2-D model of a pagoda used by Nakahara et al. (Reproduced from Nakahara et al. 2000).

Hanazato et al. also created 2-D models to represent a timber pagoda (Hanazato et al. 2004). Figure 4 shows the configuration of these two models. The first model (shown on the left) was used for static analysis. The inner frame and the outer frame of the structure are shown side by side here. When the analysis was run these frames where placed over top of each other, creating one single 2-D frame. The second model (shown on the right) was used for dynamic NLTH analysis and is simplified in order to help expedite the computation heavy analysis method. These models are more complex than the previous model shown in Figure 3 and includes additional components such as bracket complexes and shear walls. Modal analysis was carried out on the static model and it was found to have a first mode period of 1.1 s and a second mode period of 0.78 s. This model represented a pagoda other than the Horyu-ji Pagoda, accounting for the different natural periods compared to those of the previous research paper. This model was deemed accurate by the researchers when it came to representing the response of older traditional timber pagodas.

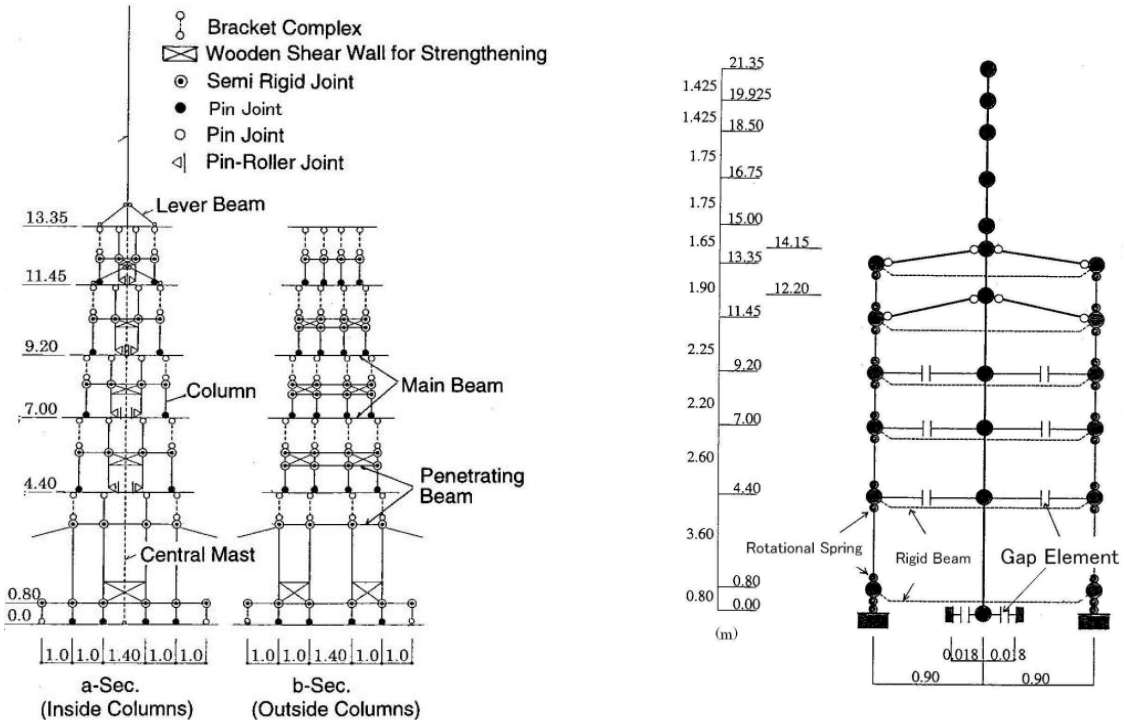

Figure 4: 2-D models of a timber pagoda created by Hanzato et al. Left shows a model used for static analysis and right shows a lumped mass model used for dynamic analysis. (Reproduced from Hanazato et al. 2004).

In this thesis a combination of the models from the two research papers were used to represent Horyu-ji Pagoda. The pagoda model will be considered accurate if it has modal periods matching those of Horyu-ji Pagoda. These modal period values were obtained through microtremor studies on the pagoda, which gave a first mode natural period of 1.1 s, a second mode period of 0.4 s and a third mode period of 0.24 s (Uchida et al. 1999). Due to the construction methods of the structure it is expected that at larger displacements the natural period of the structure will decrease. This is because the structure has increased stiffness and decreased damping ratios as these larger displacements are applied to the structure (Hanazato et al. 2010).

3. METHEDOLOGY

This section describes the process that was taken to obtain the input parameters for the multiple analyses.

When creating the model of Horyu-ji Pagoda the first step was to obtain the total mass and dimension of the structure. The dimensions of the structural members and the material properties were also obtained and are displayed in this section. This process was again repeated for the generic timber model and its variations.

The modelling of the unique non-linear joints is also described in this section. The force-displacement curves and the moment-rotation curves are calculated for each of the unique joints depending upon their location within the pagoda.

The process used to calculate the horizontal equivalent static analysis (ESA) loads that were applied to the pagoda model are described in this section. Also, the selection of the earthquake time history plots and an estimation of the wind loads that were applied to the generic timber models are also shown.

Finally, the process of modelling the structures is described. This involves placing the structural members and lumped masses as well as applying the earthquake loads and accelerations. This also involves describing the process of collecting the output data and manipulating it into a presentable form.

3.1 Pagoda Dimensions

The dimensions and floor plans of Horyu-ji Pagoda that were used is shown in Figure 5 (Nakahara et al. 2000; Hanazato et al. 2004). What can be seen is that at each floor there are 16 columns, 12 on the outer face and four in the centre. This trend follows at each level of the pagoda except at level five where there are only eight columns on the outer face of the structure; there are still the four inner columns present at level five.

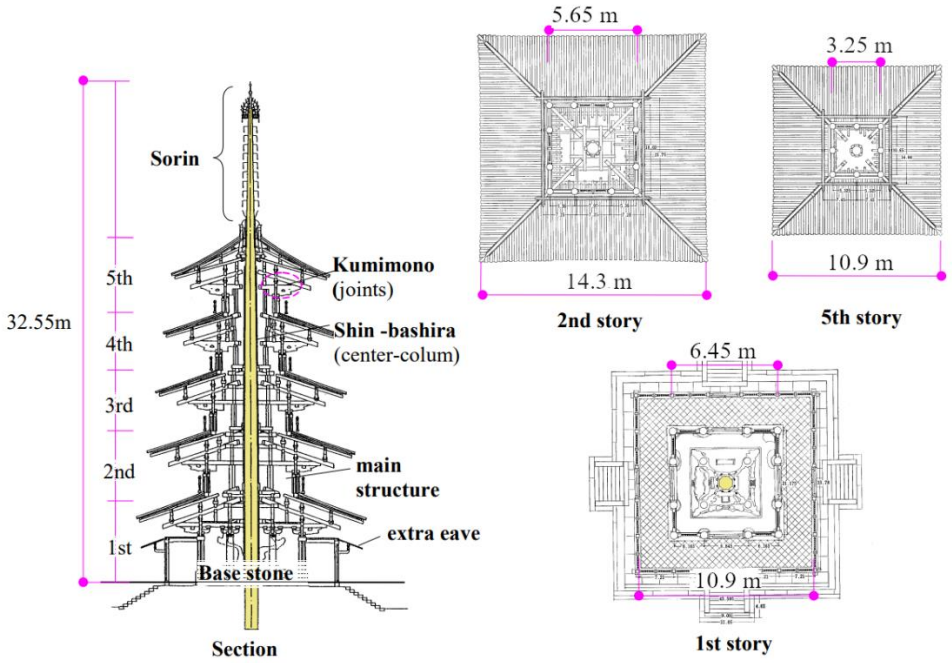

Figure 5: Cross-section of the pagoda along with the floor plans for the first, second and fifth levels. (Reproduced from Nakahara 2000).

At the ground floor there is an extra eave. This is made of a timber wall and a thin roof section and it surrounds the first level of the main structure. When considering earthquake action within the structure this extra eave was ignored. This is because the extra eave is free-standing and does not provide any horizontal resistance to the main structure. Also, because the extra eave is free-standing all of its weight is directly transferred into the foundation of the structure.

3.1.1 Elevation and floor plan dimensions

Table 1 shows the width of the main structure and the roof at each level. It can be seen that the pagoda is modular with the floor and roof spans decreasing at a constant rate with each level added. Each level is narrower than the level below it by twice the span between roof rafters. This means that as each level is added to the pagoda two roof rafters are removed from the new level. The roof narrows by 0.8 m per level meaning that the spacing between the roof rafters is 0.4 m.

Table 1: Floor and roof spans at each level within Horyu-ji Pagoda.

Floor	Floor Span (m)	Roof Span (m)
1st floor extra eave	10.9	-
1	6.45	14.3
2	5.65	13.1
3	4.85	12.0
4	4.05	10.9
5	3.25	9.74

Due to the limitations of the information that was accessible the exact height of the columns and roof sections at each level was not found in the available literature. An estimation of these values was obtained as follows. Traditional Japanese pagodas are modular in design and when the design is broken down into standardised units most traditional pagodas have the same design (Abe and Kawaguchi 2002). In this case the standardised unit is the roof rafter spacing (Zhang et al, 2015). Each level has a floor span that is a multiple of the span between roof rafters and the level above this will be narrower by two roof rafter spans. For example, Horyu-ji Pagoda has a first level floor span of 16 units while the second floor has a span of 14 units, and so on. What the investigation carried out by Zhang et al. found was that the depth of the roof at each level was the same, except for the uppermost level where the roof was twice the standard roof depth. What was also found was that the first floor has a column height that is equal to 1.6 times the second-floor column height. The columns at each level after the second level have their column heights reduced by 0.5 standardised units. Table 2 shows the column and roof section heights at each level of the pagoda.

Table 2: Column and roof section heights at each level of the Horyu-ji Pagoda.

Floor	Column Height (m)	Roof Depth (m)
1	3.41	2.05
2	2.05	2.05
3	1.84	2.05
4	1.64	2.05
5	1.44	4.09

3.1.2 Dimensions of the Members

A study by Hanazato et al. provides the dimension of members within a generic Japanese timber pagoda (Hanazato et al. 2004). A diagram of this can be seen in Figure 6. These values are slightly modified within Horyu-ji Pagoda due to the larger size of structure compared to the average timber pagoda.

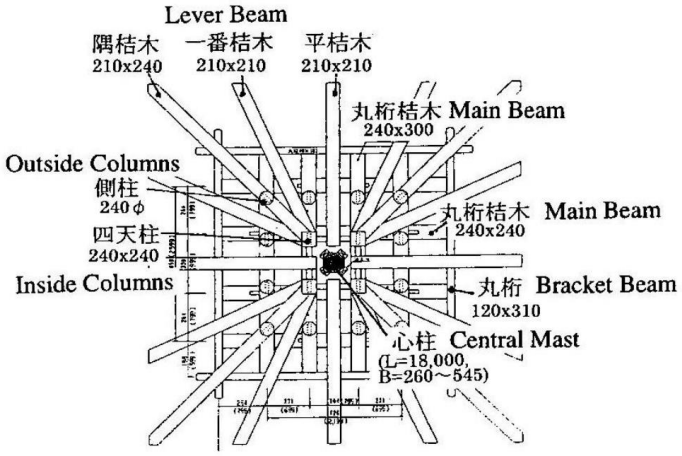

Figure 6: Member dimensions for a Japanese timber pagoda. Beam and column dimensions are in millimetres. (Reproduced from Hanazato et al. 2004).

Figure 7 shows a 3D view of the same structural members seen in Figure 6, this 3D view highlights their layout within the pagoda (Field 2008). At each level the outer frame columns have a circular cross-section while the inner columns have a square cross-section. These columns are connected by a continuous main tie beam placed along the top of the columns. These main tie beams run the length and width of the structure at each floor, except for at levels four and five where this continuous beam is broken at the midpoint of the frame. Above this main tie beam is placed a square lattice of beams labelled as bracket beams. There is an outer square bracket located above the outer columns and an inner square bracket located above the inner columns. These square bracket structures are hidden within the roof structure. Intersecting these roof brackets are two layers of diagonal roof rafters.

Within the roof structure there are also dou blocks and internal roof support members. Dou blocks are square blocks of timber that have beams and rafters sitting on top of them. These dou blocks rest upon structural members below them. They are essentially large square blocks that facilitate the vertical transfer of load between structural members within the roof (Nishioka and Kohara 2016). These dou blocks and support members both provide support within the roof structure, the only difference is that the internal roof support members provide moment resisting connections while the dou blocks act like pin joint connections.

The floor tie beams act in a similar manner to the main tie beams except that they are located at the base of the columns at each level, excluding the first floor. Table 3 lists the unique members within the structure and their dimensions.

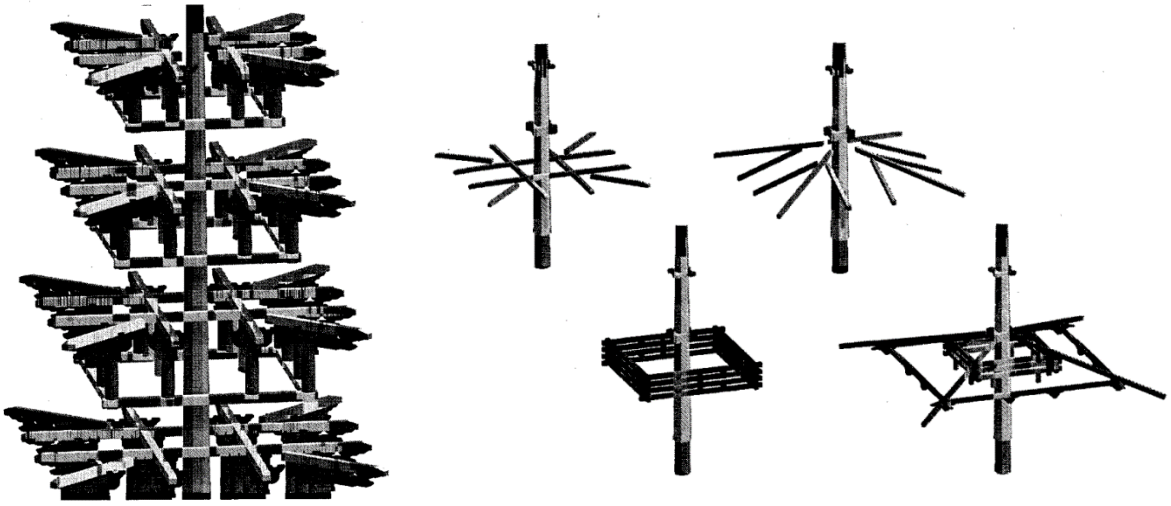

Figure 7: 3D view of sections of the internal structure of Horyu-ji Pagoda. Left side image shows the main tie beams, columns and lower tie beams. The righthand set of images shows main tie beams (top left image), lower rafters (top right image), outer bracket beams (bottom left image) and the upper rafters with the inner bracket beams (bottom right image). (Reproduced from Field 2008).

Table 3: Member cross-sectional dimensions within the Horyu-ji Pagoda.

Member	1st Floor Outer Columns	1st Floor Inner Columns	Upper Floors Outer Columns	Upper Floors Inner Columns	Main Tie Beams
Dimensions (mm × mm)	500×500	500⌀	400×400	400⌀	300×240

Member	Bracket Beams	Floor Tie Beams	Dou Blocks	Internal Roof Support	Roof Rafters
Dimensions (mm × mm)	300×180	260×260	320×320	260×260	300×240

One key aspect of all these members is that the members dimensions are consistent throughout the structure, regardless of what floor they are on. The one exception to this rule is that the ground floor columns are slightly larger in area compared to the columns in the upper levels.

3.2 Distribution of Pagoda Mass

3.2.1 Total Mass of the Pagoda

The exact mass and mass distribution of the Horyuji Pagoda was unable to be found in any of the literature available. Therefore, the mass of the pagoda was estimated by extrapolating the masses of similar pagodas. The two pagodas chosen were the Tocho-ji and the Tsu Kanon pagodas as they are both five storey pagodas with clay tile roofs. The Tocho-ji Pagoda has a main structure height (excluding the sorin) of 17.9 m and a weight of 133 tons (Hanazato et al. 2012). The Tsu Kanon Pagoda has a main structure height of 13.3 m and a weight of 74.7 tons (Fujita et al. 2004). Two graphs were plotted, one of the main structure volume versus weight and another of the entire structure volume (including roof volume) versus weight. The first graph gave an estimated weight of 290 tons and the second graph gave an estimation of 276 tons. An average of these two values gives a weight of 283 tons.

When constructing the pagoda model no live loads were considered. Horyu-ji Pagoda is used for ceremonial purposes only and the levels above the ground floor are inaccessible (Harada 2016). Therefore, when considering vertical loads within the structure only dead loads were calculated and included within the model.

The next step would be to calculate the mass of each floor of the structure. The roof is made of clay tiles and has a mass of 250 kg/m^2 (Fujita et al. 2004). We already know the floor span and roof span at each level and so we can find the area of the roof at each level. Knowing the mass per unit area and total area of the roof we find that the total roof mass is 155 tons, therefore the mass of the main structure (excluding the roof) is 128 tons. An assumption is made that main structure mass is distributed between the levels in proportion to the floor area at that level. The main structure mass and the roof mass is added together to give the total mass for each level.

Table 4 shows this distribution within Horyu-ji Pagoda and compares it to the known distribution within Tsu Kanon Pagoda. It can be seen that the mass is distributed more to the lower levels of Horyu-ji Pagoda compared to that of Tsu Kanon Pagoda. This is due to the fact that Tsu Kanon Pagoda is slenderer and the decrease in size of the upper levels is less pronounced. It can also be seen that the first level of both pagodas have a large share of the total mass. This is due to both pagodas having an extra eave surrounding the pagodas at the base level.

Table 4: Mass distribution between levels of both the Horyuji and Tsu Kanon pagodas.

	Horyu-ji				Tsu Kanon	
Level	Roof mass (tons)	Main structure (tons)	Total mass (tons)	Mass %	Total mass (tons)	Mass %
1	40.5	75.6	116	41.0	30.2	40.4
2	35.2	20.3	55.5	19.6	11.4	15.3
3	30.1	15.0	45.1	15.9	10.7	14.3
4	25.4	10.4	35.9	12.7	10.3	13.8
5	23.7	6.70	30.4	10.7	11.4	15.2
Total	155	128	283	100	74.7	100

3.2.2 Lumped Masses within the Model

The final step in this process is deciding how to distribute this weight as lumped masses within the virtual model. Lumped masses are utilised in order to simplify the model; this will not sacrifice the accuracy of the analysis (Hanazato et al. 2010). The lumped masses will be placed at the top of each column at ceiling height for each level. This lumped mass will represent the weight of the roof at that level, the top half of the main structure weight at that level and the bottom half of the main structure weight of the level above. The area on each level is divided into tributary areas and an example of this is shown in Figure 8. The red area represents the roof mass supported by the column whereas the cyan area represents the main structure mass. It is assumed that the roof mass and main structure mass is evenly distributed, meaning that the mass supported by each column is proportional to the highlighted areas.

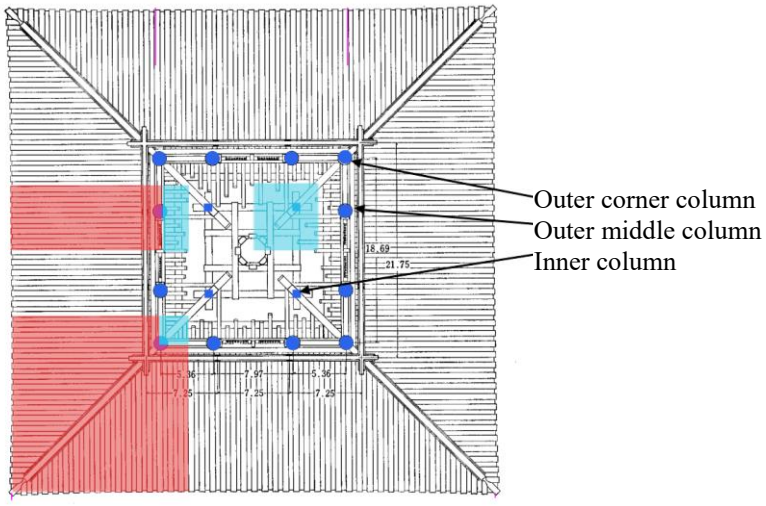

Figure 8: Tributary areas relating to the mass supported by each column.

This will leave the model with one set of lumped masses located at the top of each column, with the exception of the ground floor which will also have lumped masses at the base of the columns. Table 5 shows the weight and location of the lumped masses to be used within the model for the first and fifth levels (the full table for all levels can be found in Appendix A). There are three types of column on each level, the inner columns surrounding the shin-bashira, the outer middle columns and the outer corner columns. Level one also has the extra eave columns present.

Table 5: Lumped masses to be placed at level one and five.

	Level 1			Level 5		
Column type	Outer corner (kN)	Outer middle (kN)	Inner (kN)	Outer corner (kN)	Outer middle (kN)	Inner (kN)
Top of column	70.0	41.0	31.1	41.8	17.2	7.37
Bottom of column	13.2	14.7	16.3			

What can be seen is that the outer columns carry a larger load of the levels weight compared to the inner columns of the structure. This is more pronounced at the higher levels and is due to the large mass of the clay tile roof sections.

3.3 Material Properties

3.3.1 Hinoki Cypress

One unique aspect of Japanese pagodas is that all the structural members and their connections are made entirely out of timber. This means that all members within the pagoda model will have the same material properties. Horyu-ji Pagoda is constructed of hinoki cypress, a coniferous tree native to Japan. For this reason, when constructing the model of the pagoda, the material properties of hinoki cypress are used.

3.3.2 Radiata Pine

When constructing the computer models simulating a modern multi-storey timber structure radiata pine is used. The reason for this is that radiata pine is extensively used in timber construction within New Zealand.

The key values used are shown in Table 6 (Tenon Clearwood Ltd (2015); Yokoyama et al. 2009).

Table 6: Material properties of timber used within the computer models.

Timber	Young's Modulus (parallel to grain)	Young's Modulus (perpendicular to grain)	Compressive Strength (parallel to grain)	Compressive Strength (perpendicular to grain)	Shear Strength
Hinoki Cypress	9 GPa	450 MPa	40 MPa	4.8 MPa	7.5 MPa
Radiata Pine	8.2 GPa	410 MPa	37 MPa	4.4 MPa	12 MPa

3.4 Base Isolation Joint

The base isolation joints are located at the base of the columns on the ground floor (Figure 9). These ground floor columns are placed into shallow depressions within the foundation. The columns are able to move horizontally until they collide with the edge of the depression they sit within. This maximum horizontal motion is set as ±1.5 cm (Nakahara et al. 2000). There are 16 base isolation joints in total within the pagoda.

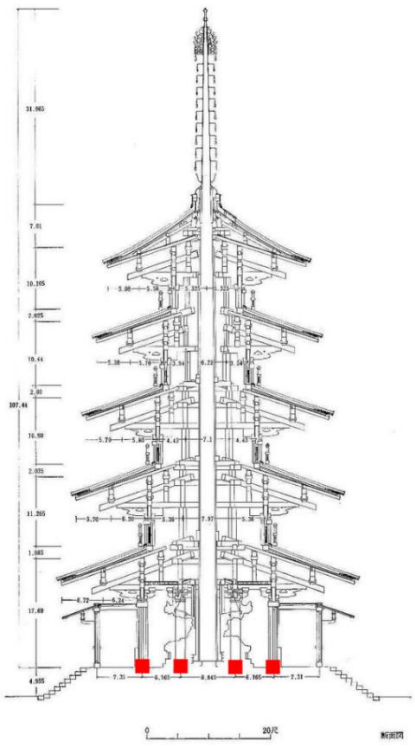

Figure 9: Diagram highlighting the location of the base isolation joints within Horyu-ji Pagoda. (Unedited image reproduced from Yasuhara et al. 2007).

The base isolation joints were assumed to act as a friction damper and were modelled as a non-linear spring. A coefficient of friction of 0.4 was used. This friction damper operates through the concept of Coulomb damping and acts as a source of energy dissipation during an earthquake event. The yield force of the joint was calculated using Equation 1.

$$Q_s = \sum W \times C_f \quad (1)$$

Q_s representing the horizontal load required for the column base to start sliding. $\sum W$ represents the total vertical weight resting upon the joint and C_f is the coefficient of friction. While the horizontal load is less than the sliding yield force the joint will not deform. When the horizontal load exceeds the sliding yield force the joint will slide until the 1.5 cm deformation limit is reached. This deformation limit was set within the program by changing the non-linear spring stiffness to an excessively large amount for any deformations exceeding ±1.5 cm. An isotropic hysteresis type (Figure 10) was chosen to model the spring within SAP2000 (Hanazato et al. 1999a).

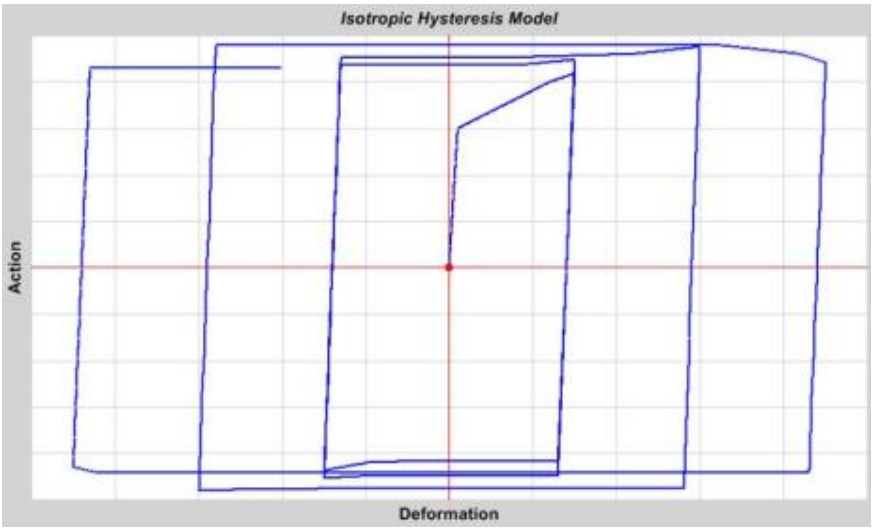

Figure 10: Hysteresis model to be used to represent the base isolation joints.

In order to calculate the force-displacement characteristics of this joint the total vertical load at the joint needs to be calculated. This is an extension of the process already used to calculate the mass distribution of the structure. The weight distribution of each level localised at the top of the columns is already known. Knowing this, the vertical loads on the columns can be calculated within the structure. For example, the weight from level five is transferred down to level four as point loads through the level five columns. This point load weight from level five is added to the previously calculated level four weight distribution in order to find the vertical load travelling through the level four columns. This weight on the level four columns represents the vertical load of all the levels

above this point. This vertical load at level four is then transferred down to level three as point loads through the columns of level four. This process continues down to level one of the pagoda.

Figure 11 shows an example of this process. In Figure 11 (a) the cross represents the level five column and the four corners of the diagram represent level four columns. Due to symmetry it can be approximated that the load from the level five column is transferred evenly by the floor diaphragm to the beams connecting the columns.

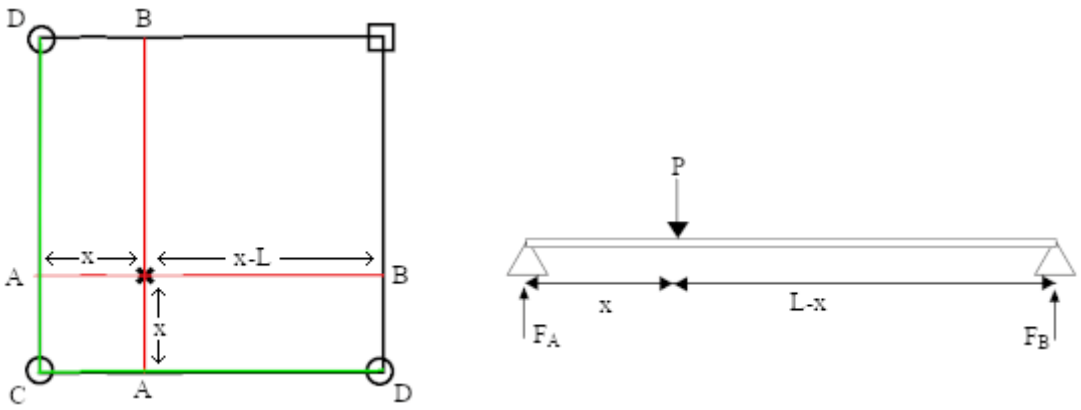

(a) (b)

Figure 11: Column support loads in response to loading from the upper level.

Looking at the example of a simply supported beam loaded with a point load, shown in Figure 11 (b), the reaction force F_A can be calculated by summing the moments acting around support B. Equation 2 shows that the support force at A is proportional to the length of the beam located between P and the opposing support compared to the total beam length.

$$F_A = \frac{P \cdot (L-x)}{L} \tag{2}$$

Knowing the reaction force at point A this process can be repeated along the beams C-D to find the support force at point C.

$$F_C = \frac{F_A \cdot (L-x)}{L} \tag{3}$$

$$F_C = \frac{P \cdot (L-x)^2}{L^2} \tag{4}$$

Equation 4 shows that the support force at column C is proportional to the ratio of the area of the opposing quadrant to the total area shown within the diagram of Figure 11 (a). From this equation the transfer of vertical loads from one level to the level below was able to be calculated. Table 7 shows the total vertical dead load at the base of the columns at level one along with the associated friction sliding loads.

Table 7: Vertical load at the base of the level one columns and the associated sliding loads.

Column type	Outer Corner	Outer Middle	Inner
W- weight (kN)	143	137	211
Q_s – sliding load (kN)	57.0	54.6	84.4

What can be seen in Table 7 is that at the lower levels of the pagoda the inner columns of the structure carry a larger share of the vertical dead load. This trend is the opposite of the one seen in Table 5 where the individual level dead load distributions are largest at the outer columns. The reason for this is that, moving up the pagoda, each level is smaller than the previous one. Because of this the columns of a level are located on the inner side of the same columns on the level below. An example of this would be that, if we focused on level five, the outer corner columns of level four will not support the full load of the outer corner columns of level five. A proportion of the level five column vertical load will be transferred to the inner columns of level four instead. This process is repeated at every level compiling the effect of load transfer towards the inner columns.

With all these calculations having been carried out the non-linear spring representing the base isolation joint was able to be created. The exact variables that were entered into SAP2000 can be seen in Appendix D.

3.5 Sliding Friction Joint

The sliding friction joints are the connections between the top of the columns and the main tie beams within the pagoda. Figure 12 shows the locations of these joints within Horyu-ji Pagoda. These joints operate in the same manner as the base isolation joints where the horizontal strength of the joint is defined by the sliding friction between the two timber members. A maximum allowable horizontal deformation of ±1.5 cm is again set. There are 40 of these joints in total within the pagoda when only considering horizontal loading.

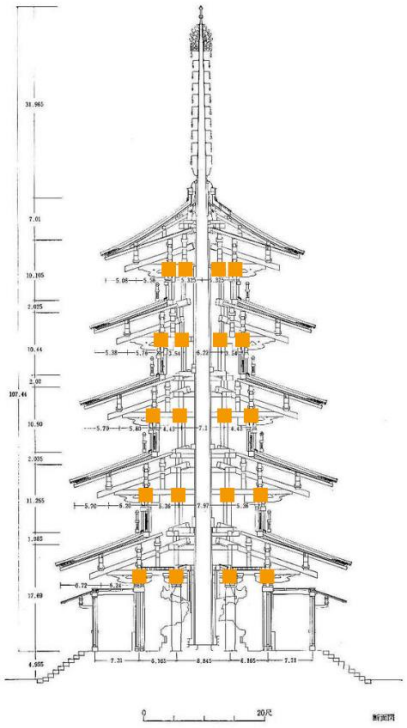

Figure 12: Diagram highlighting the location of the sliding friction joints within Horyu-ji Pagoda. (Unedited image reproduced from Yasuhara et al. 2007).

The only difference between how the sliding friction joints and the base isolation joints operate are the yielding forces at which sliding begins to occur. Equation 1 in the above section was used again to calculate these yielding forces. As a by-product of the process taken to calculate the total dead load ($\sum W$) at the ground floor columns the dead load carried by each column within the other levels of the pagoda is also known. A sliding coefficient of 0.4 was again used. Table 8 shows the total vertical load at each level as well as the horizontal yielding for each column at each level.

Table 8: The yielding force of the sliding friction joints at each level within the pagoda.

	Weight - $\sum W$ (kN)	Sliding Force (kN)	Sliding force per column -Q_s (kN)
Level 1	2270	908	56.7
Level 2	1540	615	38.4
Level 3	1020	408	25.5
Level 4	599	240	15.0
Level 5	265	106	8.80

3.6 Rocking Column Joint

The rocking column joints are located at the base of the columns at each level and represent the joint between the columns and the beam they rest upon. The exception to this is at the ground floor where the joints are instead replaced by the base isolation joints. Figure 13 shows the location of these joints within the pagoda. There are 60 rocking column joints in total within Horyu-ji Pagoda.

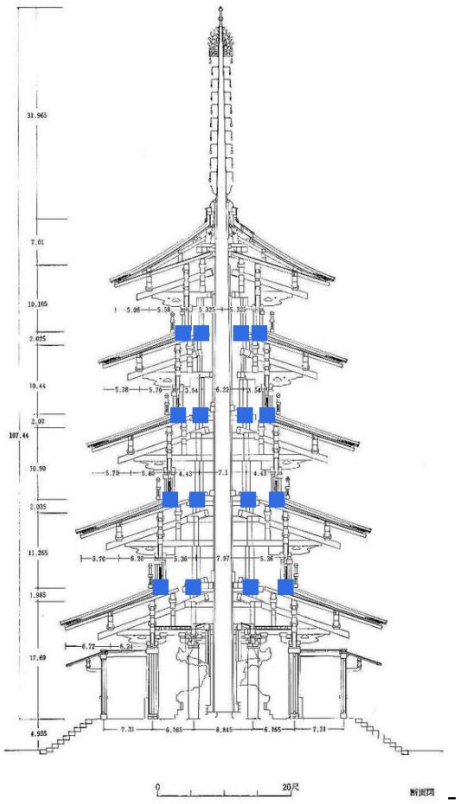

Figure 13: Diagram highlighting the locations of the rocking column joints within Horyu-ji Pagoda. (Unedited image reproduced from Yasuhara et al. 2007).

These joints are unique as they represent the columns simply resting upon the beam below them, there is no solid connection. This connection will be modelled as a non-linear rotational spring with stiffness values shown in Figure 14. These values were obtained from the research done by Hanazato et al. (Hanazato et al. 1999b).

This works on the principle that as the column rotates the vertical load (W) and the support force at the base of the column act off-centre through the column creating a moment that resists further rotation. As the column continues to rotate there is less contact between the column and the floor, leading to a gradual decrease in the restoring moment provided by the column. The y-axis is the bending moment and is a product of the vertical load and the width of the column, increasing either of

these values will cause an increase in the joint's moment resistance capacity. The x-axis is the rotation of the joint and is calculated by taking the ratio of the width to the height of the column. A larger a_0 value means that the joint is able to deform more before failure occurs. Based off of this knowledge a short wide column with a large vertical load will be able to resist a larger horizontal load compared a slender column with a light vertical load. The exact values placed before a_0 and M_0 on Figure 14 were obtained experimentally by Hanazato et al. (Hanazato et al. 1999b).

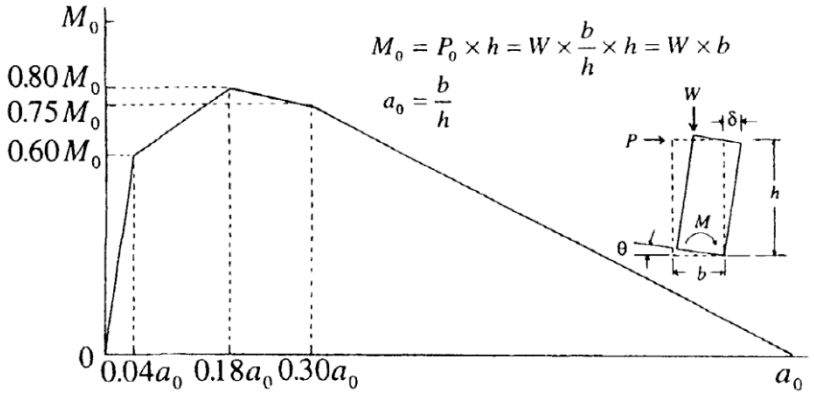

Figure 14: Rotational spring model of rocking column effect. (Reproduced from Hanazato et al. 1999b).

In order to calculate the strengths of these joints within Horyu-ji Pagoda the column widths, heights and vertical loads need to be known for every column within the structure. These values are already known and were obtained during the vertical load distribution calculations carried out earlier. Therefore, calculating the unique moment-rotation curves for each of these joints was a straight forward process.

Figure 15 shows the rotational strength of the rocking column joints at each level within Horyu-ji Pagoda. What can be seen is that these joint strengths drastically decrease at the higher levels of the pagoda. The maximum strength of these joints occur at a rotation of about 0.035-0.05 radians which translates to a storey drift of about 3.5-5%.

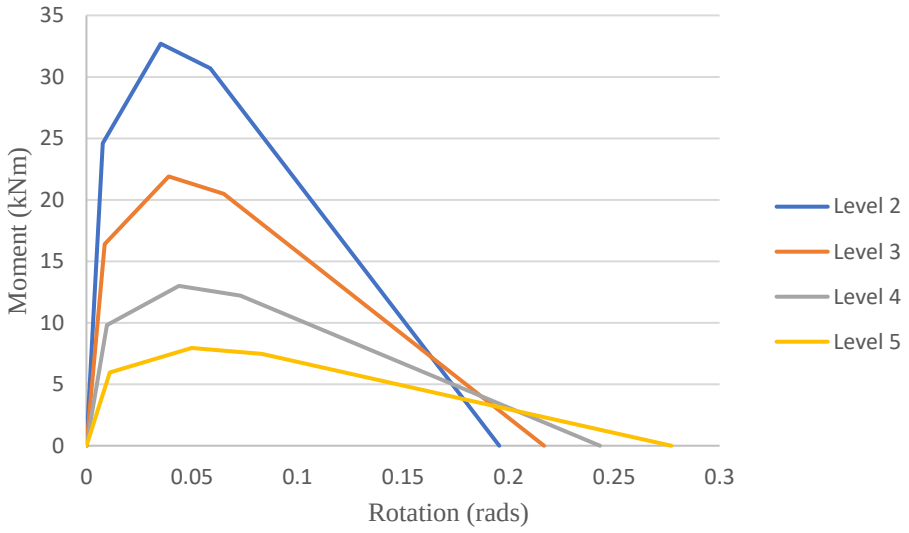

Figure 15: Moment resistance of the rocking column joints within Horyu-ji Pagoda.

3.7 Nuki Joint

The nuki joints are located at the base of the columns at levels two to five. This is coincidentally the same location as the rocking column joints, the locations having been highlighted in Figure 13. There are 38 relevant nuki joints in total within Horyu-ji Pagoda when considering horizontal loading. This joint is the connection between the columns and a continuous tie beam that penetrates them. This connection only occurs at the outer columns of each floor due to the fact that the tie beam only penetrates these columns, there is no lower tie beam connecting to the inner columns.

These nuki joints were modelled as a non-linear rotational spring. The equations used to find the stiffness of this joint was based on the research done by Chang et al. (Chang et al. 2006). Figure 16 shows the basic concepts of these joints. As the joint rotates a compressive zone forms, this is where the rotating beam is forced into the column. An initial point of contact is made at the outer edge of the column and as the joint continues to rotate the compressive zone forms and expands inwards. The largest strain within the beam occurs at this initial point of contact and linearly decreases to zero at the inner edge of the compressive zone. The far-right diagram within Figure 16 shows this strain distribution. When the strain exceeds the yielding strain perpendicular to the grain of the timber the beam begins to yield. This stress distribution is also shown in the far-right diagram within Figure 16. A compressive zone forms above and below the beam, with one zone acting upwards and the other downwards. These zones are also horizontally displaced from each other. The coupled forces caused by the compressive zones create a resisting moment within the joint. The resisting moment is capped due to the timber crushing as the yielding strength of the beam is exceeded.

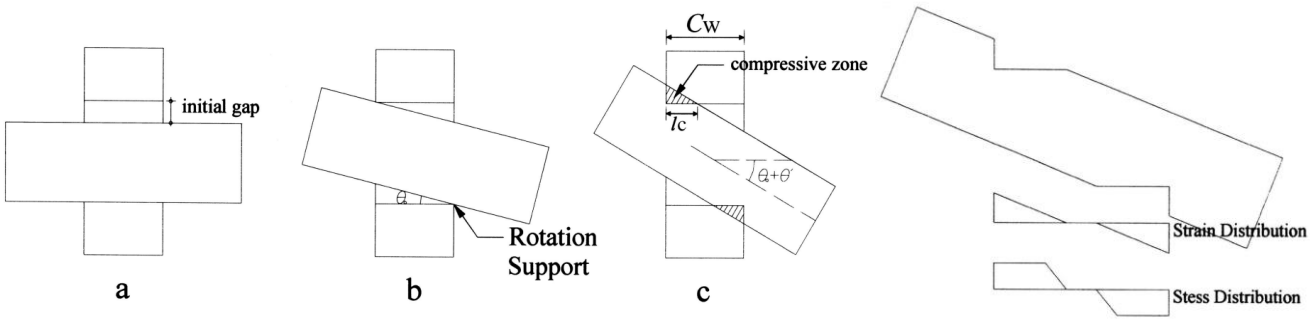

Figure 16: Basic concepts of a Nuki Joint in traditional Japanese timber structures. (Reproduced from Chang et al. 2006).

In order to find the strength of this joint it was assumed that the Young's modulus, *E*, of the wood parallel to the grain is 20 times that perpendicular to the grain. Equation 5 below shows Hankinson's Formula (Chang et al. 2006). This formula was used to calculate the modulus of elasticity during rotational deformation.

$$E(\theta) = \frac{E_{\perp} \times E_{\parallel}}{E_{\perp} cos^{3.1}(\theta) + E_{\parallel} sin^{3.1}(\theta)} \quad (5)$$

E(θ) represents the rotational modulus of elasticity, $E_{\perp}$ represents the modulus of elasticity perpendicular to the grain and $E_{/\!/}$ represents the modulus of elasticity parallel to the grain. As the beam rotated the strain at the outer edge of the beam-column compressive zone was calculated through geometric manipulation. Knowing this strain at the outer fibres of the beam compression zone the stress was calculated using Hook's law. The stress distribution was then used to calculate the bending moment created within the joint. This process was repeated for each small increment of rotation.

The key parameters that were required to calculated the moment-rotation curve of the joint were the width and depth of the beam, the width of the column, the initial gap within the joint, the timber yield strength and the timber modulus of elasticity. Figure 17 shows the rotational stiffness curve of the nuki joint. It can be seen that there is initial rigid body motion of the beam due to the small gap between the top of the beam and the column. This means that the joint has zero stiffness up to about 0.015 rads. The beam begins to yield at about 0.04 rads and has a maximum resisting moment of 47 kNm. The stiffness of the joint is roughly 1440 kNm/rad prior to the beginning of the yielding of the beam. The calculated values have an error of roughly 5.6% compared to the experimental values obtained by Chang et al. (Chang et al. 2006), validating the use of this *M-θ* relationship. Appendix C shows the MATLAB script used to calculate the rotational stiffness of the joint.

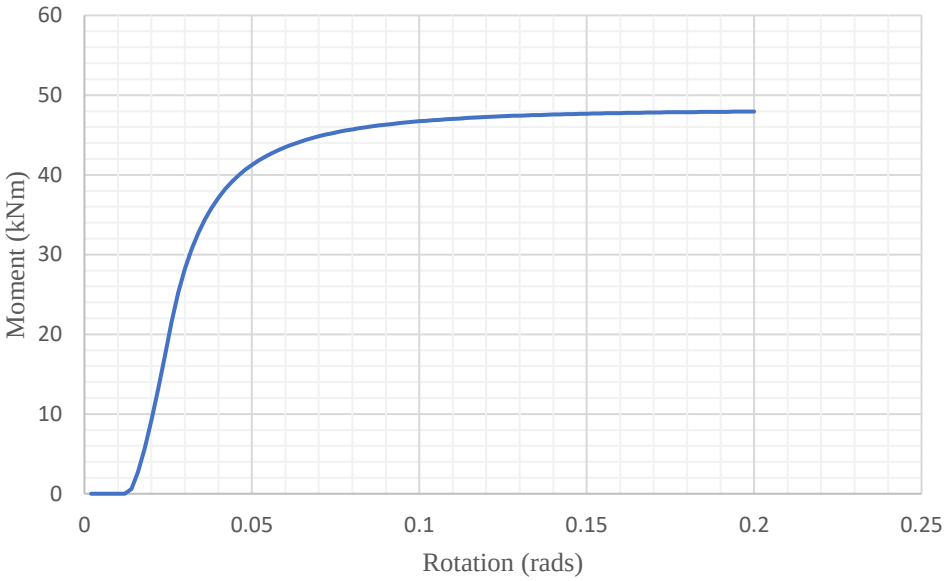

Figure 17: Moment-rotation strength curve for nuki joints within Horyu-ji Pagoda.

3.8 Balancing Toy Effect

The balancing toy effect is due to the size and weight of the roof eaves in relation to the span of the bays and this effect plays a role on the response of a timber pagoda. Figure 18 shows this concept simplified as a set of pendulums and simple springs. The pendulum masses represent the mass of the clay roof tiles while the length *l* represents the distance the centre of mass of the roof overhangs the main structure. When a rotation is forced upon the system the lever arm lengths change. The pendulum that was forced to rise has had an increase in lever arm length while the pendulum that was forced to lower has had its lever arm length decrease. This change in lever arm distance has a direct effect on the rotating moments created by the weight of the pendulums in the system. The net effect is a moment that resists the rotation of the eaves (balancing toy effect) and operates independently at each level of the pagoda. Figure 18 was obtained from the research done by Nakahara et al. (Nakahara et al. 2000).

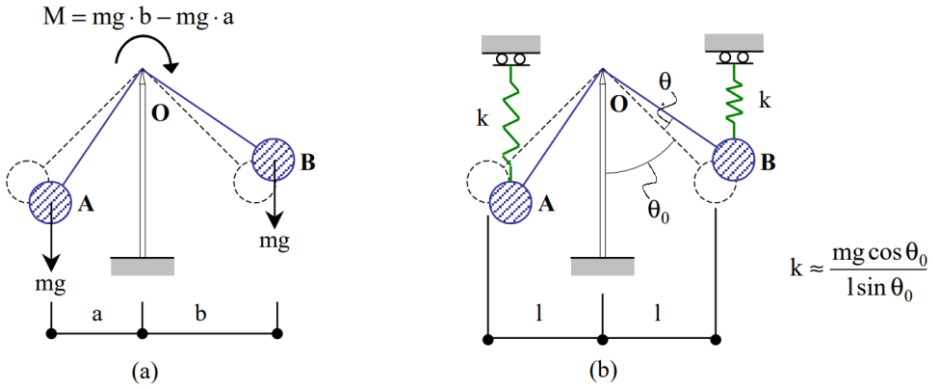

Figure 18: Balancing toy effect represented as a simple spring and pendulum model. (Reproduced from Nakahara et al. 2000).

The creation of the moment resisting rotation can be simplified further by modelling the pendulums as two vertical springs. When the angle of rotation is miniscule the spring stiffness calculation can be simplified in to Equation 6, which was shown in Figure 18.

$$k = \frac{mg \times \cos(\theta_o)}{l \times \sin(\theta_o)} \quad (6)$$

Here *k* is the stiffness if the virtual spring, *m* is the mass of the roof half, *g* is the gravitational constant, *l* is the distance between the centre of mass and centreline of the roof and θ_0 represents the slope of the roof.

Figure 19 shows where these springs were placed within the pagoda model. There were a total of 58 springs used.

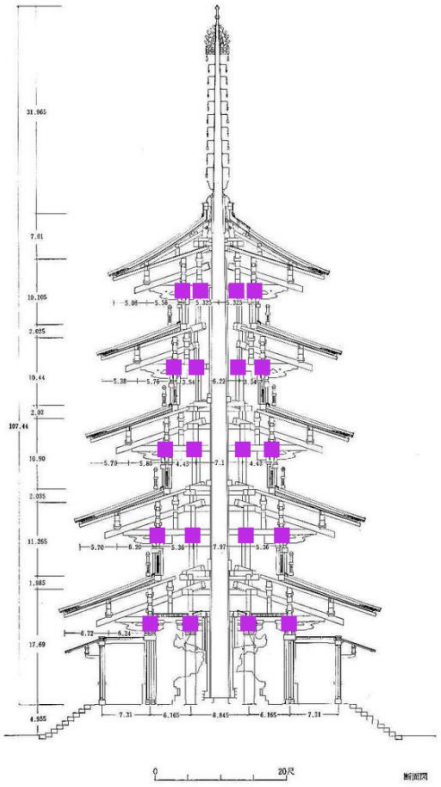

Figure 19: Diagram highlighting the locations of the springs used to simulate the balancing toy effect within Horyu-ji Pagoda. (Unedited image reproduced from Yasuhara et al. 2007).

When the spring stiffnesses to be used within Horyu-ji Pagoda were calculated the first step carried out was to find the centre of mass (COM) of the roof at each level. The horizontal area of the roof was split into two halves, a left half and a right half. Each half would represent one of the two pendulums within the model. The roof halves were then further split into regular shaped segments. Because the floor plan at each level of the pagoda was known the areas and the distance of the centres of these regular shaped segments to the roof centreline were also able to be calculated. The centre of mass of the roof half at each level was then calculated by taking a weighted summation of the distance of the segment centres to the roof centreline. The summation was weighted based upon the area of the segments. Equation 7 was used to find the centre of mass of the roof at each level. It was assumed that the weight of the roof was evenly distributed over the entire area of the roof.

$$l = \frac{\sum_i^n (A_i \times l_i)}{\sum A} \tag{7}$$

Here A_i represent one of the roof segment areas, l_i represents the distance of the segment centre to the roof centreline and ΣA represent the total area of the half of the roof.

Finally, the mass of the roof at each level was calculated. This step was completed previously during the process of calculating the total mass of the structure and is shown in Table 1. Table 9 shows the values calculated for the roof at each level using Equation 6 and Equation 7.

Table 9: Values used to calculate the strength of the virtual springs modelling the balancing toy effect within Horyu-ji Pagoda.

	Centre of Mass – l (m)	Roof Angle – θ_o	Roof Mass – m (kN)	Spring Stiffnes – k (kN/m)
Level 1	4.07	27.6°	199	91.2
Level 2	3.71	28.7°	172	82.8
Level 3	3.35	29.8°	148	74.8
Level 4	2.99	30.9°	125	67.0
Level 5	2.64	40.0°	116	45.8

The spring stiffnesses calculated above are for springs placed directly above the centre of mass of the roof. In order to further simplify the model the springs were moved so that they are instead directly above the columns of each floor. The spring stiffnesses have been adjusted in order to compensate for this shift in location. The values obtained from Equation 7 are entered into Equation 8 to find the final spring stiffnesses. The derivation of Equation 8 is shown in Appendix B.

$$k_c = \frac{{l_r}^2}{{l_c}^2} \cdot k_r \tag{8}$$

Here l_r represents the distance between the virtual springs at the roof COM and the centreline of the roof. l_c represents the distance between the column and the roof centreline. k_r represents the stiffness of the springs at the roof COM and k_c represents the stiffness of the springs at the columns.

Table 10 shows the values of the spring stiffnesses used to simulate the balancing toy effect of Horyu-ji Pagoda. These values are for springs placed at each column whereas the values shown within Table 9 are for one spring per half roof. These springs will be placed at the joint between the top of the columns and the main tie beams at every level.

Table 10: Spring stiffnesses used to simulate the balancing toy effect of Horyu-ji Pagoda.

Location	Spring Stiffness – k_c (kNm)
Level 1	33.3
Level 2	32.8
Level 3	32.8
Level 4	33.7
Level 5	36.1

3.9 Shin-bashira (Tuned Mass Damper)

The shin-bashira is a continuous piece of timber that is located at the very centre of the pagoda. This member extents from the ground floor up through the core of the structure all the way to the top floor. The member then continues above the roof as spire, extending a further 9.8 m. The shin-bashira is technically two separate members that are fused at the fourth floor. This central column was modelled as a beam member with continuous joints placed at each level. This method of modelling the shin-bashira has given accurate results in past analyses (Hanazato et al. 2010). The central column is suspended from the beams of the fifth floor and does not make contact with the foundation at the ground floor (Hanazato et al. 2004).

Attached to the side of this shin-bashira are wooden battens, they are located at the roof sections of floor one to floor three and again at floor five. These battens are not present at the fourth floor as this is the location of the shin-bashira fusion point. These battens are short timber members that act as a buffer between the internal members within the roof sections and the shin-bashira column. Therefore, the shin-bashira is able to make contact with each floor, but only in compression. This interaction was modelled as a compression only gap spring within SAP2000. The gap at which the spring had no stiffness was set as 1 mm (Field 2008). Figure 20 shows the location of the special shin-bashira connection points within the pagoda. There are a total of eight of these connection points within Horyu-ji Pagoda.

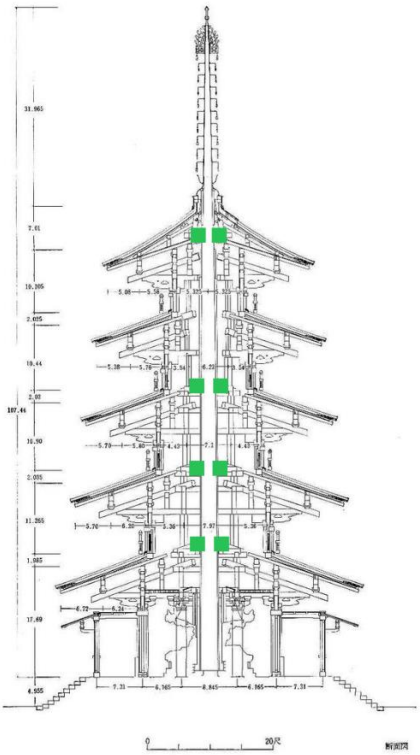

Figure 20: Diagram highlighting the locations of the shin-bashira connections within Horyu-ji Pagoda. (Unedited image reproduced from Yasuhara et al. 2007).

The stiffness of the spring during compression was calculated using Equation 9.

$$k = \frac{E \cdot A}{L} \tag{9}$$

Where E is the young's modulus of the timber, A is the area of compression and L is the depth of the timber batten being compressed. The stiffness of the shin-bashira compression connections used in the modelling was 6.74 GPa.

The shin-bashira does not help carry vertical load within the structure. However, it does help transfer shear loads between levels within the pagoda. This, in theory, should help decrease displacements and storey drifts during an earthquake event.

As a side note the sorin (vertical spire attached to the top level of the structure) acts as a TMD (tuned mass damper) that helps absorb inertial forces from the main structure.

3.10 Selection of Earthquake Time History Plots

In order to more accurately gauge the response of the modelled structures to earthquake excitation NLTH (non-linear time history) analysis was performed on the models. The earthquake time history graphs are plots representing horizontal ground acceleration over time. This horizontal ground acceleration would then be applied to the foundation of the model and the response of the model to this ground excitation would be recorded over time. The key parameters recorded are the accelerations and displacements of each joint within the structure as well as internal forces within the joints and members. These values were recorded at each time-step of the NLTH analysis. Three different recorded earthquake events were chosen, two mid-range earthquakes and one larger one. This was done in order to avoid a situation where an outlier could potentially skew the output information.

The first earthquake time history used was a recording taken at array 6 of the 1940 El Centro earthquake. This earthquake recording had a PGA (peak ground acceleration) of 0.38 G. Figure 21 shows the function as plot over time. The total period of this recording is 39 seconds and the input timestep was 0.01 s. This earthquake case will be referred to as Array 6.

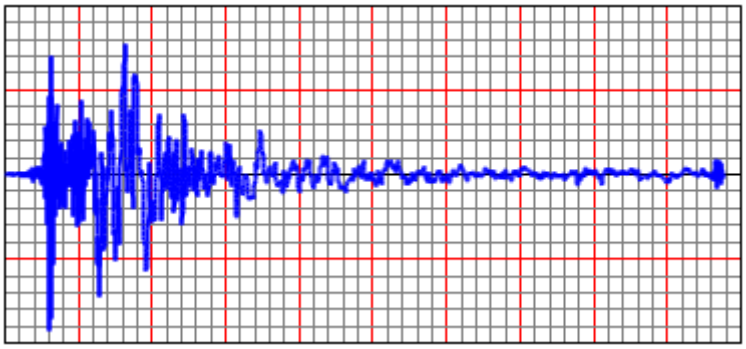

Figure 21: Time history function of the Array 6 recording. Horizontal axis is time and the vertical axis represents ground acceleration.

The second earthquake time history used is a recording taken at Newhall of the 1994 Northridge earthquake. This earthquake recording had a PGA of 0.59 G, roughly 50% larger than the other two earthquake recordings chosen. Figure 22 shows a plot of this time history function. The total period of this recording is 60 seconds and the input timestep was 0.02 s. This case will be referred to as Newhall.

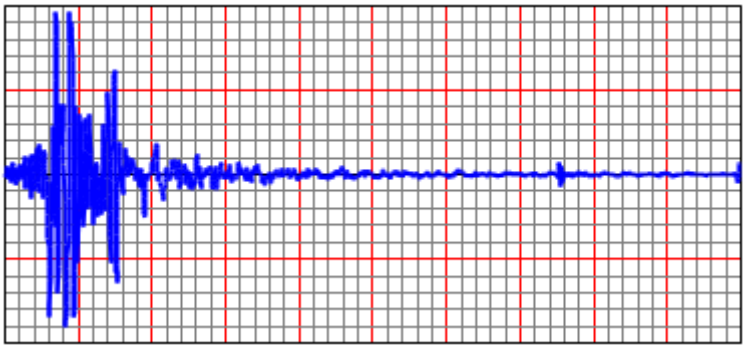

Figure 22: Time history function of the Newhall recording. Horizontal axis is time and the vertical axis represents ground acceleration.

The third earthquake time history used is a recording taken at Hollister of the 1989 Loma Prieta earthquake. This earthquake recording had a PGA of 0.37 G, similar to the first earthquake chosen. Figure 23 shows a plot of this time history function. The total period of this recording is 60 seconds and the input timestep was 0.02 s. This case will be referred to as Hollister.

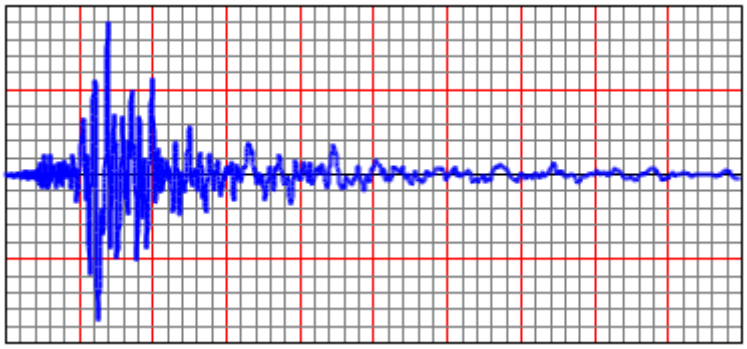

Figure 23: Time history function of the Hollister recording. Horizontal axis is time and the vertical axis represents ground acceleration.

3.11 Construction of Horyu-ji Pagoda Model

Once the unique joint parameters have been calculated the model was created in SAP2000. Figure 24 shows the completed 2D model. The pagoda model was created in order to validate that the unique virtual joints would accurately represent the real physical joints within Horyu-ji Pagoda. If the pagoda model gave outputs similar to what was recorded from the microtremor tests then that would give us confidence that these virtual joints could be used on other structure models in order to estimate their earthquake responses.

Two loading cases were tested on the pagoda, the first being modal analysis. If the pagoda model had similar modal time periods compare to what was observed during microtremor tests on Horyu-ji Pagoda then the model would be considered validated.

The second loading case was a non-linear static analysis or ESA. In this case the NZS 1170.5 method was followed in order to calculate a force distribution that would reasonably simulate an earthquake loading on the structure. If the pagoda model had reasonable horizontal displacements and storey drifts for the loading case then the model would be validated.

The pagoda was modelled as a two-dimensional structure. This was done in order to reduce the computational requirements of the analysis. The model consists of four frames in parallel placed over top of each other, two outer frames and two inner frames. Therefore, each column in the model represents four columns within the real structure. The other structural members, lumped masses and unique joints were also combined in this way.

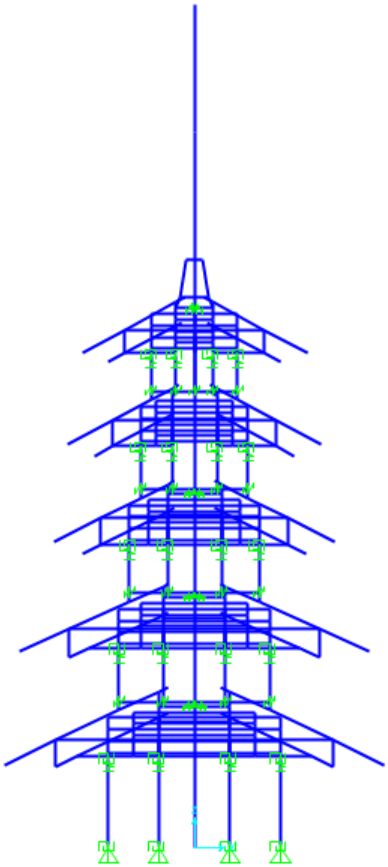

Figure 24: 2D Model of Horyu-ji Pagoda created in SAP2000. Blue lines represent the structural members, green represents the unique non-linear joints.

3.11.1 Modal Analysis

Modal analysis was carried out on the pagoda model. A damping ratio of 4% was used for all modes. This was all completed internally within SAP2000. The stiffness and mass matrices were constructed based upon the structural member and lumped mass locations within the model. The mode with the largest participating mass ratio was labelled the first mode and the mode with the second largest ratio was labelled the second mode and so on. This process continued until the accumulative value of the participating mass ratios was greater than 99%. This 99% threshold was chosen as it was sufficiently large enough to ensure an accurate representation of Horyu-ji Pagoda.

The key output values taken from this analysis were the modal periods and the modal mass participation ratios.

3.11.2 ESA Loading Case

When calculating the horizontal force distribution between levels the NZS1170.5 procedure was followed (Council of Standards New Zealand 2004). The reason a New Zealand standard was used for a Japanese building was because the NZS 1170.5 method gives a reasonable approximation for earthquake loading that is applicable to a wide variety of structures. Also, if these construction techniques are to be used within New Zealand in the future then knowing how these structures will theoretically perform when New Zealand design standards are applied to them will be relevant.

A few assumptions were made. Firstly, it was assumed that the ground was classed soil type C. Soil type C is defined as shallow intermediate stiffness soil with underlying bedrock. Secondly, a hazard factor (*Z*) of 0.4 was chosen, which is a good estimation for the Christchurch or Wellington regions. Next it was assumed that the near-faulty factor (*N(T,D)*) was 1.0, this corresponds to a site located 20 km from the fault-line. A risk factor (*R*) of 1.0 was chosen, this corelates to an earthquake with a return period of 500 years. Equation 10 is used to calculate the elastic site spectra.

$$C(T) = C_h(T) \cdot R \cdot N(T, D) \cdot Z \tag{10}$$

The variable $C_h(T)$ represents the spectral shape factor and its value is dependent on the modal time period value and the soil type. There will be a unique spectral shape factor for each of the three modal periods of the model. Equation 11 and Equation 12 are used to calculate the spectral shape factors for soil type C cases.

For $0.1 < T < 0.3\ s$

$$C_h(T) = 2.93 \tag{11}$$

For $0.3 \leq T \leq 1.5\ s$

$$C_h(T) = 2 \cdot (0.5/T)^{0.75} \tag{12}$$

Equation 11 will be used to calculate the spectral shape factor for the third modal period while Equation 12 will be used for the first and second mode of the pagoda model. Once the elastic site spectra values are calculated for each mode Equation 13 will be used to calculate the design action coefficients.

$$Cd(T) = C(T) \cdot \frac{S_p}{\mu} \tag{13}$$

Here μ represents the ductility factor and is the ratio between the yield strain and ultimate limit strain within the plastic hinge zones of the structure. This was calculated to be 1.5 assuming the mode of failure was due to plastic hinges forming within the columns as horizontal displacement occurred. The next variable was S_p which represents the structural performance factor. This value was set as 1.0 due to the low ductility factor (μ < 2) and the high first modal period (T_1> 1 s) of the model. Table 11 shows the calculated values for the three modal periods.

Table 11: Earthquake design factors and coefficients for the first three modes of the pagoda model, following NZS 1170.5 design procedures.

	Modal period - T (s)	Spectral Shape Factor - C_h	Elastic Site Spectra - C(T)	Design Action Coefficient - $C_d(T)$
1st Mode	1.14	1.10	0.44	0.29
2nd Mode	0.46	2.28	0.91	0.61
3rd Mode	0.22	2.93	1.17	0.78

In order to calculate the base shear created by each of these modes the design action coefficient value is multiplied by the effective weight of that mode. This effective weight is simply calculated by multiplying the total weight (W) of the structure to the mass participation ratio (MPR) of that mode. Equation 14 shows this calculation. The subscript i relates to each individual mode.

$$V_{b,i} = C_d(T) \cdot W \cdot MPR_i \tag{14}$$

Equation 15 is used to calculate the horizontal applied load at each level for each mode.

$$F_{n,i} = 0.08 \cdot V_{b,i} + 0.92 \frac{W_n \cdot h_n}{\sum(W_n \cdot h_n)} \cdot V_{b,i} \quad (15)$$

The subscript *i* relates to the mode number while the subscript *n* relates to the level within the pagoda model. Here w_n represents the weight of each level of the pagoda and h_n represents the height at which this weight is located. The second term of the equation will be used at every level while the first term will only be included when considering the top level. This is to account for the increased effect the higher modes have on the upper levels of the structure.

In order to calculate the loads and base shears of all three modes combined the square root of the sum of the squares (SRSS) method is used (Equation 16). This is to account for the fact that the probability of the maximum effect of all three modes acting simultaneously is very slim. The SRSS method will give a more reasonable estimation of earthquake loading.

$$S = \sqrt{\sum_{i=1}^{n} S_i^2} \quad (16)$$

This SRSS method was carried out separately for each level applied load and then again for the total base shear. Table 12 shows the calculated values that were then applied to each level of the pagoda model. When the loads were applied to the model the horizontal loads were placed at the same joints that the lumped masses were located, this being the joint connecting the top of the columns to the main tie beams in the roof sections. The applied loads were distributed within the level in proportion to the lumped mass values. For example, if a lumped mass represented 30% of that levels total mass then 30% of the horizontal applied load for that level would be placed at that same joint.

Table 12: Horizontal applied loads at each level of the pagoda model following the ESA method outlined in NZS 1170.5.

	Force (kN)
Level 1	71.0
Level 2	110
Level 3	136
Level 4	143
Level 5	192
Base Shear	653

The base shear calculated is 26% of the total structure weight.

3.12 Construction of the Modified Generic Multi-storied Timber Structure Models

A generic 2D timber structure was created in SAP2000. It was decided that this model would be three stories high and would have a square plan with each face having two bays. The unique joints used within the pagoda model was then added to the generic structure in order to observe the change in earthquake response. Five separate models were tested, a short description of each is given in the list below:

1. Unmodified structure model: This model does not have any unique joints added to it. All of the joints are modelled as moment resisting joints.
2. Base isolation model: The ground floor joints are modified to be base isolation joints modelled in the same manner as the pagoda model joints.
3. Sliding friction model: This model has the sliding friction joints placed at the top joint of each column within the structure.
4. Rocking column and nuki joint model: Due to the fact that both these joint types occur in conjunction with each other in the pagoda model they were both included together in the modified generic structure. These were placed at the base joint of each column, excluding the ground floor.
5. Combined mechanisms model: this structure included the base isolation, sliding friction, nuki and rocking column joints all present in one model.

It was decided that the balancing toy effect would not be included in the model as this did not seem practical to modern building design. The inclusion of it would require the addition of mass to the roof and would lead to a large increase in roof span. This change would lead to an increase in horizontal displacements and storey drifts within the structure (Muai and Tanaka 2012). It was also decided that the shin-bashira would not be included for two reasons, one is that is takes up floor space at every level of the structure and the second reason is that it is not effective when considering low-rise buildings.

3.12.1 Unmodified Timber Structure Model

The unmodified model was made to be three stories high with a total height of 9 m. The floor plan was 10 m by 10 m with each face of the structure consisting of two bays. NZS 3604 (timber-framed buildings) was referenced in order to obtain a reasonable mass and stiffness for the structure (Council of Standards New Zealand 2011). Table 13 shows the vertical loads assumed.

Table 13: Live and dead loads assumed for the generic timber structure based on recommendations made by NZS3604.

Live loads – Q	Dead loads - G		
Floors	Walls	Floors and Roof	Services
3 kPa	0.4 kPa	0.4 kPa	0.16 kPa

This model used lumped masses to represent the mass distribution. These lumped masses were located at the ceiling of each level at the joint connecting the columns to the main beams. The lumped masses represented the weight of the ceiling/floor and half the weight of the walls above and below the ceiling/floor. It was assumed that the floors and walls of the structure had an even weight distribution. Because of this assumption the value of each lumped mass was calculated using the tributary area of each column. The process for this method is the same one that was used when calculating the pagoda lumped masses and has been outlined previously in this paper.

Due to the fact that the 2D model represented a 3D structure each column in the frame actually represented three columns overlapping. This meant that once the lumped masses for each column were calculated the overlapping lumped masses were added together and entered into the SAP2000 model. Table 14 shows these combined lumped mass values that were used within the SAP2000 model at each level and column location.

Table 14: Lumped mass values distributed within the generic timber model.

	Lumped mass location	
	Outer frame (kN)	Inner frame (kN)
Foundation	8.40	16.8
Level 1	95.8	192
Level 2	95.8	192
Level 3	18.4	36.8

The columns were designed with cross-sectional dimensions of 300 mm by 300 mm while the beams were designed with dimensions of 240 mm by 240 mm. The material properties of radiata pine were used when defining the structural member material parameters. Figure 25 shows the completed model.

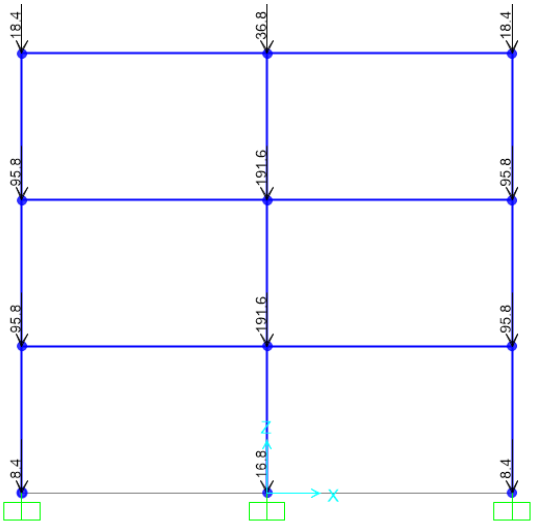

Figure 25: 2D model of the unmodified generic timber structure built within SAP2000. Lumped mass weights (kN) and locations are also shown.

3.12.2 Base Isolation Model

The unmodified timber structure model was taken and the ground floor joints were changed into base isolation joints. Because using base isolation joints only changed how the ground floor joints were constructed the rest of the model, including member dimensions and lumped masses, did not change between this model and the unmodified one.

The process of calculating the parameters of these joints followed the same process carried out for the pagoda model. Again, a coefficient of friction value of 0.4 and a maximum allowed sliding displacement of ±1.5 cm was used. An isotropic hysteresis curve was chosen to represent the friction sliding mechanism of the joint. The base isolation joints were model as non-linear springs where Equation 1 was used to calculate the yielding force of the joint. The vertical weight at each ground floor joint was easily calculated by simply combining the weights of all the lumped masses directly above each of these ground floor joints. Table 15 shows the vertical load at each base isolation joint as well as the horizontal sliding load. Each of these values actually represent three joints in parallel due to the model being 2D.

Table 15: Vertical weight and horizontal sliding load of the base isolation joints within the generic timber model.

Column type	Outer Column	Inner Column
W- weight (kN)	218	437
Q_s – sliding load (kN)	87.4	175

While the horizontal shear load within the joint is less than the calculated sliding load the joint will not displace horizontally. As soon as the sliding load value is exceeded the joint is able to displace horizontally up to the maximum of ±1.5 cm. Figure 26 shows the completed base isolation model with the base isolation joints highlighted.

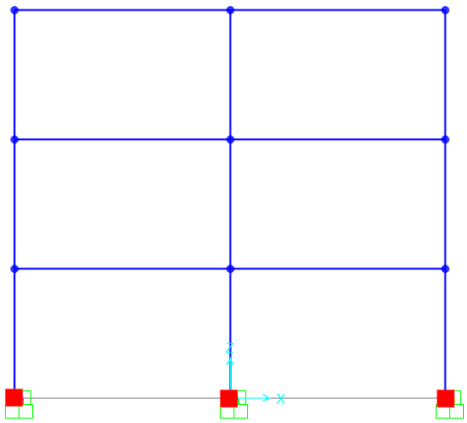

Figure 26: 2D model of the base isolation timber structure with the base isolation joints highlighted in red.

3.12.3 Sliding Friction Model

The sliding friction model is exactly the same as the unmodified structure model except that the joints connecting the top of the columns to the beams are replaced with sliding friction joints. These joints are modelled using a non-linear spring acting in the horizontal direction. Equation 1 is used to calculate the sliding load of the joints. The process used to calculate these joint parameters is the same as the one used to calculate the base isolation joints. Table 16 shows the relevant values for each column at each level. The coefficient of friction is 0.4 and the maximum allowed displacement due to sliding is ±1.5 cm.

Table 16: Vertical load and subsequent sliding load of each sliding friction joint within the model.

	Outer Columns		Inner Columns	
	W- Weight (kN)	Q_s – Sliding Load (kN)	W- Weight (kN)	Q_s – Sliding Load (kN)
Level 1	210	84.0	420	168
Level 2	114	45.7	228	91.4
Level 3	18.4	7.36	16.8	6.72

Figure 27 shows the completed sliding friction model with the sliding friction joints highlighted.

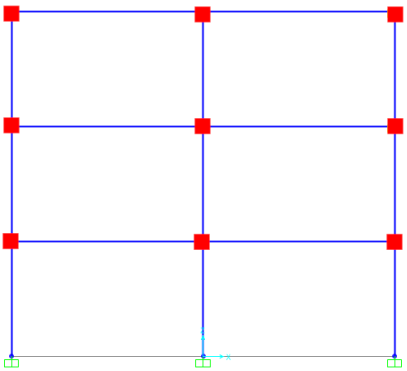

Figure 27: Sliding friction model with the sliding friction joints highlighted in red.

3.12.4 Rocking Column and Nuki Joint Model

For this model the rocking column joints and nuki joints where combined into a single connection and replaced the previous joints connecting the base of the columns to the beams. This occurred at every floor except the ground floor, this changing of joints mirrors the joint layout within Horyu-ji Pagoda.

In order to calculate rocking column rotational strength component, the same procedure that was used for the pagoda model was followed. Figure 14 in the above sections shows the theory behind the calculations. In this case *b*, the column width, is 300 mm while *h*, the column height, is 3 m. *W*, the vertical weight on the joint, is calculated by summing the lumped masses above each joint. This vertical weight value is then divided by 3 in order to get the vertical weight on each individual joint at that location. This is done because of the fact that the 2D model represents a 3D structure with three frames in parallel. Appendix D shows the full table of these calculated values for each of the joints.

In order to calculate the nuki joint strength component the MATLAB script shown in Appendix C was used again. This is the exact same process that was used for the pagoda model except now the young's modulus and yielding strength of radiata pine is used instead. Also, the dimensions of the beams are updated within the script to reflect the new beam dimensions used within the generic timber model. Because of the similar values in in the timber material properties and the beam dimensions between the generic timber model and the pagoda model the two nuki joint strength plots where almost identical. The pagoda model had a maximum nuki joint strength of 47.9 kNm while the generic timber model had a maximum strength of 46.0 kNm.

Once the rocking column joint and nuki joint strengths were calculated the two components were added together to find the final joint strength curves. The strength values were then multiplied by a factor of three in order to account for the fact that each joint within the 2D model represents three joints in parallel. Figure 28 shows the plot of these curves for each of the unique joints. These curves were entered directly into SAP2000. What can be seen is that the nuki joint component dominates the strength profile of the joint. The rocking column component has an initial stiffness which helps compensate for the fact that the nuki joint has no stiffness below a rotation of 0.02 radians. Both of these components together help give a joint with a linear initial stiffness and a clear yielding strength.

Both the level two and level three joints have the same yielding strength of roughly 145 kNm however the initial stiffness of the joints vary. The level two joints are roughly 50% stiffer than the same joints located at level three. The reason for this is that the total vertical weight acting on the level two joint is larger than the weight on the level three joint directly increasing the rocking column stiffness component.

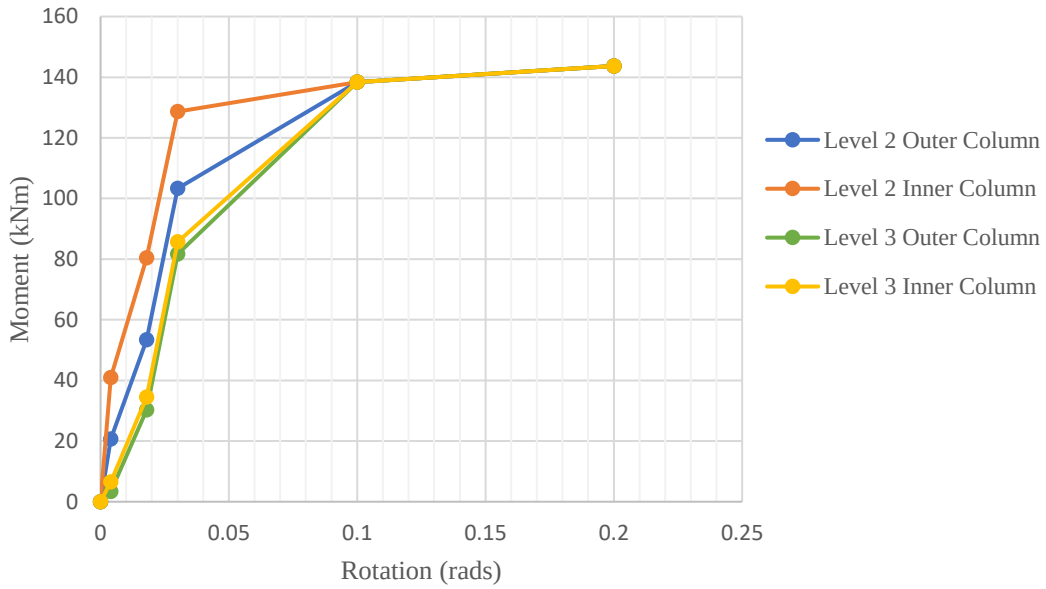

Figure 28: Rotational strength curves for the rocking column and nuki joints within the generic model.

Figure 29 shows the completed rocking column and nuki joints model with the unique joint locations highlighted.

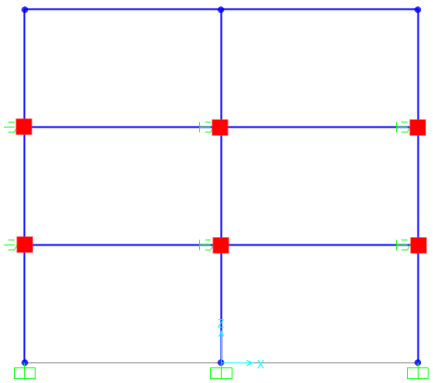

Figure 29: Rocking column and nuki joint model with the unique joints highlighted in red.

3.12.5 Combined Mechanisms Model

The combined mechanisms model takes the unmodified timber model and adds the base isolation joints, sliding friction joints and the rocking column and nuki joints all onto one structure. All three of the unique joint types added to the model only change the layout of the joints and do not affect the total mass or dimensions of the structure. Because of this fact the parameters of the unique joints are unchanged from the previous models. Figure 30 shows the combined mechanism model within SAP2000 with the different joint types highlighted.

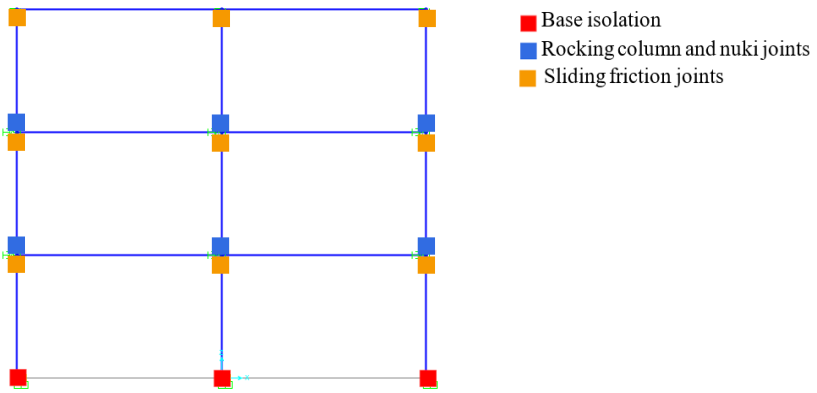

Figure 30: Combined mechanisms model with the unique joints highlighted.

3.12.6 Application of the Earthquake Time History Plots

Once the five separate generic timber models were constructed the three different earthquake time history accelerations were applied to each of these models. This gave a total of 15 unique tests. For each of the three earthquake time histories only the first ten seconds of the earthquake recording was applied to the structure. The reason for this is that the process of NLTH analysis is calculation intensive and so by cutting down the length of the applied acceleration the total analysis time would be reduced also. By the ten second mark the structures would have experienced upwards of ten complete cycles of loading and unloading, providing an ample amount of information with which to draw conclusions from. This ten second threshold was also chosen as it was a time period that ensured that the peak acceleration of the earthquake excitation had been experienced by the structure.

The key parameters that were extracted from the output data were the peak displacements, peak storey drifts, peak accelerations, average accelerations and the energy within the system.

When considering displacements of the storeys within the models the relative displacement was the focus. Relative displacement is the displacement of a joint in relation to the ground motion. This parameter is of importance as it would indicate if the structure is likely to collide with neighbouring buildings. The maximum relative displacement of a floor was calculated by taking the displacement of each floor and negating the displacement of the ground from it at each timestep. The maximum absolute value obtained from this list was then recorded. This was repeated for every floor. The peak relative displacement for a floor did not necessarily occur at the same time for every level within the model.

The peak storey drift was calculated in a similar manner. For each test run the relative displacement for a floor was compared to the relative displacement of the floor above it at each timestep. The maximum of the absolute values was then recorded as the peak storey drift between those two levels. This was then repeated for every level within the model. Again, the peak storey drift for a level did not necessarily occur at the same time as the peak value for another level.

When calculating the peak acceleration for a level the absolute acceleration was the focus. Absolute acceleration considers the acceleration experienced by the motion of the structure as well as the acceleration of the ground at that timestep. This parameter is of importance as it most accurately describes the intensity of the sensation of shaking at that location or level, it is what the occupants of the structure experiences. The peak acceleration of a level will only occur once during the earthquake event for a short duration of time. This value was calculated by taking the absolute acceleration of the

level at each timestep and recording the maximum value from the list as the peak acceleration. This was then repeated for each level within the model.

The average acceleration was also considered when looking at outputs from the analyses. The average acceleration represents a uniform function that would match the earthquake time history plots in terms of total excitation. It would give a fair estimation of the average experienced acceleration at each level of the model over the entire ten second event rather than just the peak acceleration which would usually only occur very briefly. This value would be more representative of the total potential damaging forces the structure will experience over the course of the earthquake event. Because the earthquake excitation is a wave function the root mean square (RMS) value of the acceleration will represent this average acceleration. Equation 17 shows the equation used.

$$RMS = \sqrt{\frac{1}{n}(\sum x^2)} \tag{17}$$

The average acceleration was calculated for every level within the model. Here *x* represents the level's acceleration at each timestep and *n* represents the total number of timesteps.

The final step in the NLTH analyses was the calculation of the energy and energy dissipation within the models. SAP2000 calculated these values internally when running NLTH analyses. This was done by calculating and combining three components within the system at each timestep. The first component is the inertial energy of the lumped masses, the second component is the kinetic energy of the structure as it sways and the last component is the potential energy stored within the structural members of the model as they bend and deform. There are five key energy parameters that were recorded, these are:

1. Total input energy: this is the total energy transferred into the structure over the course of the earthquake excitation.
2. Modal energy: this is the total energy dissipated by the system through the process of modal damping.
3. Maximum internal energy: this represents the maximum energy within the system at any one point during the earthquake event.
4. Link total energy: this represents the total energy dissipated through the action of the unique non-linear joints within the model.
5. Residual energy: this represents the total energy still present within the system at the end of the ten second excitation period.

3.12.7 Wind Loading

In theory the addition of the unique joints talked about above will decrease the effects of an earthquake on a structure. Another form of horizontal loading to consider is that of wind loads. These unique joints potentially decrease the rotational stiffness of connections and allow for horizontal sliding of joints. The consistent horizontal loading from wind may cause an increase in the displacements and drifts of storeys within the structure. This possibility was investigated through the process of running non-linear static analyses on the models with horizontal wind loads applied.

NZS 3604 was referenced to find a suitable wind load value. A wind speed of 44 m/s was chosen, this was considered a high wind speed. At sea level a 44m/s wind speed translates to 1162 Pa (The Engineering Toolbox 2011). Equation 18 shows the equation used to calculate the drag force of the timber model:

$$F_D = P \cdot C_D \cdot A \tag{18}$$

F_D represents the drag force and would be applied on the windward side of the structure and again on the leeward side. P represents the pressure due to wind speed, A represents the area of the side of the structure and C_D is the coefficient of drag, which is 1.05 for a cube (Daemei et al. 2019). Using Equation 18, it was found that the wind load was 110 kN. It was assumed that this wind load was evenly distributed over the windward face of the structure and again over the leeward face. The model was simplified by changing the horizontal wind loads to point loads where the value of the load was proportional to the area that that point load represented. These point loads where placed at column-beam joints at each level. Figure 31 shows the model with the wind load applied. This wind load value was consistent between the five unique models tested. The key output values recorded were the horizontal displacements and the storey drifts between each level.

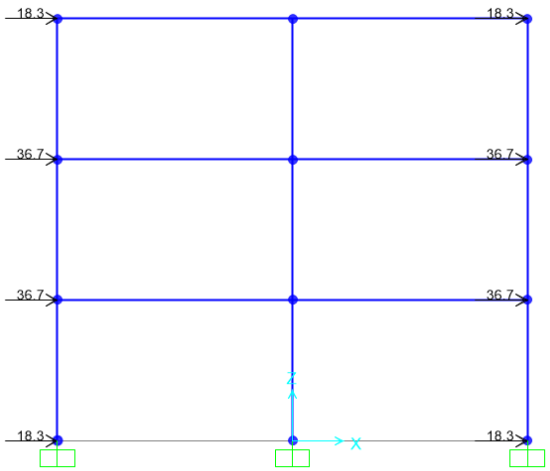

Figure 31: Generic timber model with the wind load applied. The wind load force values are shown in kN.

4. RESULTS AND ANALYSIS

This section looks at the data outputs gathered from the analyses. The modal analysis data and ESA loading data of the Horyu-ji model is presented. This data shows that the modelling of the unique non-linear joints is accurate.

The data gathered from the five variations of the generic timber model is also presented. The NLTH accelerations, displacements and internal energy values have been collated in order to compare the similarities and differences between different model types. The data gathered from the static pushover analysis with the wind load applied has also been investigated in this section. This data will highlight the strengths and weaknesses of each joint type and will also show the benefit of using all four unique joints simultaneously within a structure.

An interesting aspect of the analysis was the fact that the input energy was not consistent between the model types. The time history plots were applied as a horizontal acceleration at the foundation joints of the structures. This ground acceleration is translated into velocity and displacement of the structural members and masses within the structure. The more a structure is isolated from ground motion the lower the fraction of this ground motion transfers into the structure. The use of the unique non-linear joints increase the isolation of the structure, leading to lower accelerations, velocities and displacements within its members. The lowering of these parameters leads to a decrease in the total energy within the structure as a whole.

Another reason for this discrepancy between input energies of the models is the fact that the unique non-linear joints have a decreased stiffness compared to those within the unmodified model, especially at higher deformations. This lowering of joints stiffness leads to an increase in the modal periods of the model. The increase in modal periods causes the frequency ratio (β) to increase. The frequency ratio is the ratio between the excitation force frequency and the structure's frequency. Figure 32 shows the trends of the dynamic amplification factors in relation to a change in the frequency ratio (Paultre 2011). The dynamic amplification factors are unitless values that are a ratio between the excitation forces and the structures displacement, velocities or accelerations. As the frequency ratio increases above a value of one the amplitude of resonance within the system decreases. Because the modified models have a higher modal period they have less resonance within the structure, leading to lower values of internal kinetic and elastic potential energy.

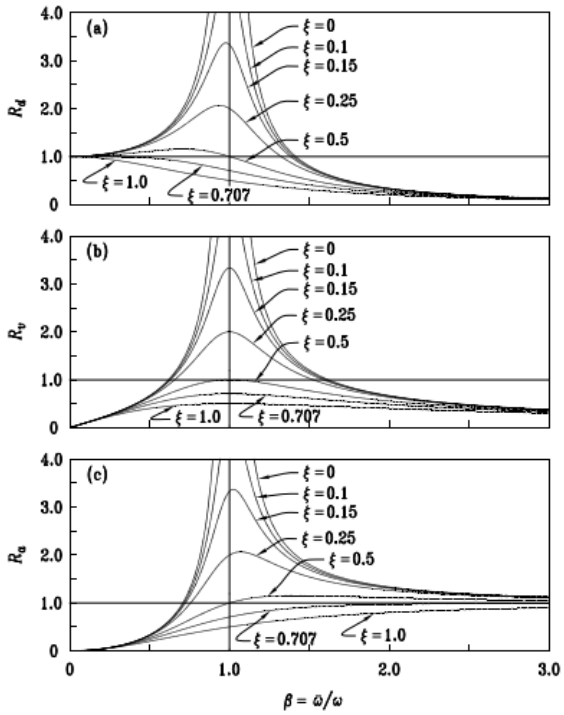

Figure 32: Dynamic amplification factors as a function of frequency ratio and damping ratio. (Reproduced from Paultre 2011).

4.1 Horyu-ji Pagoda

4.1.1 Modal Analysis

The modal analysis output data was obtained from SAP2000 and compared to the microtremor test modal periods. Table 17 compares the model outputs to the expected results. These microtremor modal periods were obtained through physical testing carried out on Horyu-ji Pagoda (Uchida et al. 1996).

Table 17: Model modal periods compared to modal periods of Horyu-ji Pagoda obtained through microtremor testing.

	Modal Periods		
	T_1 (s)	T_2 (s)	T_3 (s)
Microtremor Test	1.11	0.42	0.24
Model Output	1.14	0.46	0.22
Participating Mass Ratio	78%	20%	2%
Difference (%)	+2.7%	+9.5%	-8.3%

The results show that analysing the first three modes only are sufficient due to the combined participating mass ratios of the first three modes being greater than 99% of the total mass. The higher modes of the structure can be effectively ignored as their contribution to the model response is negligible. The first mode period of the model is 2.7% larger than the microtremor results. This difference is minor and so the models first mode period is in range of what was expected. The second and third mode periods are out by a larger amount. However, because the participating mass ratios of these modes are smaller the difference of these modal periods are not as crucial to the accuracy of the model. Overall, the modal analysis results indicate that the model's modal periods match the microtremor data. This indicates that the stiffness matrix and mass matrix of the model can be used to accurately represent Horyu-ji Pagoda during horizontal loading. The validation of this stiffness matrix also validates the unique non-linear joints within the model.

4.1.2 ESA Loading

The horizontal loads shown in Table 12 were applied to the pagoda model and a non-linear static pushover analysis was carried out. Table 18 shows that displacements and storey drifts at each level. The maximum storey drift was 2% and occurred at level four. When considering the ultimate limit state of the structure a storey drift of 2% is acceptable (Council of Standards New Zealand 2004). When looking at the member stresses within the model the largest value was found to be a compressive stress of 32 MPa. This occurred at level one within the main tie beam above the columns. This maximum stress is below the yielding strength of hinoki cypress indicating that collapse of the structure is not likely to occur for this magnitude of horizontal loading.

Table 18: Displacements and storey drifts due to the horizontal loading of the pagoda model during the ESA analysis.

	Displacement (cm)	Storey Drift (cm)	Storey Drift (%)
Level 1	4.14	4.14	1.2%
Level 2	8.26	3.25	1.6%
Level 3	13.7	3.49	1.9%
Level 4	19.0	3.35	2.0%
Level 5	23.1	2.04	1.4%

Based upon the output data of the ESA case the displacements, storey drifts and maximum stresses are all reasonable and expected values when considering the NZS 1170.5 earthquake design methodology. This outcome, along with the modal analysis outcome, validates the accuracy of the model and the unique non-linear joints. This means that when the unique joints are used within

SAP2000 on models of various layouts the output data can be used to accurately represent real structures.

4.2 Generic Timber Models Modal Analysis

Modal analysis was carried out on the five different models of the generic timber structure. This was done in order to verify that the models were operating as expected and that no major errors were made during the modelling of the structures. For example, a change of up to ±20% in the first mode period is expected, however a ±200% change would indicate an error. The first three modal periods for each model are shown in Table 19.

The unmodified model, base isolation model and sliding friction model all have the same first mode period. This is because the base isolation and sliding friction joints have the same initial joint stiffnesses as that of the unmodified model's joints. Modal analysis is based on a linear analysis method which cannot capture the non-linear properties of the unique joints accurately. This leads to the modal periods of these three models being identical. In reality, especially at larger joint deformations, it is expected that the base isolation and sliding friction model modal period values are higher than what is shown. The reason for this is that at higher deformations the stiffness of the joints decreases, leading to a modified stiffness matrix. As the structure stiffness decreases the modal periods will increase. This is not reflected in the analysis output data.

This observation is also true for both the rocking column and nuki joints model and the combined mechanisms model. The modal periods of these models are expected to increase with an increase in joint deformation. This is again due to the joints yielding in a non-linear fashion. The reason for these two models having modal periods differing from the unmodified model is due to the unique joints having different initial stiffnesses compared to those of the unmodified model's joints. The combined mechanisms model has multiple different types of unique non-linear joints present, with all of these joints interacting. This interaction leads to an overall increase in the initial stiffness matrix of the structure. This is reflected in the model having a lower first modal period compared to the unmodified model.

Table 19: Modal periods of the generic timber models.

Model Type	Modal Periods		
	T_1 (s)	T_2 (s)	T_3 (s)
Unmodified	0.86	0.24	0.15
Base Isolation	0.86	0.24	0.15
Sliding Friction	0.86	0.24	0.15
Rocking Column and Nuki Joints	1.00	0.34	0.31
Combined Mechanisms	0.79	0.24	0.15

The accuracy of the modal period values is important as these values are directly tied into the NLTH analysis process. The first, second and third mode periods of the models are within range of what was expected with a maximum change of 16% seen in the first mode period values. The validation of this data allows the NLTH analyses to take place with the knowledge that the input data is correct.

4.3 Array 6 Earthquake Time History

4.3.1 Acceleration

The Array 6 time history was applied as a horizontal acceleration to the foundation joints of the different models. Figure 33 shows the peak horizontal acceleration at each level plotted against the height of the level for each of the models.

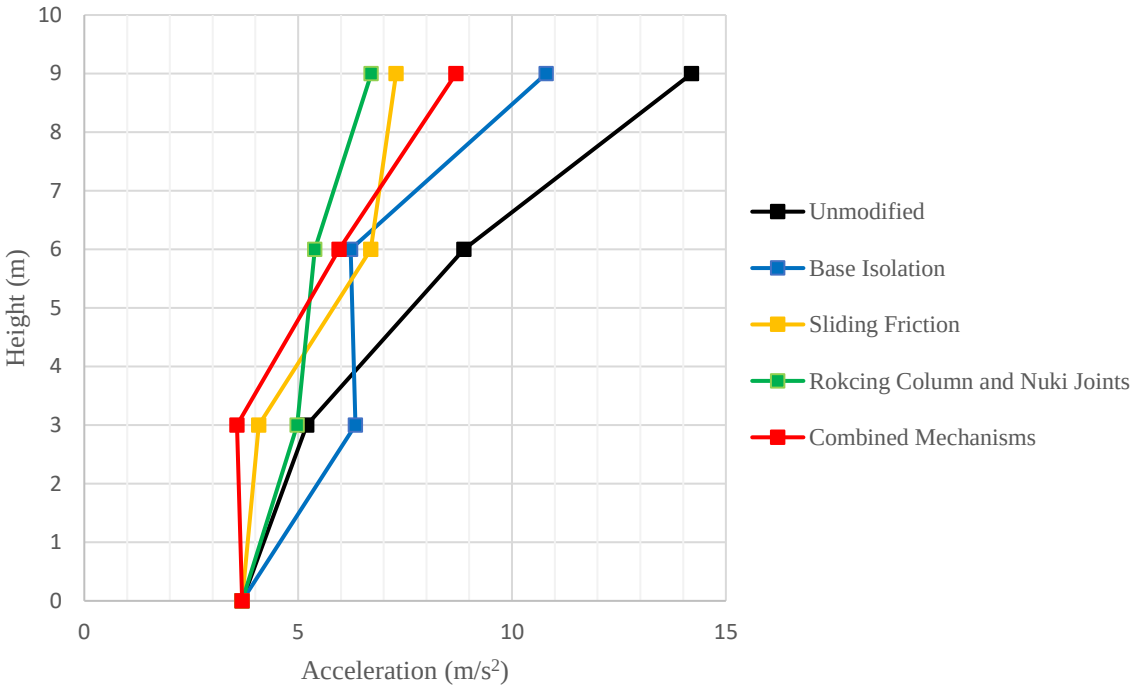

Figure 33: Peak acceleration at each level of the model caused by the Array 6 time history.

When looking at the data, the largest acceleration occurred at the ceiling of level three for all of the models. In order to evaluate the effectiveness of the unique joints the reduction in peak acceleration was investigated at this location. Table 20 shows the percentage decrease in peak acceleration at roof level of each of the model types compared to the unmodified model.

Table 20: Percentage differences of the peak acceleration at roof level of the different model types compared to the unmodified model during the Array 6 time history analysis.

Model	Base Isolation	Sliding Friction	Rocking Column and Nuki Joints	Combined Mechanisms
Difference	-23.9%	-48.7%	-52.7%	-38.8%

All four of the models containing unique joints had a decrease in peak acceleration. The sliding friction model and the rocking column and nuki joints model performed the best, decreasing the largest peak acceleration within the structure by roughly 50%.

The one outlier was the base isolation model which had an increase in peak acceleration at level one compared to the unmodified model. This may be because of the fact that the earthquake excitation is a complex wave function and leads to minor resonance within the structure. The peak acceleration only

occurs once, and for a short duration, during the earthquake event and is due to this minor resonance. Changing the parameters of the structure has caused this resonance to peak at a higher value for this specific earthquake time history at level one of the base isolation model. The largest benefit of the unique joints is demonstrated at the higher levels of the structure where there is a consistent decrease in peak acceleration.

Figure 34 shows the RMS of the horizontal acceleration at each level versus height for each of the five model variations. What can be seen is that all four of the modified models have had a significant decrease in the average acceleration at all levels compared to the unmodified model.

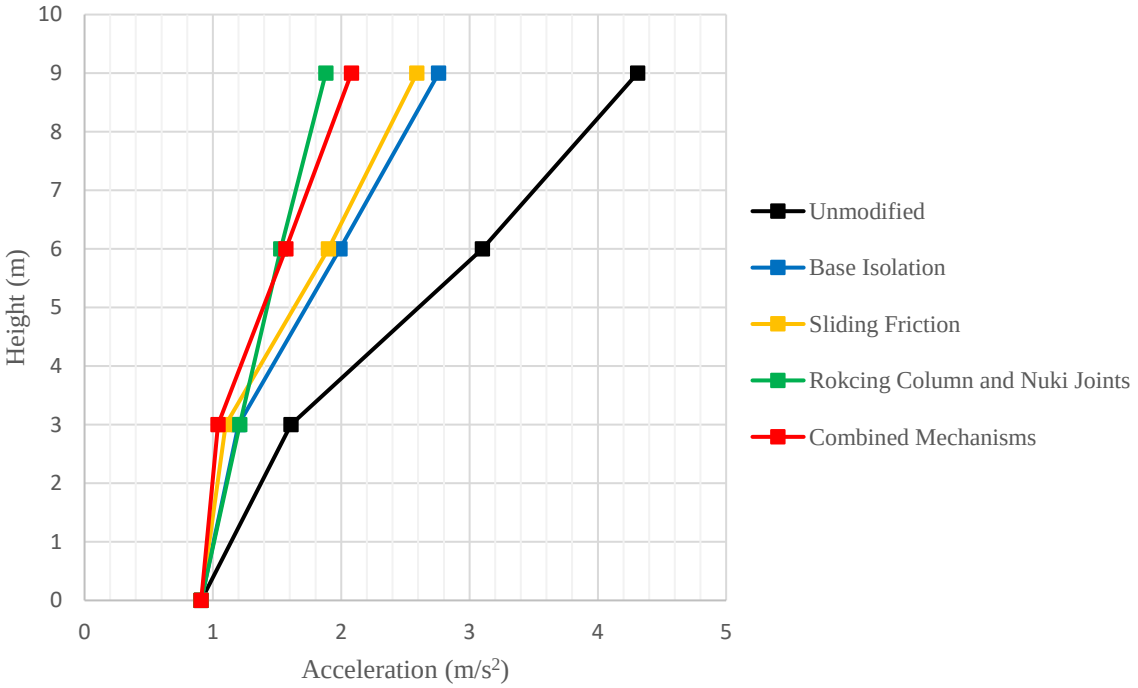

Figure 34: Average acceleration at each level of the model caused by the Array 6 time history.

Table 21 shows the percentage decrease in average acceleration at roof level for the four modified models. The combined mechanisms model and the rocking column and nuki joints model performed the best with a decrease of over 50%.

Table 21: Percentage differences of the average acceleration at roof level of the different model types compared to the unmodified model during the Array 6 time history analysis.

Model	Base Isolation	Sliding Friction	Rocking Column and Nuki Joints	Combined Mechanisms
Difference	-36.0%	-39.9%	-56.4%	-51.7%

The percentage decreases for each model is different between the peak and average acceleration. There is more variation in the values and trends of the peak acceleration graph due to the fact the peak acceleration is a single datapoint that occurs once during the analysis. The average acceleration takes into consideration every single datapoint throughout the earthquake loading and so removes the effects of larger or smaller outliers within the data. The average acceleration more clearly shows the effect of each unique joint.

4.3.2 Displacement

Figure 35 shows the largest horizontal displacements at each level for the five different models during the Array 6 earthquake excitation. All four modified models had a decrease in displacement compared to the unmodified model. The percentage decrease for each model is shown in Table 22. This decrease is specifically for the displacements at the roof level and is chosen as this is the site of the largest displacements within all five of the models.

The base isolation model had a displacement at the ground floor due to the horizontal sliding of the base isolation joints. The combined mechanisms model also had these base isolation joints present however they did not move horizontally as the required sliding force of the joints was never exceeded during the loading.

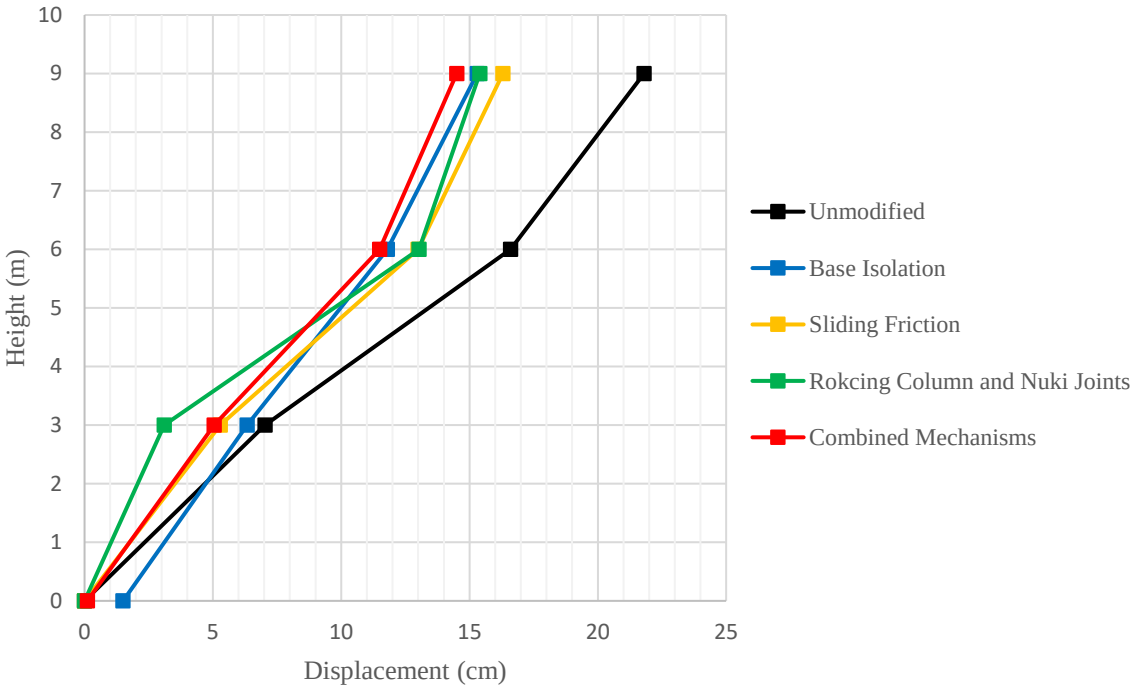

Figure 35: The displacement at each level of the model caused by the Array 6 time history.

Table 22: Percentage differences of the displacement at roof level of the different model types compared to the unmodified model during the Array 6 time history analysis.

Model	Base Isolation	Sliding Friction	Rocking Column and Nuki Joints	Combined Mechanisms
Difference	-29.8%	-25.2%	-29.4%	-33.5%

Figure 36 shows the maximum storey drift at each level for the five models. This maximum storey drift is the largest storey drift at any point during the earthquake loading and is independent of the storey drifts of the other levels. What can be seen is that the largest storey drift occurs at level two within all of the models. Because of this fact the reduction in storey drift of the modified models is calculated for level two and is shown in Table 23.

In general, all of the modified models have a decrease in the largest storey drift. The exception to this is the rocking column and nuki joints model where the level two storey drift is larger than the unmodified model storey drift. The reason for this is that the rocking column and nuki joints have a lower joint stiffness than the same joints in the other models. When sideways swaying of the structure occurs the lumped masses within the model have inertia, the inertias being similar between models. As the structure deforms this kinetic energy is transformed into elastic potential energy. The lowering

of the joint stiffnesses within this model leads to an increased horizontal deflection as this conversion of energy occurs. The reason that the largest storey drift occurs at level two for the rocking column and nuki joints model is because this level has a large mass, and therefore large kinetic energies, while at the same time having a low horizontal joint stiffness. This leads to the creation of a soft storey. If more levels were to be added to the structure the expectation would be that every middle level (i.e. every level other than the first and the last) of the rocking column and nuki joint model would have a larger storey drift than the unmodified model.

The base isolation model and the combined mechanisms model performed the best in reducing the largest storey drift within the structure with a decrease of roughly 30-35%. All of the modified models, excluding the rocking column and nuki joints model, had a decrease in storey drift at every level within the structure.

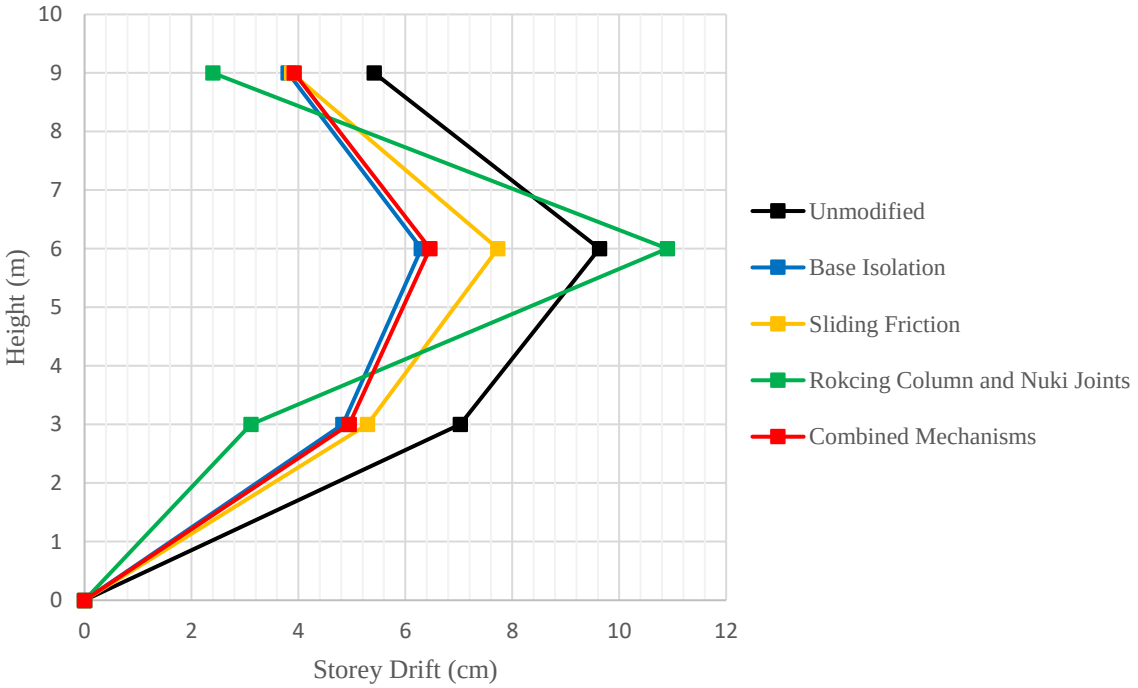

Figure 36: Storey drift between each level of the model caused by the Array 6 time history.

Table 23: Percentage differences of the storey drift at the second level of the different model types compared to the unmodified model during the Array 6 time history analysis.

Model	Base Isolation	Sliding Friction	Rocking Column and Nuki Joints	Combined Mechanisms
Difference	-34.6%	-19.7%	+13.2%	-32.9%

4.3.3 Energy Dissipation

Figure 37 shows the input energy and energy dissipation within the five models during the Array 6 time history analysis. The input energy is the total energy entering the superstructure over the ten second analysis. The modal energy is the total energy dissipated through means of modal damping. The maximum internal energy is the largest internal energy value at any one timestep during the analysis, this considers both the kinetic energy and elastic potential energy within the structure. The link total energy represents the total energy dissipated through the unique non-linear joints added into the structure. The residual energy is the total energy remaining within the superstructure at the end of the ten second duration of the analysis. The input energy is the sum of the modal, link total and the residual energies.

The unmodified model relies solely on modal damping in order to dissipate energy while the modified models dissipate energy through both modal damping and deformation of the unique non-linear joints. It can be seen that the modified models dissipate a larger proportion of the internal energy through the unique joints than through modal damping. This proportion becomes the largest within the combined mechanisms model since there are more unique joints, and therefore more points for the energy to dissipate.

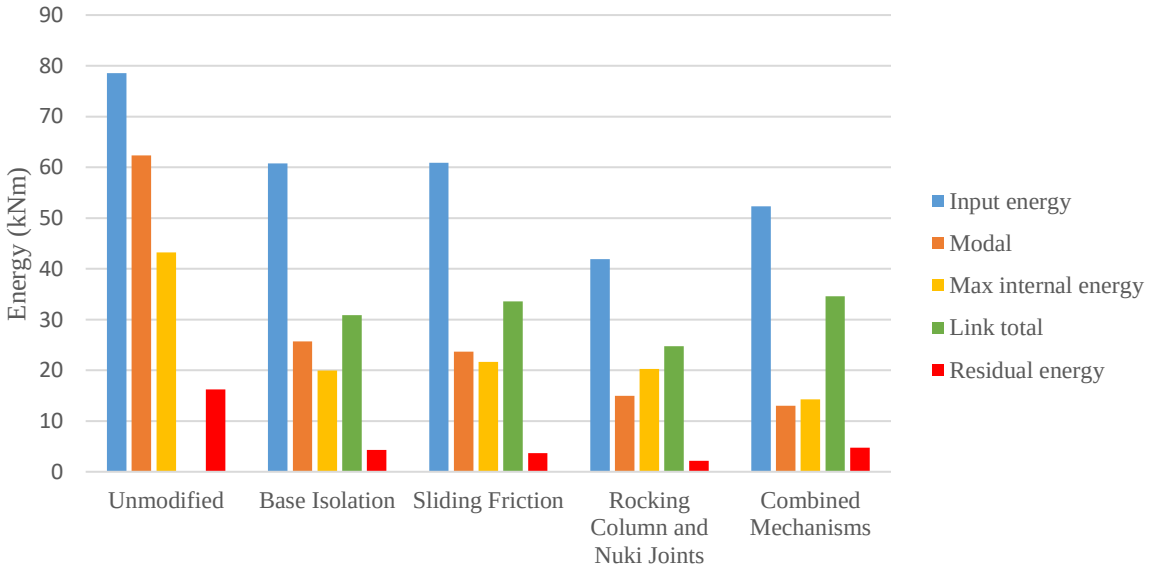

Figure 37: The energy dissipation within each model during the Array 6 time history excitation.

Table 24 shows the percentage decrease in internal energies between the modified models and the unmodified one. What can be seen is that there is a decrease in the maximum internal energy for all of

the modified models. The maximum internal energy is a measure of the velocities and deformations of the structural members and a decrease in internal energy indicates a decrease in these parameters. This is reflected in Figure 33 and Figure 35 where the peak acceleration and displacements of the modified models have decreased compared to the unmodified one. The combined mechanisms model performed the best with a 79% decrease in the maximum internal energy with the rocking column and nuki joints model close behind with a 75% decrease. This indicates that these models will have the least risk of structural damage during the Array 6 earthquake excitation.

In terms of a residual energy decrease the rocking column and nuki joints model performed the best with a decrease of 87%. This indicates that a higher proportion of the total input energy was dissipated over the ten second excitation period compared to the unmodified model. This also implies that once the earthquake event has passed the rocking column and nuki joints model will cease to sway and become stationary sooner than the other models. Regardless of the fact that the rocking column and nuki joints model had the largest decrease, all of the modified models had a decrease in residual energy in excess of 70%.

Table 24: Percentage differences of the energy dissipation within the difference model types compared to the unmodified model during the Array 6 time history analysis.

	Base Isolation	Sliding Friction	Rocking Column and Nuki Joints	Combined Mechanisms
Input Energy Difference	-22.6%	-22.5%	-46.7%	-33.4%
Max Internal Energy Difference	-53.8%	-62.1%	-75.9%	-79.1%
Residual Energy Difference	-73.6%	-77.3%	-86.8%	-70.8%

As discussed earlier, the modified models had lower input energy values compared to the unmodified model. This implies that the amount of the earthquake's energy entering the superstructure is less for the modified models. This is due, in part, to the unique non-linear joints having lower stiffness values at higher deformations compared to the linear joints found within the unmodified model. This change in stiffness causes the modal frequency of the structure to decrease and the frequency ratio (β) of the system to increase. For example, the rocking column and nuki joint model had the largest modal period and therefore it had the lowest total input energy out of the five models.

4.4 Newhall Earthquake Time History

4.4.1 Acceleration

The Newhall earthquake time history has a PGA of 0.59 G, roughly 50% larger than the previous Array 6 time history. The output data reflects this with the accelerations, displacements and energy inputs increasing between analyses. Figure 38 shows the peak horizontal accelerations at each level for the five different models.

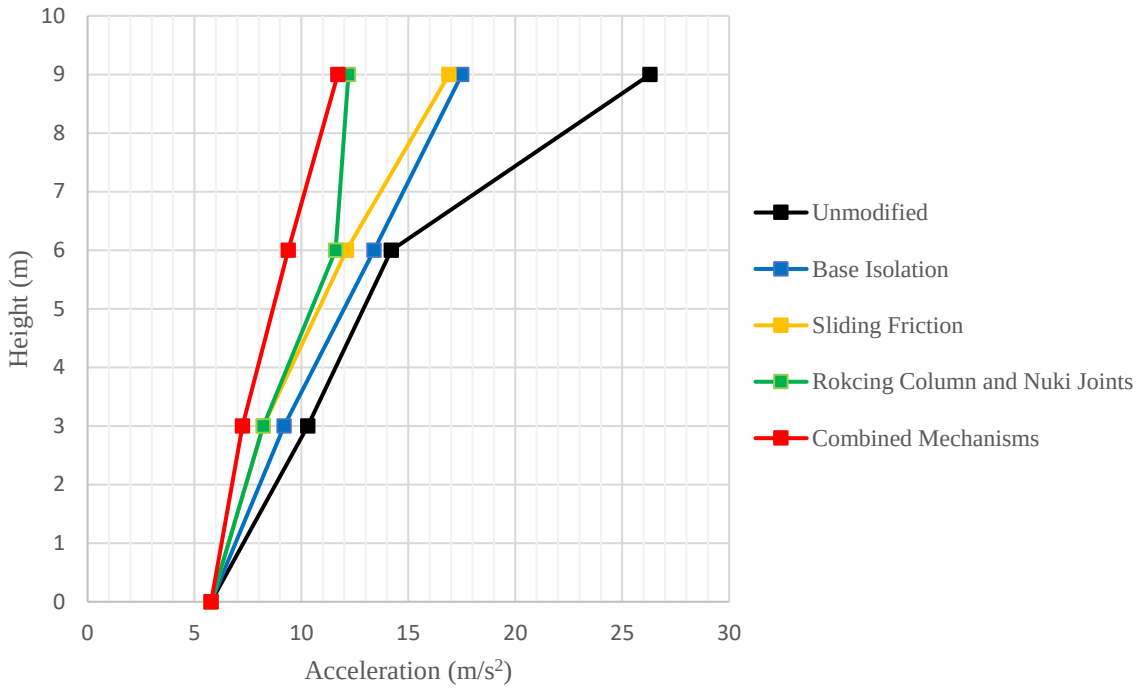

Figure 38: The peak acceleration at each level of the model caused by the Newhall time history.

The largest accelerations again occurred at the roof level of the structure. All four of the modified structures had a decrease in the peak acceleration compared to the unmodified model. These percentage decreases at roof level are shown in Table 25. The combined mechanisms model performed the best with a decrease of 56%, the rocking column and nuki joints model had a similar decrease with 54%.

The combined mechanisms model performed better during the Newhall earthquake compared to the Array 6 earthquake with the peak acceleration decrease changing from 39% to 56% between the earthquake analyses. The sliding friction model performed worse which a peak acceleration decrease

changing from 49% to 36% between analyses. These changes can be explained by the nature of the peak acceleration value. The peak acceleration value is a single datapoint in the output data an is sensitive to any initial input and system parameter changes.

Another key difference between this figure and the one for Array 6 is the fact that all levels within all of the modified models have a lower peak acceleration than those within the unmodified model. Previously the peak acceleration at level one of the base isolation model was greater than the peak acceleration of level one within the unmodified model, this is not the case for the Newhall analysis. This could be due to the variability of the peak acceleration explained above or it could be due to the possibility that the base isolation model performs better with the intensity of the earthquake increasing.

Table 25: Percentage differences of the peak acceleration at roof level of the different model types compared to the unmodified model during the Newhall time history analysis.

Model	Base Isolation	Sliding Friction	Rocking Column and Nuki Joints	Combined Mechanisms
Difference	-33.5%	-35.7%	-53.6%	-55.5%

Figure 39 shows the RMS average horizontal acceleration at each level for the five models. The trends in this graph are very similar to those seen in Figure 34, which shows the Array 6 RMS accelerations. Again, all of the modified models have a decrease in the average acceleration at all levels of the structure.

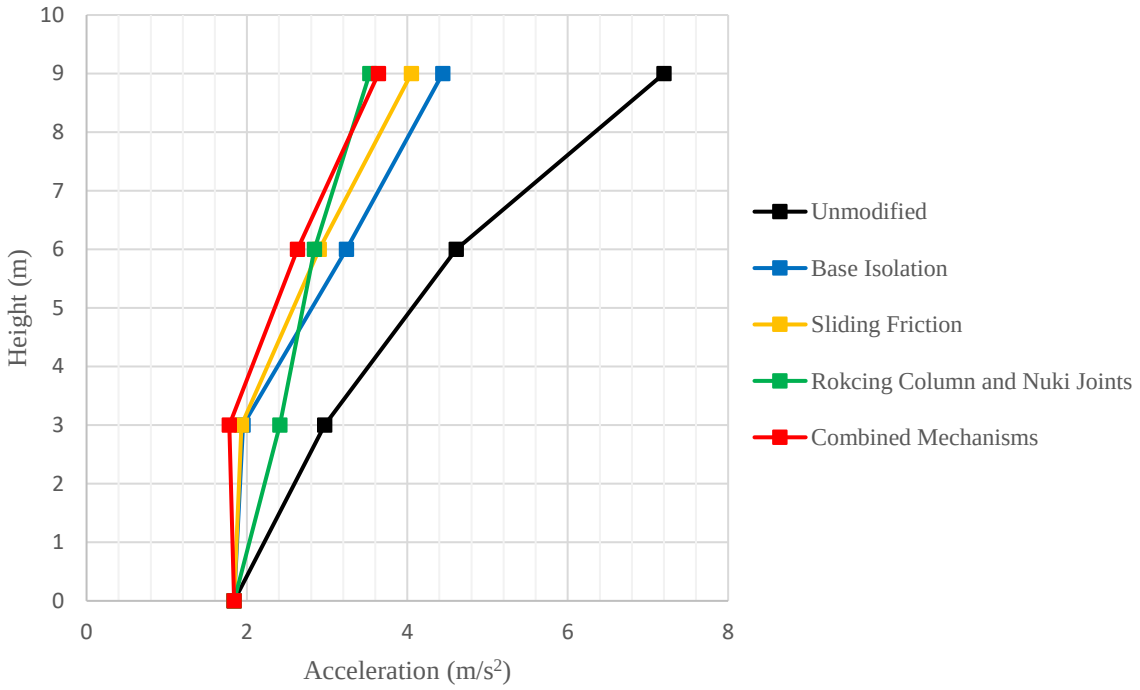

Figure 39: The average acceleration at each level of the model caused by the Newhall time history.

Table 26 shows the percentage decrease in the RMS acceleration values at roof level for the modified models compared to the unmodified one. These values are very similar between the Array 6 and Newhall analyses with the values only changing between 2-5% for each of the models. Again, the rocking column and nuki joints model and the combined mechanisms model performed the best with both the models decreasing the average acceleration by roughly 50%. The base isolation model and sliding friction model also performed well with both having roughly a 40% decrease.

Table 26: Percentage differences of the average acceleration at roof level of the different model types compared to the unmodified model during the Newhall time history analysis.

Model	Base Isolation	Sliding Friction	Rocking Column and Nuki Joints	Combined Mechanisms
Difference	-38.3%	-43.8%	-51.0%	-49.4%

4.4.2 Displacement

Figure 40 shows the peak horizontal displacement at each level for the five models during the Newhall time history analysis. The modified models all had a decrease in the largest displacement compared to the unmodified model but when compared to the Array 6 data the decrease was not as substantial. Table 27 shows the percentage decrease in horizontal displacement for the modified models. The combined mechanisms model performed the best with a 28% decrease at roof level compared to the unmodified model. This value was 34% during the previous Array 6 earthquake analysis. The other three modified models only had a 14-15% decrease which is far less than the 25-30% decrease experienced in the Array 6 analysis.

This data would imply that, when considering horizontal displacement, as the intensity of an earthquake increases the benefits gained from using the unique non-linear joints decreases. This may be due to the fact that the unique non-linear joints have a maximum amount of energy that they are able to dissipate per cycle of loading and unloading. As the intensity of the earthquake increases this limit is reached and the expected decrease in displacement is not met. This can be seen in Figure 40 where there is a decrease in the displacement, but not to the same level which was experienced in the weaker Array 6 earthquake analysis. The reason for the combined mechanism model performing at a similar level between analyses is due to the model's energy dissipation capacity being larger. This model has a higher capacity compared to the other modified models simply due to the presence of a larger number of unique non-linear joints.

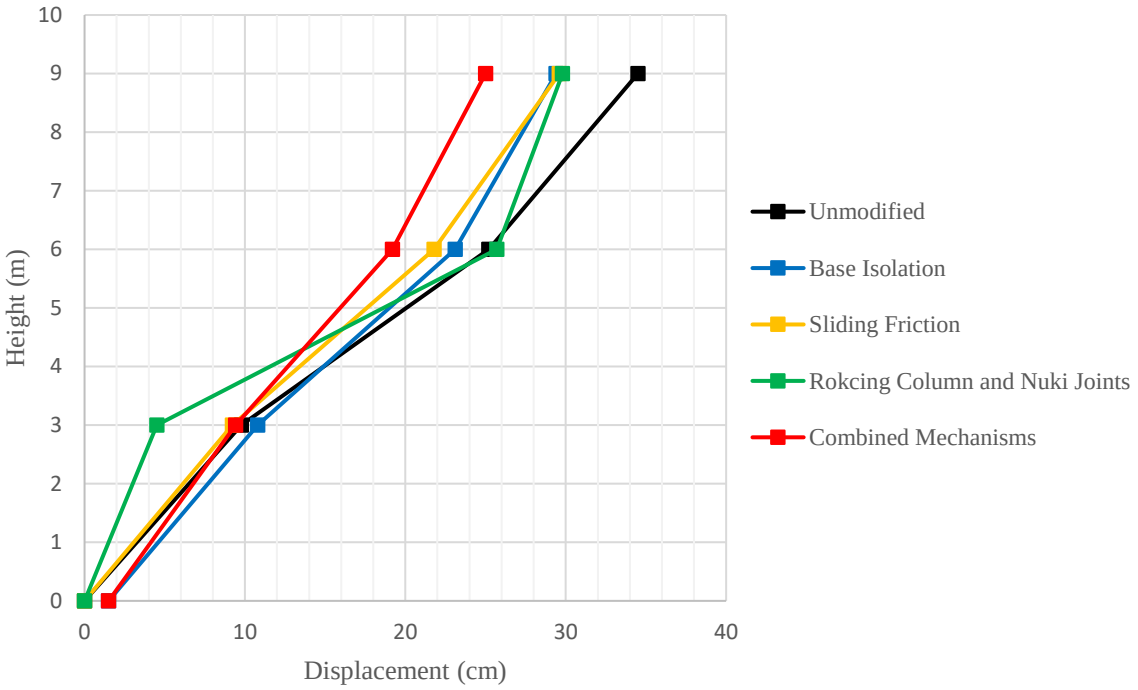

Figure 40: The displacement at each level of the model caused by the Newhall time history.

Both the base isolation model and the combined mechanisms model had horizontal displacements at the ground floor joints. This is in contrast to the Array 6 earthquake analysis where only the base isolation model had displacement at the ground floor. The reason for this is that the intensity of the Newhall time history was large enough to generate the horizontal forces required to engage the base isolation joints within the combined mechanisms model.

Table 27: percentage differences of the displacement at roof level of the different model types compared to the unmodified model during the Newhall time history analysis.

Model	Base Isolation	Sliding Friction	Rocking Column and Nuki Joints	Combined Mechanisms
Difference	-14.8%	-14.2%	-13.6%	-27.5%

Figure 41 shows the storey drifts of each level within the models during the Newhall analysis. Again, the largest storey drift occurred at level two of the structure. The base isolation, sliding friction and combined mechanisms models all had a decrease in the storey drifts at every level compared to the unmodified model. The rocking column and nuki joints model had a large increase in the storey drift at level two.

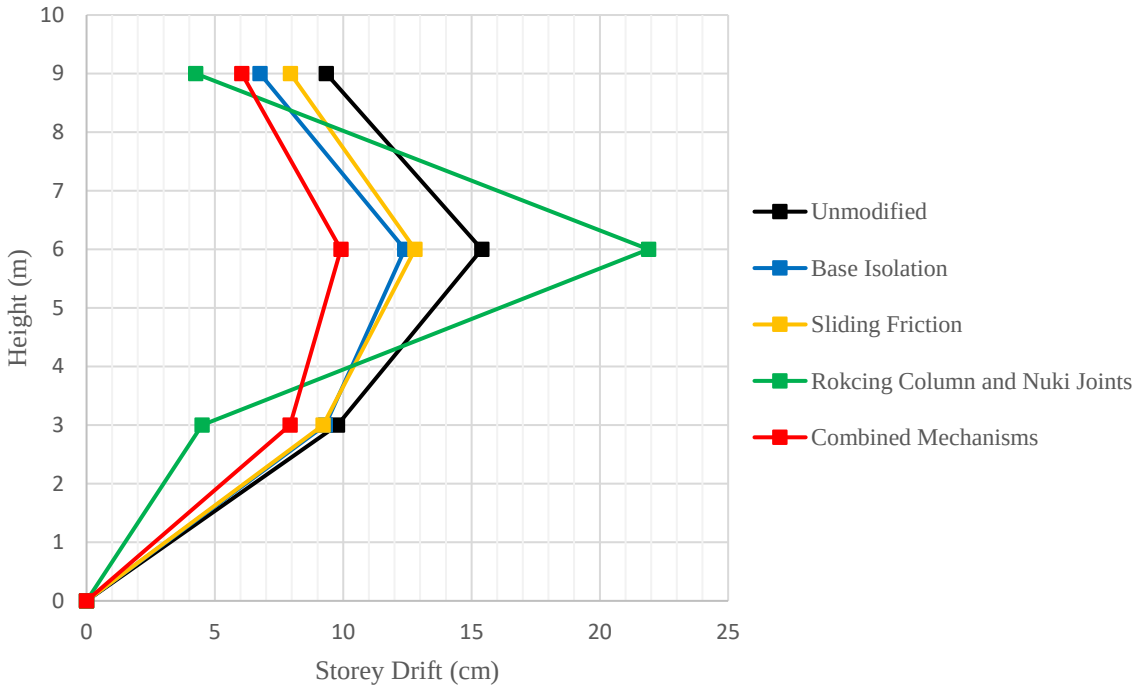

Figure 41: The storey drift between each level of the model caused by the Newhall time history.

Table 28 shows the percentage changes of the storey drift at level two for each of the models. The combined mechanisms model performed the best with a 36% decrease, very similar to the results of the Array 6 analysis. The rocking column and nuki joints model performed the worst with a 42% increase in the largest storey drift, this is a vast increase compared to the 13% observed in the Array 6 analysis. This trend implies that the effects of a soft storey within the model is enlarged by an increase in earthquake intensity.

Table 28: Percentage differences of the storey drift at the second level of the different model types compared to the unmodified model during the Newhall time history analysis.

Model	Base Isolation	Sliding Friction	Rocking Column and Nuki Joints	Combined Mechanisms
Difference	-19.5%	-16.9%	+42.2%	-35.6%

4.4.3 Energy Dissipation

Figure 42 below compares the energy input and dissipation between the different models for the Newhall time history excitation. Looking at the chart, all of the modified models had a decrease in maximum internal energy and residual energy compared to the unmodified model. This trend matches the one seen in the Array 6 analysis data. The percentage decreases of these values are shown in Table 29.

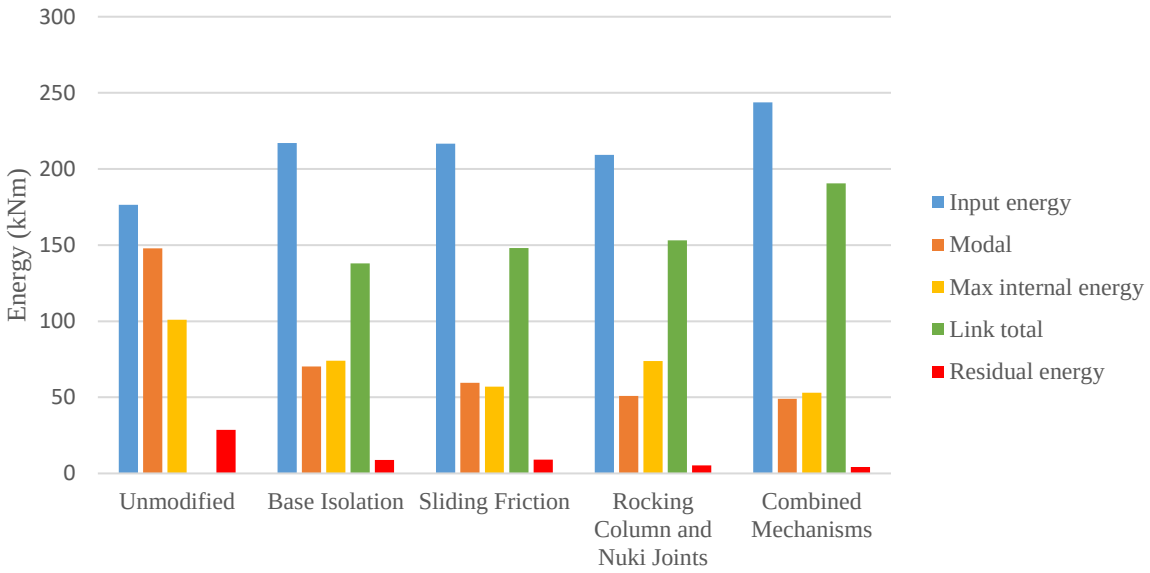

Figure 42: The energy dissipation within each model during the Newhall time history excitation.

Looking at the maximum internal energy data the combined mechanisms model performed the best with a 47% decrease compared to the unmodified model. This decrease is far less than the 79% decrease seen in the Array 6 analysis. In fact, all of the modified models had a reduction in the decrease of the max internal energy between analyses. This trend highlights the fact that the model unique joints have an energy dissipation capacity and as the intensity of the earthquake increases the likelihood that this cap is reached increases.

When looking at the residual energy data the reduction provided by the modified models is similar between the Array 6 analysis and the Newhall analysis. All of the modified models had a significant decrease in the residual energy. The combined mechanisms model performed the best with an 85% decrease, followed closely by the rocking column and nuki joints model with a decrease of 82%. This data implies that during the peak of the earthquake loading the proportion of total energy that the unique joints are able to dissipate is less for the Newhall time history excitation. However, once the peak loading has passed the unique joints are still able to dissipate energy as efficiently as before.

Table 29: Percentage differences of the energy dissipation within the difference model types compared to the unmodified model during the Newhall time history analysis.

	Base Isolation	Sliding Friction	Rocking Column and Nuki Joints	Combined Mechanisms
Input Energy Difference	+22.9%	+22.7%	+18.6%	+38.1%
Max Internal Energy Difference	-26.6%	-43.5%	-26.9%	-47.4%
Residual Energy Difference	-69.4%	-68.0%	-81.9%	-85.0%

4.5 Hollister Earthquake Time History

4.5.1 Acceleration

The Hollister time history intensity is very similar to the first Array 6 time history plot. The results are expected to reflect this with the trends matching between the two datasets. Figure 43 shows the peak acceleration at each level for the five different models. The largest peak acceleration occurred at roof level for each model. The percentage decrease in this acceleration is shown in Table 30.

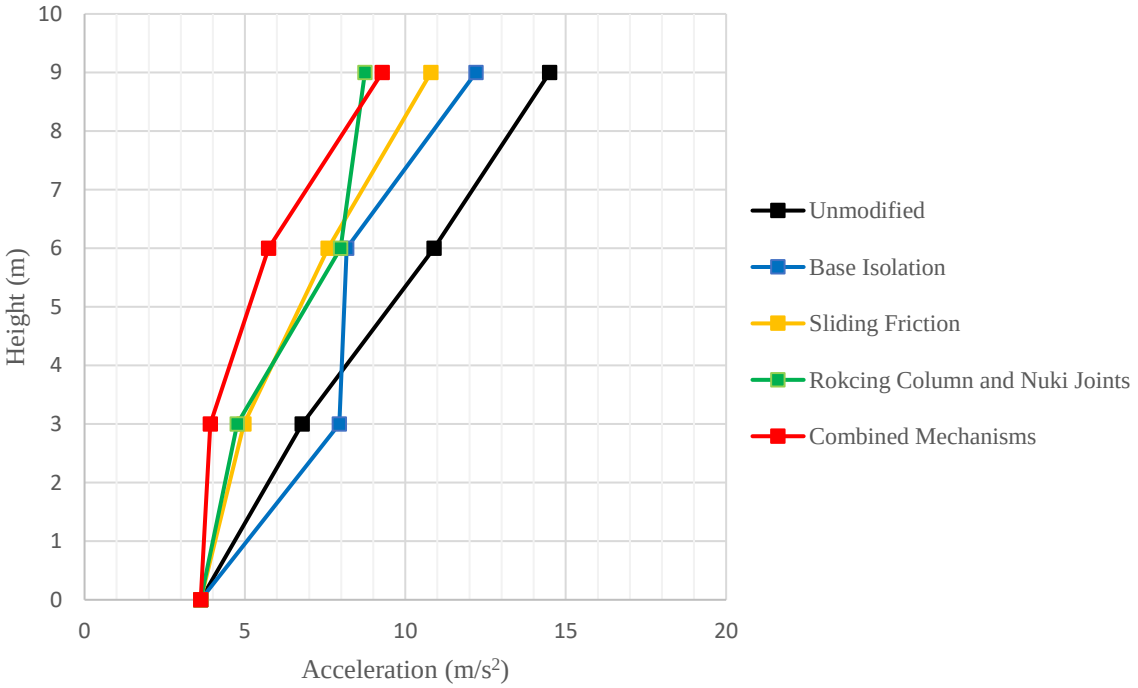

Figure 43: The peak acceleration at each level of the model caused by the Hollister time history.

The rocking column and nuki joints model performed the best with a 40% decrease in peak acceleration at roof level. The combined mechanisms model performed at a similar level with a 36% decrease over the unmodified model. This data is similar to the Array 6 data.

Table 30: Percentage differences of the peak acceleration at roof level of the different model types compared to the unmodified model during the Hollister time history analysis.

Model	Base Isolation	Sliding Friction	Rocking Column and Nuki Joints	Combined Mechanisms
Difference	-15.9%	-25.5%	-39.7%	-36.0%

Figure 44 shows the RMS average horizontal acceleration data for the Hollister analysis. Table 31 shows the percentage decrease of these values at roof level for the modified models. The rocking column and nuki joints model and the combined mechanisms model performed the best, both with a 48% decrease compared to the unmodified model's average acceleration. The base isolation and sliding friction models both performed well too, with a roughly 35-40% decrease. This outcome is very similar to those seen in the previous two analyses.

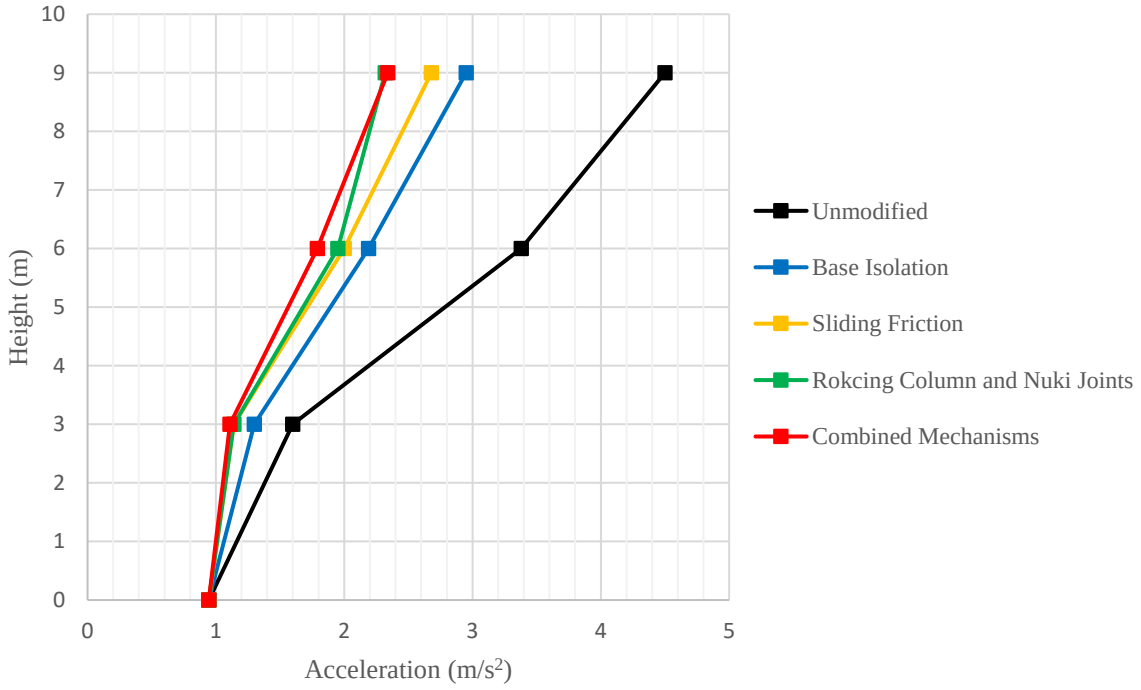

Figure 44: The average acceleration at each level of the model caused by the Hollister time history.

Table 31: Percentage differences of the average acceleration at roof level of the different model types compared to the unmodified model during the Hollister time history analysis.

Model	Base Isolation	Sliding Friction	Rocking Column and Nuki Joints	Combined Mechanisms
Difference	-34.4%	-40.4%	-48.4%	-48.0%

4.5.2 Displacement

Figure 45 shows the relative displacement of each level within the five models during the Hollister time history analysis. Again, all of the modified models had a decrease in the horizontal displacements at all levels. Table 32 shows the percentage decrease of this displacement at roof level compared to the unmodified model.

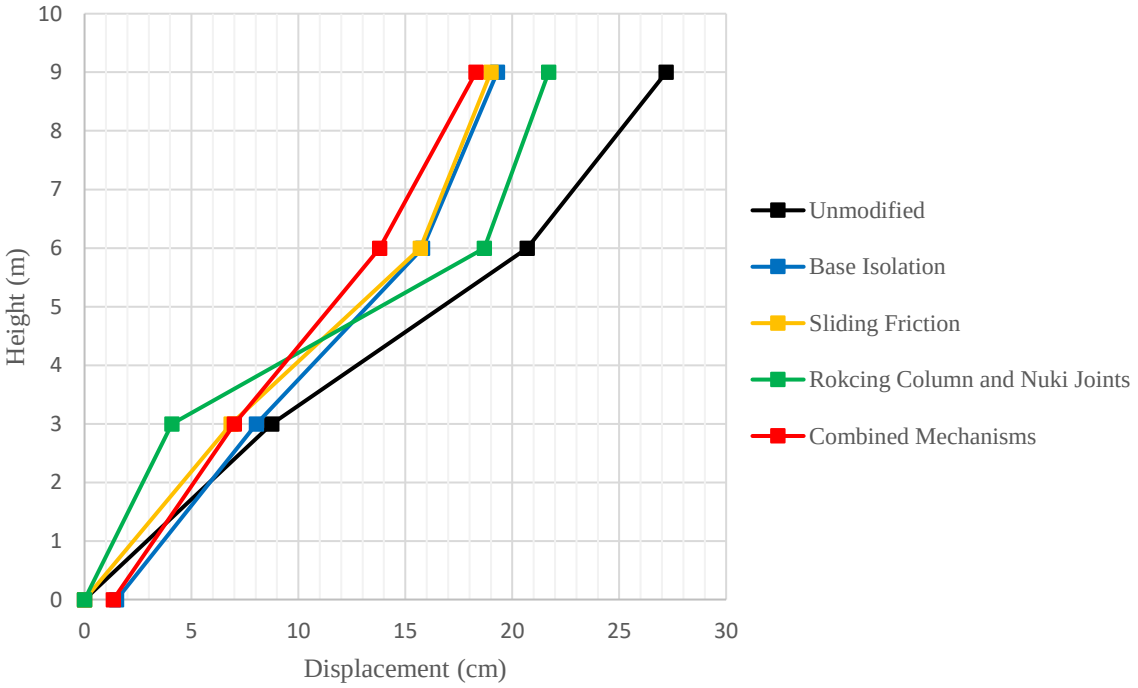

Figure 45: The displacement at each level of the model caused by the Hollister time history.

The base isolation, sliding friction and combined mechanisms models all performed at a similar level with a decrease of roughly 30% at roof level. This outcome is very similar to what is seen in the Array 6 analysis.

Table 32: Percentage differences of the displacement at roof level of the different model types compared to the unmodified model during the Hollister time history analysis.

Model	Base Isolation	Sliding Friction	Rocking Column and Nuki Joints	Combined Mechanisms
Difference	-29.0%	-30.1%	-20.2%	-32.7%

Figure 46 shows the storey drift of each model. This graph follows the trends of the previous two analyses. Again, the largest storey drift occurred at level two of the structure. At level two the rocking column and nuki joints model had an increase in storey drift compared to the unmodified model. The other three modified models all had a decrease in storey drift at every level. Table 33 shows the percentage decrease of these values at level two for the modified models when compared to the unmodified one.

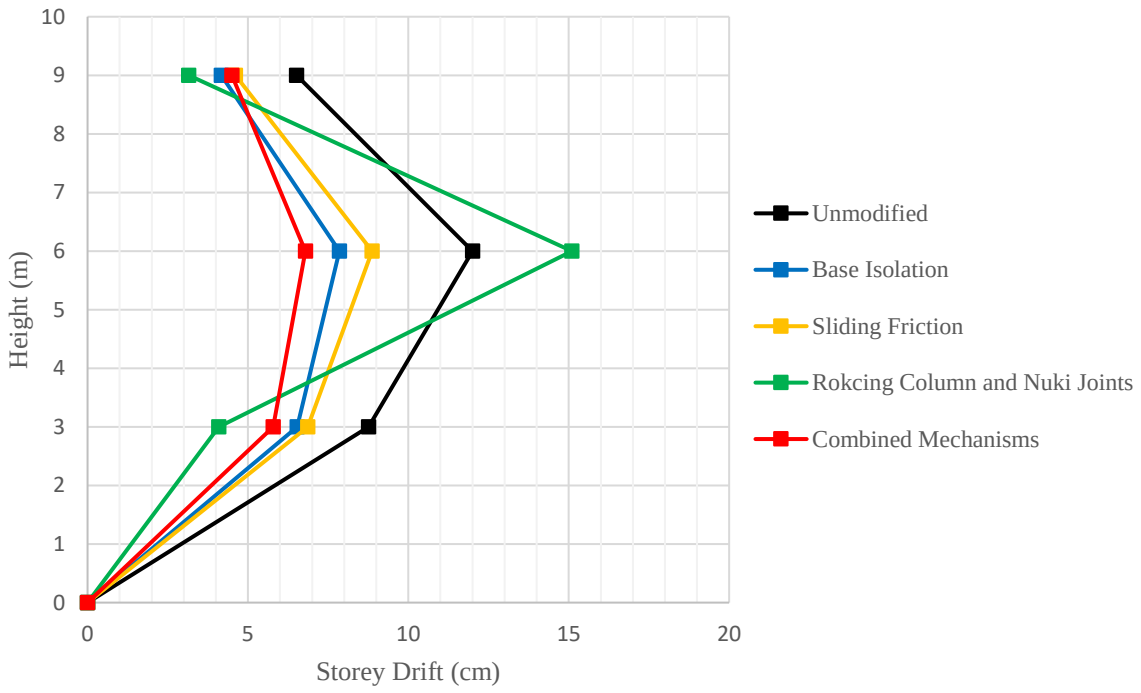

Figure 46: The storey drift between each level of the model caused by the Hollister time history.

The combined mechanisms model performed the best with a 43% decrease in maximum storey drift. This decrease is larger than those experienced by the same model in the Array 6 and Newhall analyses where the values were 33% and 36% respectively. This could simply be due to the potential variability of the data when considering a complex excitation frequency such as an earthquake time history plot.

Table 33: Percentage differences of the storey drift at the second level of the different model types compared to the unmodified model during the Hollister time history analysis.

Model	Base Isolation	Sliding Friction	Rocking Column and Nuki Joints	Combined Mechanisms
Difference	-34.6%	-26.1%	+25.8%	-43.4%

4.5.3 Energy Dissipation

Figure 47 shows the energy input and energy dissipation within the models during the Hollister analysis. This graph is very similar to the Array 6 energy dissipation graph. Again, the input energy, maximum internal energy and the residual energy is decreased within the modified models when compared to the unmodified one. Table 34 shows the percentage decrease of these values.

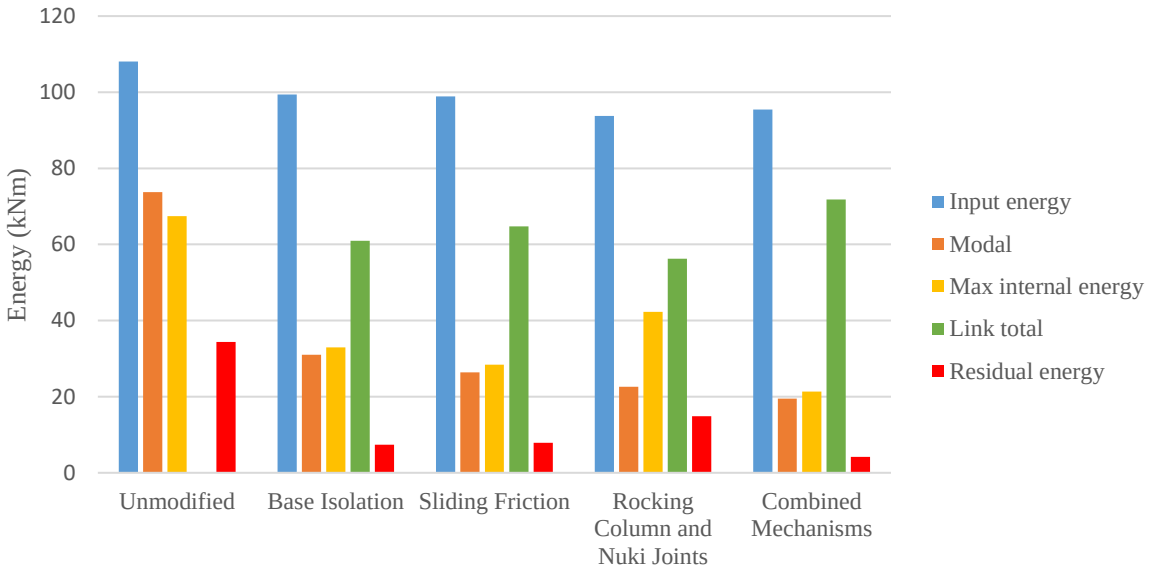

Figure 47: The energy dissipation within each model during the Hollister time history excitation.

The combined mechanisms model had the largest decrease in the maximum internal energy, with a decrease of 68%. The sliding friction and base isolation models performed well too, with a decrease exceeding 50%. This data is very similar to the values seen within the Array 6 data. One exception to this is the rocking column and nuki joints model. Within the Hollister data the model had a 37% decrease in max internal energy while the same model had a 76% decrease during the Array 6 analysis. This difference indicates that at a single timestep during the Hollister analysis the total energy within the model was higher than within the same model during the Array 6 analysis. This can be seen in Figure 45 where the maximum internal energy of the rocking column and nuki joints model is clearly larger than those within the other modified models. The reason behind this could be due to

the complexity of the system as the maximum internal energy is the maximum value for a single datapoint. Ideally, including multiple datapoints would result in more trustworthy data. Therefore, this maximum internal energy datapoint will be considered alongside the maximum internal energy datapoints of the other earthquake time history analyses.

Looking at the residual energy data, the combined mechanisms model performed the best with an 89% decrease compared to the unmodified model. The base isolation and sliding friction models had similar decreases of 77% and 79% respectively. For these three models, the data matches those seen in the previous two analyses. The rocking column and nuki joints model again has a lower rate of decrease compared to the other models, matching the trend seen in the maximum internal energy of the Hollister earthquake analysis.

Table 34: percentage differences of the energy dissipation within the difference model types compared to the unmodified model during the Hollister time history analysis.

	Base Isolation	Sliding Friction	Rocking Column and Nuki Joints	Combined Mechanisms
Input Energy Difference	-8.1%	-8.5%	-13.3%	-11.7%
Max Internal Energy Difference	-51.1%	-57.9%	-37.3%	-68.4%
Residual Energy Difference	-78.6%	-77.1%	-56.9%	-87.9%

4.6 Wind Load

The wind load static pushover analysis was carried out on the five models. Figure 48 shows the horizontal displacement at each level for the different model types. It can be seen that the peak displacements occurred at the roof level for all of the models. The modified models' peak displacement at roof level was compared to the unmodified model's peak roof displacement. Table 35 shows the percentage change of these values.

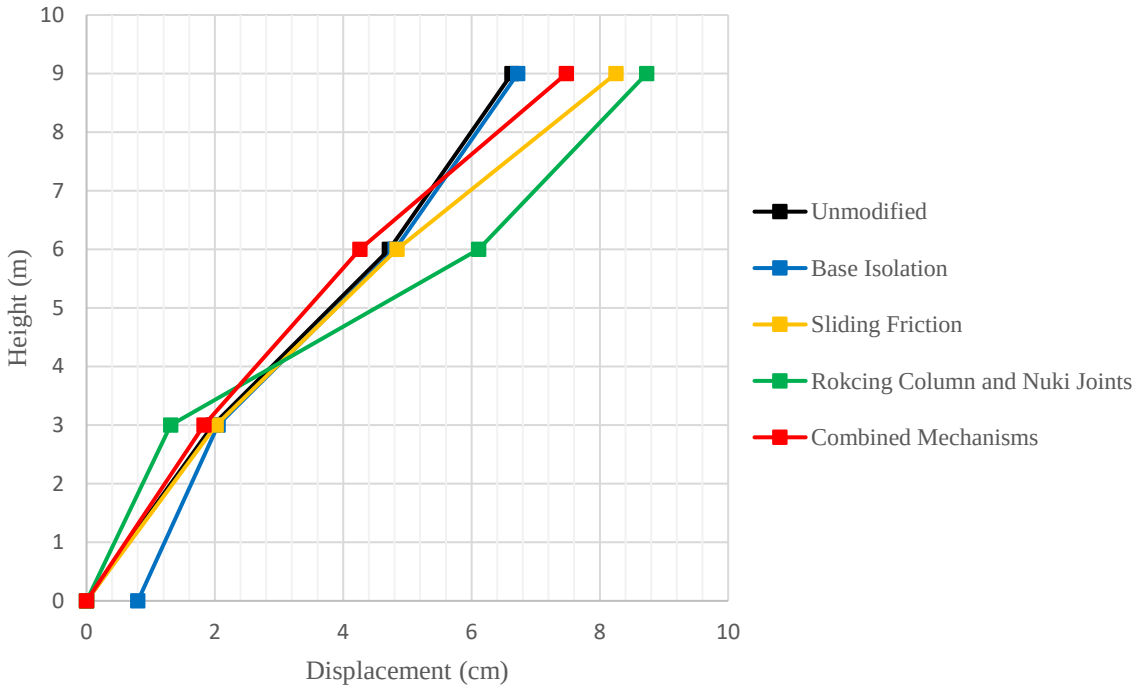

Figure 48: The displacement at each level of the model caused by the applied wind load.

All of the modified models had an increase in the peak displacement compared to the unmodified model. This outcome was expected and is due to the modified models' unique non-linear joints having a lower stiffness compared to the linear moment resisting joints within the unmodified model. When a horizontal load is applied to the non-linear joints they deform to a greater extent compared to when the same load is applied to the unmodified model's joints. This larger joint deformation translates into a greater peak horizontal displacement within the structure. This wind load has a constant direction and magnitude, there is no loading and unloading cycle within the joints. The non-linear joints are not able to dissipate energy meaning that the benefits seen during an earthquake event are not seen here.

Table 35: Percentage differences of the displacement at roof level of the different model types compared to the unmodified model for wind load.

Model	Base Isolation	Sliding Friction	Rocking Column and Nuki Joints	Combined Mechanisms
Difference	+1.4%	+24.4%	+31.7%	+12.8%

When considering the modified models, the base isolation model performed the best with an insignificant increase of roughly 1%. The combined mechanisms model also performed well with a 13% increase in maximum displacement. The unmodified model had a displacement of 6.6 cm at roof

level, the combined mechanisms model had less than a 1 cm increase over this value. This is a minor increase considering that the total height of the structure is 9 m.

Figure 49 shows the storey drifts at each level created by the wind loading. There is not a consistent trend between models. The unmodified model, the rocking column and nuki joints model and the base isolation model all had the peak storey drift occur at level two. The combined mechanisms model and the sliding friction model had the peak storey drift occur at level three. When comparing the percentage changes of the modified models to the unmodified one the levels that are compared are the ones where the peak storey drift occurred. For example, the combined mechanisms model level three storey drift is compared to the unmodified model's level three storey drift and so on. Table 36 shows these percentage changes.

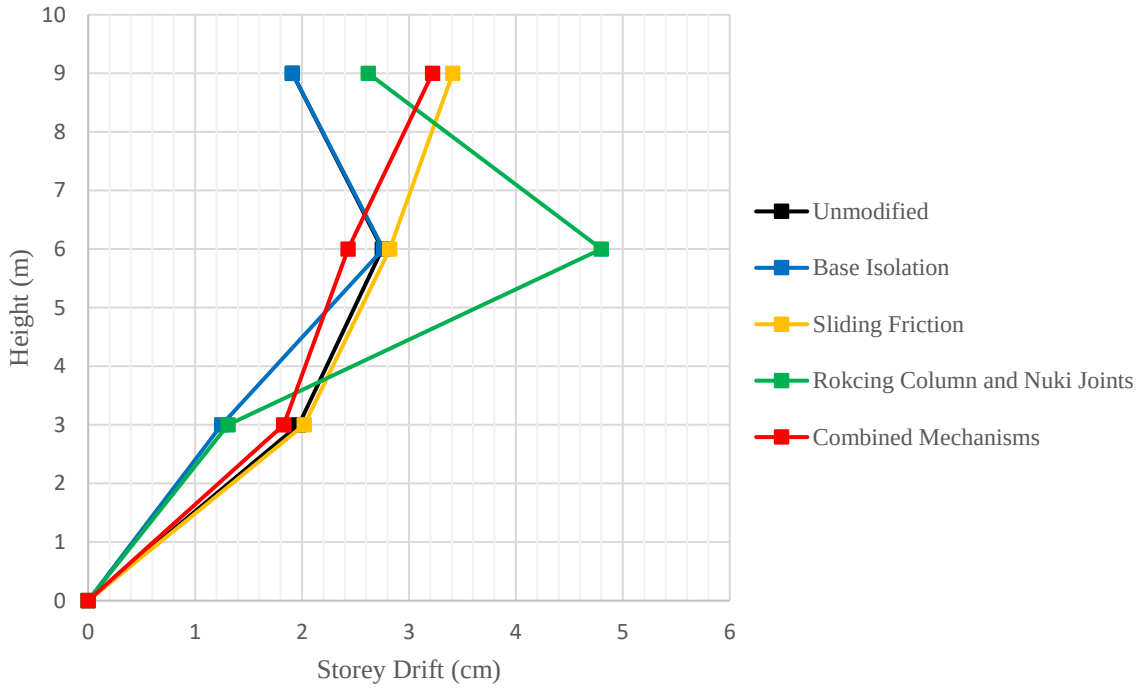

Figure 49: The storey drift between each level of the model caused by the applied wind load.

The base isolation model performed the best out of the four modified models. The storey drift of this model matched that of the unmodified model's storey drift. The other three modified models all had a significant increase in peak storey drift. Again, the rocking column and nuki joints model had a large increase in the storey drift at level two. This matches the trends seen during the earthquake time history analyses.

Table 36: Percentage differences of the storey drift of the different model types compared to the unmodified model for wind load. The comparison is made at the level with the highest percent difference.

Model	Base Isolation	Sliding Friction	Rocking Column and Nuki Joints	Combined Mechanisms
Difference	+0.4%	+78.5%	+74.5%	+68.6%

The combined mechanisms model had a 69% increase. This percent change is significant but when looking at the absolute change in the value the severity is decreased. The storey drift of the unmodified model at level three is 0.6%. This is the ratio of the horizontal drift compared to the total storey height. The storey drift of the combined mechanism model at level three is 1.1%. So, for a high wind load (as defined by NZS3604), the largest storey drift within the combined mechanisms model is 1.1%. This value is below the ultimate limit state of the structure, which is set as 2.5% by NZS 1170.5 (Council of Standards New Zealand 2004). This model is currently only a frame of a structure, once timber shear walls have been included in the design the maximum storey drift is expected to decrease.

5. DISCUSSION

In order to gauge the effectiveness of each of the model configurations all three time history analyses need to be considered. This is done by taking the accelerations, displacements and energy dissipation of the models for each of the three time history analyses and averaging the percentage decreases. This average percentage change is then compared between the five models. Table 37 and Table 38 displays these averaged values.

The general trends between the earthquake analyses are consistent. Therefore, the values between the earthquakes can be averaged without risk of losing the trends seen in the individual datasets.

Table 37: Averaged percentage differences of the output parameters of the modified models compared to the unmodified model considering all three time history excitations.

Averaged Percent Difference	Base Isolation	Sliding Friction	Rocking Column and Nuki Joints	Combined Mechanisms
Peak Acceleration	-24.4%	-36.6%	-48.7%	-43.4%
Average Acceleration	-36.2%	-41.4%	-51.9%	-49.7%
Displacement	-24.5%	-23.2%	-21.1%	-31.2%
Storey Drift	-29.6%	-20.9%	+27.1%	-37.3%

Table 38: Averaged percentage of the energy dissipation within the models compared to the unmodified model considering all three time history excitations.

Averaged Percent Difference	Base Isolation	Sliding Friction	Rocking Column and Nuki Joints	Combined Mechanisms
Input Energy	-2.6%	-2.8%	-13.8%	-2.3%
Max Internal Energy	-43.8%	-54.5%	-46.7%	-65.0%
Residual Energy	-73.9%	-74.1%	-75.2%	-81.2%

5.1.1 Acceleration

When considering the largest peak acceleration within the structure all of the modified models had a decrease of over 24%. The rocking column and nuki joints model performed the best with an average percentage decrease of 49%. The combined mechanism model also had an excellent result with an average decrease of 43%. The expected outcome was that the combined mechanism model would perform the best. The reasoning was that the inclusion of the different unique joints within one model would have an accumulative effect, leading to a greater decrease in peak acceleration, however this was not the case. When looking at the modal periods of the five models it was seen that the combined mechanisms model had the lowest modal period. This implies that this model has a higher initial stiffness compared to that of the other models. This increased stiffness is due to the inclusion of a greater number of joints within the structure as a whole. Because of this increased initial stiffness, when the pulse of the peak ground acceleration is applied to the structure the model acts similar to a rigid body with a large proportion of this ground acceleration being felt by the upper levels of the structure. The opposite is true for the rocking column and nuki joints model which has the lowest stiffness of the five models. This would account for why the rocking column and nuki joints model outperformed the combined mechanisms model when it came to decreasing the peak horizontal acceleration.

When considering the largest RMS average acceleration within the structure both the combined mechanisms model and the rocking column and nuki joints model had an average decrease of roughly 50%. These results were consistent between the three earthquake time history analyses implying that the models are able to consistently reduce the average acceleration within the structure.

During an earthquake event the occupants of a building experience shaking or a sense of motion. This shaking can be dangerous as it increases the chance of injury from falling or from unrestrained objects crushing people. The intensity of this shaking is directly related to the magnitude of the acceleration within the structure. When designing a structure to be earthquake resistant decreasing the magnitude of this horizontal acceleration is key. Both the peak acceleration and the average acceleration are metrics that need to be considered and decreased. Looking at the data obtained from the analyses the combined mechanisms model is the best option for decreasing the internal horizontal accelerations. When compared to an unmodified model, this model was able to decrease the peak acceleration by 43% and the average experienced acceleration by 50%. The rocking column and nuki joints model slightly outperformed this model but is not considered due to drawbacks that are discussed later.

5.1.2 Displacement

When considering an urban setting, reducing the peak horizontal displacement of a structure is important. When a structure's horizontal displacement becomes excessively large there is a possibility that the structure will collide with neighbouring structures, especially if those structures are swaying also. If contact occurs between two swaying structures the collision will lead to damage, and could even lead to the structural failure of the buildings. If the structure is not constructed in close proximity to other structures this peak displacement is not as crucial of a parameter to consider. Regardless, the peak horizontal displacement needs to be kept within a reasonable range in order to reduce the P-delta effect internally within the structure.

When considering the peak horizontal displacements within the structure the combined mechanisms model performed with best with an average decrease of 31%. This model had consistent results between all three analyses. The other three modified models performed within a similar range of each other, having a decrease of between 21% and 25%.

Storey drift is the horizontal displacement between the floor of a level compared to the ceiling of the same level. It is a metric relating to the horizontal deformation within a level. If this value is excessively large the internal services within the walls (e.g. pipes, wiring etc), as well as the cladding on the structure, will be damaged and could potentially dislodge from the structure. This will lead to injuries and potential fatalities within the structure and at the ground level outside. Therefore, when designing a structure to be earthquake resistant the peak storey drifts need to be considered.

The combined mechanisms model had the greatest average decrease in the largest storey drift. This model had an average decrease of 37%. The base isolation model also had a significant effect with a 30% average decrease.

The one unexpected result within the data was the fact that the rocking column and nuki joints model had a consistent increase in the largest storey drift compared to the unmodified model. At the same time, this model had the best results when considering the reduction in peak and average acceleration. This implies that this model's strong point is reduction in acceleration while its weak point is only a minor reduction in displacement and an increase in the storey drift. This weakness is not carried over into the combined mechanisms model. The reason for this is that the base isolation and the sliding friction joints excel at reducing the displacement and storey drift. When these joints are incorporated into the combined mechanisms model they counteract the drawbacks that come with the use of the rocking column and nuki joints. The conclusion is that each of these unique non-linear joints have a benefit and a drawback but when they are all used in tandem within a structure the strengths of one

joint type outweigh the drawbacks of another. This allows the combined mechanisms model to consistently perform the best during an earthquake event.

5.1.3 Energy Dissipation

The input energy is the total energy entering the superstructure over the course of the loading event. This energy translates into the motion and deformation of the structural members within the model. If this input energy is increased the potential accelerations and deformations within the structure also increase. This will lead to a larger amount of damage and potentially the failure of the structure. Therefore, decreasing this input energy, or at least preventing an increase, is crucial to earthquake design.

When averaging the change in input energies between the modified models and the unmodified one it was found that the decrease was minor. The largest change was from the rocking column and nuki joints model, with an average decrease of 14%. The other three modified models only had a 2-3% decrease.

The maximum internal energy is the maximum value at a single timestep, which considers the combined value of the kinetic and elastic potential energy within the system. This energy value is a measure of the magnitude of motion and deformation within the structure. As this value increases the potential damage of the structure increases as well. As with the input energy, any potential decrease in the maximum internal energy is beneficial in earthquake design.

All four of the modified models had a significant decrease of at least 44% in the maximum internal energy of the system. The combined mechanisms model performed the best with a 65% decrease.

The residual energy is the measure of the total internal energy within the system at the final timestep of the analysis. The difference between the input energy and the residual energy is the total energy dissipated within the structure over the course of the analysis. If a model has a low residual energy value then this model is capable of dissipating energy efficiently after the earthquake peak has passed and will return to a stationary position sooner. This is beneficial as it reduces the number and the magnitude of the loading and unloading cycles post-earthquake peak. This will help mitigate some of the potential damage that could have occurred within the structure otherwise.

The residual energy of the modified models was significantly decreased. All of the models had a decrease of 74% or greater. The combined mechanisms model performed the best with a decrease of 81%. This means that at the final timestep of the earthquake analyses the combined mechanisms model had on average only 19% of the internal energy that the unmodified model had at the same timestep.

5.1.4 Wind Load

Wind load is always a consideration when designing structures within New Zealand. The intensity of the load is dictated by the location of the site, both nationally and topographically. For example, a building located on a hilltop in Wellington will have to be designed considering very high wind speeds while a building located at the base of a hill in Hamilton will be designed considering low or medium wind speeds. Regardless of location, the expected wind load will need to be calculated and accounted for in the design.

Because the wind load is a horizontal force there is potential for excessive horizontal displacements within the structure. As described in the previous sections, excessively large horizontal deformations can lead to structural damage of the building, or adjacent buildings. The unique non-linear joints used within the models help decrease earthquake effects, however their performance during wind loading needs to be considered also. It is expected that the structures horizontal displacements increase with the use of the non-linear joints. If this increase in displacement is minor then the use of these non-linear joints in earthquake resistant structures can be considered.

The combined mechanisms model performed the best during earthquake loading and so this model's performance during wind loading is the most important result. This model had a 13% increase in peak displacement, an increase of less than 1 cm compared to the unmodified model. The combined mechanisms model also had a 69% increase in peak storey drift, however this storey drift corresponded to a 1.1% drift during high wind speeds which will not lead to the collapse of the structure. Once the timber frame of the structure is infilled with timber shear walls this peak storey drift is expected to decrease further.

6. CONCLUSION

Horyu-ji Pagoda was investigated in order to discover the reason for its excellent performance during earthquake events. Six key construction techniques were identified. These were base isolation joints, sliding friction joints, rocking column joints, nuki joints, the presence of the shin-bashira (central column) and the balancing toy effect. These construction techniques were virtually modelled within SAP2000. Based upon the modal analysis and static pushover analysis results it was found that the pagoda model accurately modelled the response of Horyu-ji Pagoda during horizontal loading. This result validated the accuracy of the unique virtual joints, allowing them to be used within a wider range of model configurations.

A generic three storey timber structure was modelled within SAP2000. This model was then edited to include the unique non-linear joints. The base isolation joints, sliding friction joints, rocking column joints and nuki joints were investigated. These four joints were chosen for practicality reasons as they only required a change in the joint configuration and allowed the structural floorplan and usable space to remain unchanged. The effects of the shin-bashira and the balancing toy effect were not investigated further. This meant that there were five unique models to be analysed, an unmodified model, a base isolation model, a sliding friction model, a rocking column and nuki joints model and finally a combined mechanisms model, which included all four unique joints within one model. Three recorded earthquake time history excitations were chosen and applied as the ground accelerations to the models. The key output data collected was the peak horizontal acceleration, average acceleration, peak horizontal displacement, peak storey drifts and the energy dissipation within the models.

When looking at the results, each model had certain strong points and weak points. The base isolation model and the sliding friction model had moderate decreases in accelerations and displacements. The rocking column and nuki joints model had a significant decrease in accelerations, a minor decrease in displacement and a moderate increase in peak storey drift. However, when these unique joints are used in conjunction within a model the strong points of one type of joint nullify the drawbacks of the other joints. This was seen in the combined mechanisms model.

The combined mechanisms model had an average decrease in the peak acceleration of 43%. This model also had a 50% decrease in the average acceleration experienced. The peak displacement was decreased by 31% while the peak storey drift was decreased by 37%. When looking at energy dissipation the maximum internal energy was decreased by 65% and the residual energy was decreased by 81%. When a high wind speed was experienced by the model the horizontal displacement increased by 13% and the largest storey drift increased from 0.6% to 1.1%. These changes were calculated when comparing the combined mechanisms model to the unmodified model.

When designing multi-storeyed timber structures with regular floor plans it is recommended to consider the use of the four unique joints outlined in this study. The construction of these joints are simple and the joints themselves are not large or bulky. This means that they are able to be incorporated easily into new builds. However, in order for consistent sizable decreases to be seen all four unique joint types need to be present within the structure simultaneously.

7. FUTURE RESEARCH

This study only considered very specific scenarios. These scenarios and cases need to be expanded upon in order to observe the potential versatility of these unique joints. Some recommendations are:

1. Varying structure heights. For example, analysing the performance of the joints in a three, six and nine storey model will be important in the future.
2. Irregular floor plans. The observing performance of the joints in structures with irregular floor plans is also beneficial.
3. Larger variety of earthquake intensities. This study included two 0.4 G PGA earthquakes and one 0.6 G PGA earthquake. Including a 1.5 G PGA earthquake or larger may highlight any unforeseen drawbacks associated with the use of the unique joints.
4. Physical testing of the joints. Constructing a scale model and testing it on a shake table will be crucial in validating the performance of the joints before their potential use in real world scenarios.

REFERENCES

Abe, M., and Kawaguchi, M. (2002). "Structural Mechanism and Morphology of Timber Towers in Japan*." Journal of Asian Architecture and Building Engineering*, 1(2), 25-32.

Chang, W., Hsu, M. and Komatsu, K. (2006). "Rotational Performance of Traditional Nuki Joints with Gap I: Theory and Verification." *The Japan Wood Research Society*, 52, 58-62.

Council of Standards New Zealand (2004). *NZS 1170.5 Supp 1:2004. Structural Design Actions Part 5: Earthquake Actions – New Zealand – Commentary*, Standards New Zealand, Wellington, New Zealand.

Council of Standards New Zealand (2011). *NZS 3604:2011. Timber-framed Buildings*, Standards New Zealand, Wellington, New Zealand.

Daemei, A.B., Khotbehsara, E.M., Nobarani, E.M. and Bahrami, P. (2019). "Study on Wind Aerodynamic and Flow Characteristics of Triangular-shaped Tall Buildings and CFD Simulation in order to Assess Drag Coefficient." *Ain Shams Engineering Journal*, 10, 541-548.

The Engineering Toolbox (2011). "Wind Speed vs. Wind Load." Accessed February 11, 2022. https://www.engineeringtoolbox.com/wind-load-d_1775.html.

Field, E. M. (2008). "Chapter two – The Central Core Structural System: A Three-Dimensional Analysis of the Five-Story Pagoda of Horyuji." In *Horyuji Reconsidered*, Cambridge Scholars Publishing, Newcastle, UK.

Fujita, K., Hanazato, T. and Sakamoto, I. (2004). "Earthquake Response Monitoring and Seismic Performance of Five-Storied Timber Pagoda." *13WCEE Canada 2004*, 13, paper no. 54.

Hanazato, T., Ogiwara, Y., Inayama, M., Okura, Y., Misho, K. and Sakamoto, I. (1999a). "Structural Design of Traditional Wooden Five-Storied Pagoda." *AIJ J. Technical Des.*, 7, 33-38.

Hanazato, T., Nagai, T., Yanagisawa, K., Hidaka, K., Sakamoto, I. and Watabe, M. (1999b). "Greek Temple and Timber Pagoda in Japan - Comparison of the Aseismic Structural Performances." *Transactions on the Built Environment*, 39, 291-300.

Hanazato, T., Fujita, K., Sakamoto, I., Inayama, M. and Ohkura, Y. (2004). “Analysis of Earthquake Resistance of Five-Storied Timber Pagoda.” *13WCEE Canada 2004*, 13, paper no. 1223.

Hanazato, T., Minowa, C., Nitsu, Y., Nitto, K., Kawai, N., Maekawa, H. and Morii, M. (2010). “Seismic and Wind Performance of Five-Storied Pagoda of Timber Heritage Structure.” *Advanced Materials Research*, 133-134, 79-95.

Hanazato, T., Ayaki, D., Ogiwara, Y., Uchida, R., Sato, N., Misu, M., Takayama, M. and Sakamoto, I. (2012). “Seismic Design and Construction of a Traditional Timber-Made Five-Storied Pagoda by Applying Coupled Vibration Control.” *15WCEE Lisboa 2012*, 15, 3353-3362.

Harada, K. (2016). “Structural Characteristics of Wooden Five Storied Buddhism Temple Pagodas and Application to the Modern Architecture in Japan.” *Proceedings of Structural Engineering and Construction Conference*, ISEC Press, North Dakota, USA, 221-226.

Konishi, A. (2011). “Structural Design of Tokyo Sky Tree.” *CTBUH 2011 World Conference*, Council on Tall Buildings and Urban Habitat, Seoul, Korea, 513-520.

Muai, Y. and Tanaka, E. (2012). “Performance Evaluation for Traditional Japanese Wooden Pagodas based on Micro-tremor Measurement and Numerical Frame Model Analysis.” *15WCEE Lisboa 2012*, 15, 6810-6817.

Nakahara, K., Hisatoku, T., Nagase, T. and Takahashi, Y. (2000). “Earthquake Response of Ancient Five-Story Pagoda Structure of Horyu-ji Temple in Japan.” *12WCEE New Zealand 2000*, 12, paper no. 1229.

Nishioka, T. and Kohara, J. (2016). *The building of Horyu-ji: the technique and wood that made it possible*, Japan Publishing Industry Foundation for Culture, Tokyo, Japan.

Ogawa, I. (2006). *High Rise Office, Structural Design*, Mitsubishi Sekkei, Tokyo, Japan.

Paultre, P. (2011). *Dynamics of Structures*, ISTE Ltd, London, UK, 90.

Tenon Clearwood Ltd (2015). “Radiata Pine Clearwood Properties.” Accessed August 28, 2021. https://tenonclearwood.com/radiata-pine/properties.aspx.

Uchida, A., Kawai, N. and Maekawa, H. (1999). “Dynamic Characteristics of Traditional Wooden Building, Part2: Micro Tremor Measurements on Horyuji Pagada.” *Summaries of Tech Papers 1996 Annual Meeting,* AIJ, Tokyo, Japan, 171-172.

Walley, A. (2006). “Instant Bliss: Enactment of the Miraculous Appearance of Relics in the Horyuji Nested Reliquary Set.” *Ar Orientalis*, 46, 137-172.

Yasuhara, M., Sakiyama, T. and Iibuchi, K. (2007). “Characterization of Space Around Japanese Traditional Buildings: Visible Music on the Approach to Horyuji Temple, Saiin (West Compound).” *WIT Transactions on The Built Environment*, 95, 53-60.

Yokoyama, M., Gril, J., Matsuo, M., Yano, H., Sugiyama, J., Clair, B., Kubodera, S., Mistutani, T., Sakamoto, M., Ozaki, H., Imamura, M. and Kawai, S. (2009). “Mechanical Characteristics of Aged Hinoki Wood from Japanese Historical Buildings.” *C. R. Physique*, 10, 601-611.

Zhang, Y., Tang, H. and Xue, S. (2015). “Investigation into the Architectural Design of a Traditional Japanese Wooden Pagoda.” *Journal of Asian Architecture and Building Engineering*, 14(2), 241-246.

APPENDIX A – SUPPLEMENTARY TABLES AND FIGURES

Table A.1: Horyu-ji Pagoda weight of the structure at each of the columns.

Level	Column Type	Roof Area (m^2)	Main Structure Area (m^2)	Roof Weight (ton)	Main Structure Weight (ton)	Total Weight (ton)	Total Weight Considering Upper Levels (ton)	Total Weight Considering Upper Levels (kN)
1	Outer corner	22.6	0.88	5.65	0.56	8.35	14.53	143
	Outer middle	8.9	2.15	2.23	1.37	5.24	13.92	137
	Inner	0	5.23	0	3.33	3.33	21.50	211
	Total	162	41.7	40.5	26.5	116.1	283.0	2776
2	Outer corner	20.2	0.68	5.04	0.43	5.47	9.98	97.9
	Outer middle	7.50	1.65	1.87	1.05	2.92	8.90	87.3
	Inner	0	4.01	0	2.55	2.55	13.92	137
	Total	140.6	31.9	35.2	20.3	55.5	166.8	1637
3	Outer corner	17.85	0.50	4.46	0.32	4.78	7.89	77.4
	Outer middle	6.15	1.21	1.54	0.77	2.31	5.99	58.7
	Inner	0	2.95	0	1.88	1.88	7.98	78.3
	Total	120.6	23.5	30.1	15.0	45.1	111.4	1093
4	Outer corner	15.7	0.35	3.91	0.22	4.14	6.06	59.5
	Outer middle	4.89	0.85	1.22	0.54	1.76	3.41	33.5
	Inner	0	2.06	0	1.31	1.31	3.67	36.0
	Total	101.8	16.4	25.4	10.4	35.9	66.3	650
5	Outer corner	16.35	0.54	4.09	0.35	4.43	4.43	43.5
	Outer middle	6.04	0.77	1.51	0.49	2.00	2.00	19.6
	Inner	1.32	1.32	0.33	0.84	1.17	1.17	11.5
	Total	94.8	10.5	23.7	6.7	30.4	30.4	298

Table A.2: Horyu-ji Pagoda lumped mass values at each of the columns throughout the structure.

Level	Column Type	Lump Mass at the Top of Each Column (kN)	Lump Mass at the Base of Each Column (kN)
1	Outer corner	70.0	13.2
	Outer middle	41.0	14.7
	Inner	31.1	16.3
	Total	868	370.9
2	Outer corner	52.5	
	Outer middle	26.7	
	Inner	23.7	
	Total	518	
3	Outer corner	45.9	
	Outer middle	21.0	
	Inner	17.2	
	Total	420	
4	Outer corner	40.2	
	Outer middle	15.8	
	Inner	11.6	
	Total	334	
5	Outer corner	41.8	
	Outer middle	17.2	
	Inner	7.37	
	Total	265	

Table A.3: Horyu-ji Pagoda rocking column joint curvature plot values.

	Level 2			Level 3			Level 4			Level 5		
	outer corner	outer middle	inner	outer corner	outer middle	inner	outer corner	outer middle	inner	outer corner	outer middle	inner
b	0.4	0.4	0.4	0.4	0.4	0.4	0.4	0.4	0.4	0.4	0.4	0.4
h	2.05	2.05	2.05	1.84	1.84	1.84	1.64	1.64	1.64	1.44	1.44	1.44
W	97.9	87.3	137	77.4	58.7	78.3	59.5	33.5	36.0	43.5	19.6	11.5
θ1	0	0	0	0	0	0	0	0	0	0	0	0
θ2	0.0078	0.0078	0.0078	0.0087	0.0087	0.0087	0.0097	0.0097	0.0097	0.0111	0.0111	0.0111
θ3	0.0352	0.0352	0.0352	0.0390	0.0390	0.0390	0.0438	0.0438	0.0438	0.0499	0.0499	0.0499
θ4	0.0587	0.0587	0.0587	0.0651	0.0651	0.0651	0.0730	0.0730	0.0730	0.0831	0.0831	0.0831
θ5	0.1956	0.1956	0.1956	0.2168	0.2168	0.2168	0.2433	0.2433	0.2433	0.2771	0.2771	0.2771
M1	0	0	0	0	0	0	0	0	0	0	0	0
M2	23.5	21.0	32.8	18.6	14.1	18.8	14.3	8.0	8.6	10.4	4.7	2.8
M3	31.3	28.0	43.7	24.8	18.8	25.1	19.0	10.7	11.5	13.9	6.3	3.7
M4	29.4	26.2	41.0	23.2	17.6	23.5	17.8	10.0	10.8	13.0	5.9	3.5
M5	0.0	0.0	0.0	0.0	0.0	0.0	0.0	0.0	0.0	0.0	0.0	0.0

Table A.4: Generic timber model rocking column joint curvature plot values.

	Level 2		Level 3	
	Outer frame	Inner frame	Outer frame	Inner frame
b	0.3	0.3	0.3	0.3
h	3.00	3.00	3.00	3.00
W	38.2	76	6.2	12.1
θ1	0	0	0	0
θ2	0.0040	0.0040	0.0040	0.0040
θ3	0.0180	0.0180	0.0180	0.0180
θ4	0.0300	0.0300	0.0300	0.0300
θ5	0.1000	0.1000	0.1000	0.1000
M1	0	0	0	0
M2	6.9	13.6	1.1	2.2
M3	9.2	18.2	1.5	2.9
M4	8.6	17.1	1.4	2.7
M5	0.0	0.0	0.0	0.0

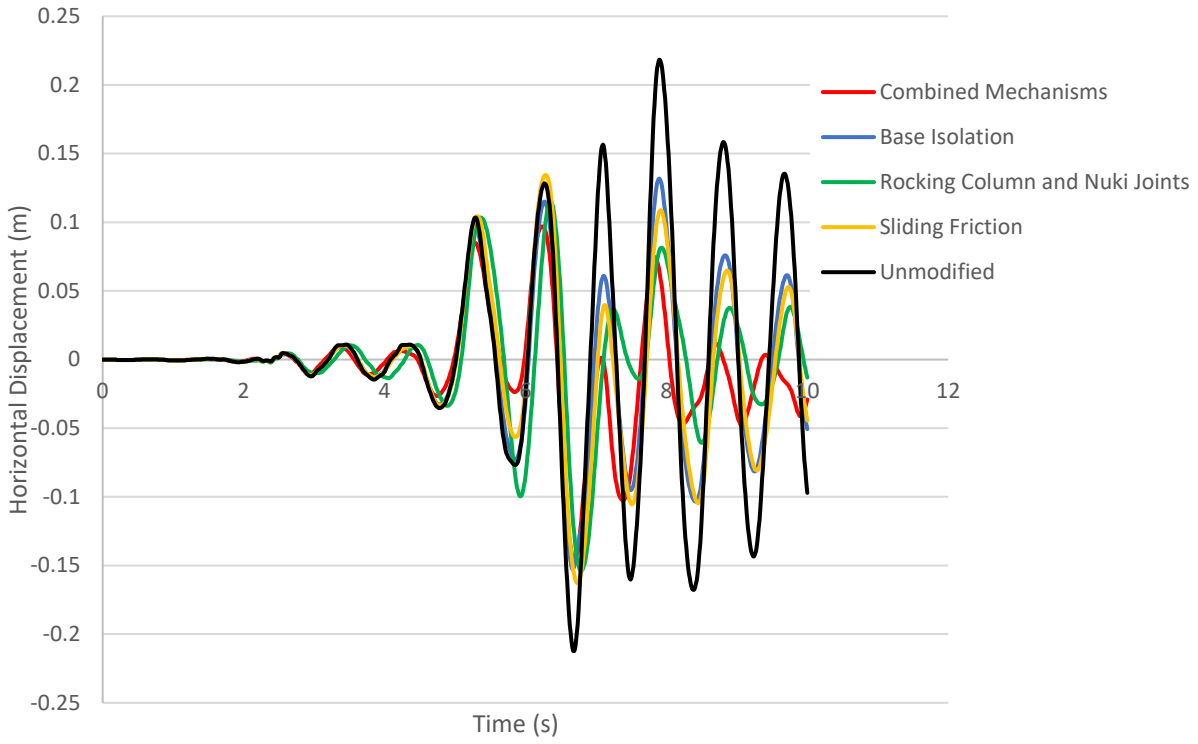

Figure A.1: Horizontal displacement at roof height for the five model types during the Array 6 earthquake.

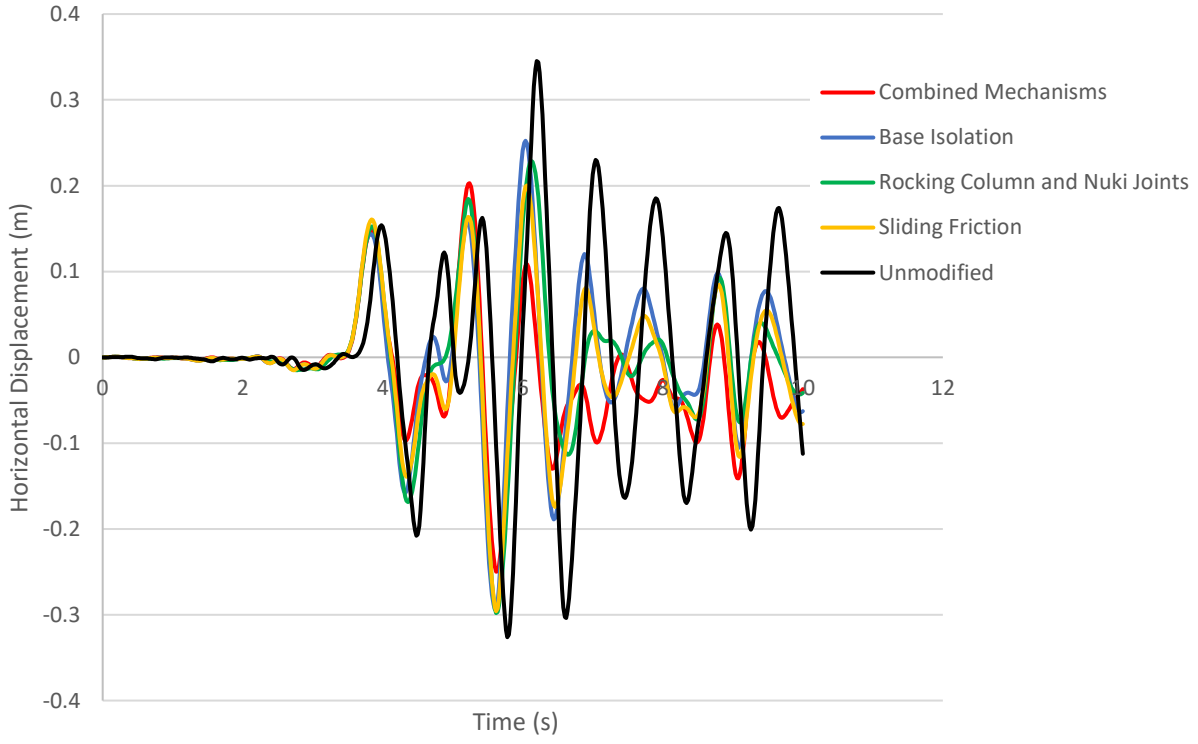

Figure A.2: Horizontal displacement at roof height for the five model types during the Newhall earthquake.

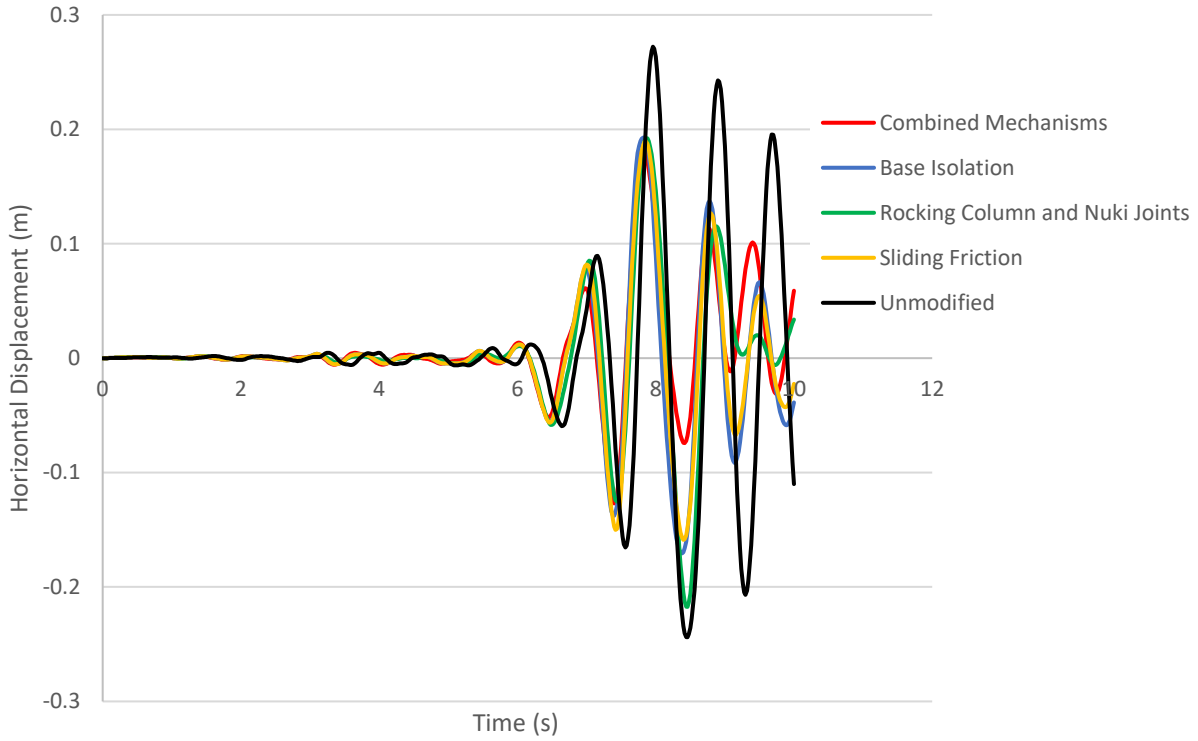

Figure A.3: Horizontal displacement at roof height for the five model types during the Hollister earthquake.

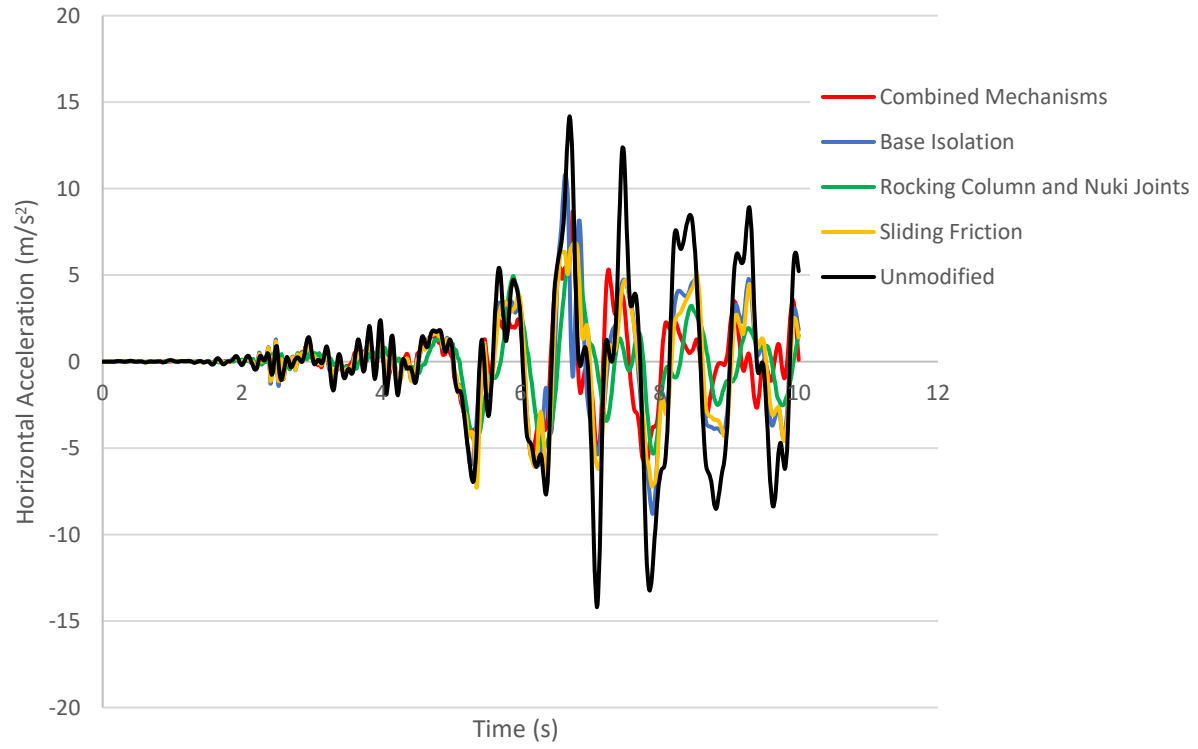

Figure A.4: Horizontal acceleration at roof height for the five model types during the Array 6 earthquake.

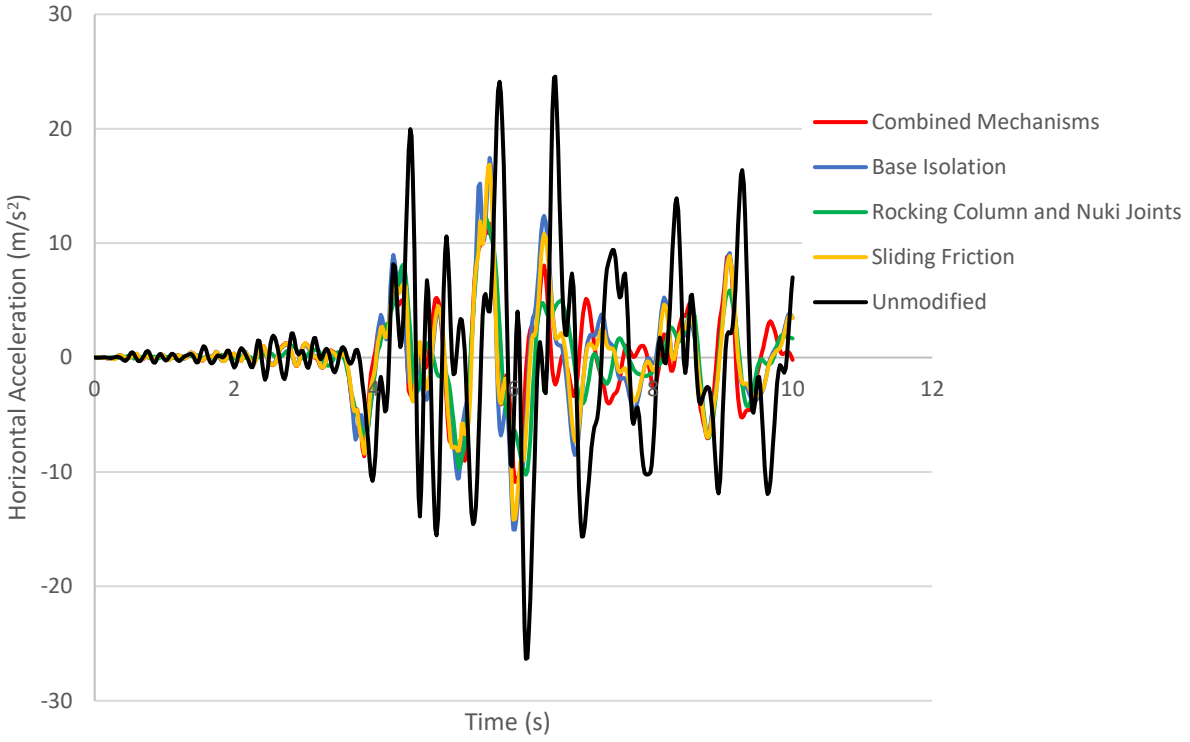

Figure A.5: Horizontal acceleration at roof height for the five model types during the Newhall earthquake.

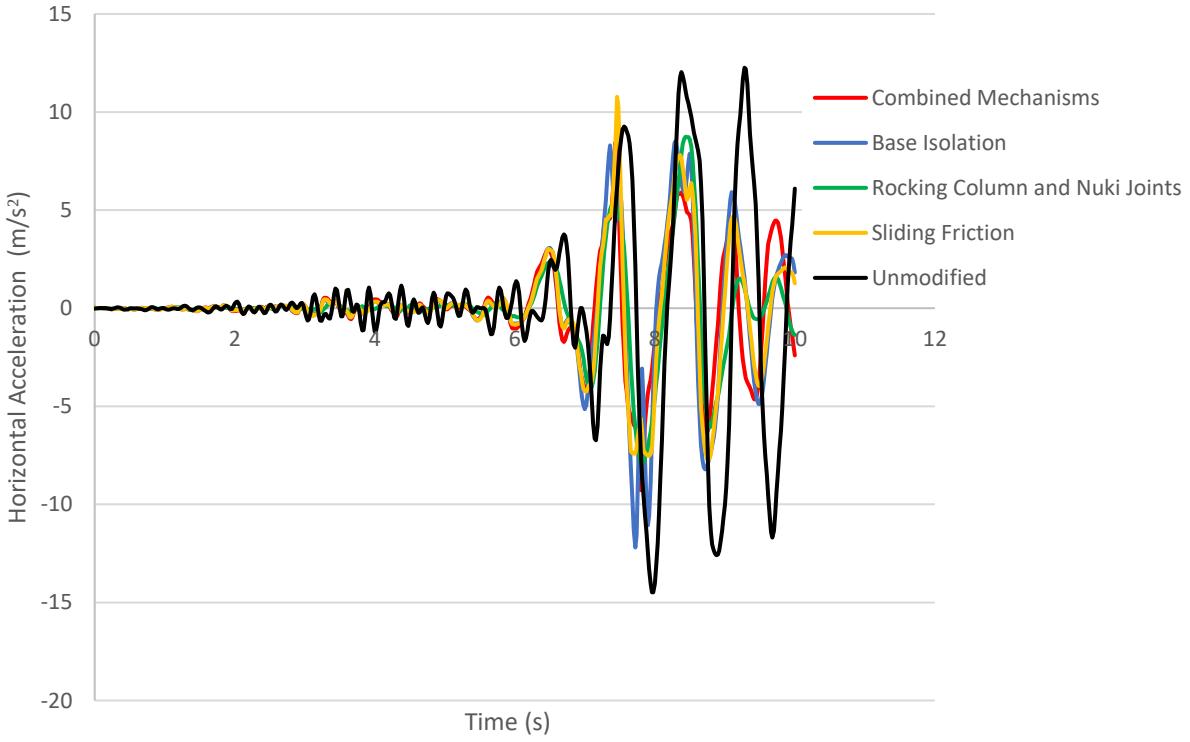

Figure A.6: Horizontal acceleration at roof height for the five model types during the Hollister earthquake.

APPENDIX B – DERIVATIONS

Derivation of Equation 8:

Equation B.1 shows Hook's law and Equation B.2 – B.5 shows this equation modified so that the new spring stiffnesses can be calculated.

$$F = k \cdot x \tag{B.1}$$

$$M = F \cdot l \tag{B.2}$$

Equation B.1 is substituted into Equation B.2 to give Equation B.3.

$$M = k \cdot x \cdot l \tag{B.3}$$

The virtual springs placed at the columns will create an equal moment compared to the springs placed at the roof COM.

$$k_c \cdot x_c \cdot l_c = k_r \cdot x_r \cdot l_r \tag{B.4}$$

Equation B.4 is rearranged to give Equation B.5.

$$k_c = \frac{x_r}{x_c} \cdot \frac{l_r}{l_c} \cdot k_r \tag{B.5}$$

The variable *x* represents spring displacement in the vertical direction while *l* represents the distance between the spring location and the centreline of the structure in the horizontal direction. The subscript *c* denotes variables relating to the column springs while the subscript *r* relates to the springs located at the roof centre of mass. In the case of Equation B.5, the vertical displacements x_c and x_r are unknown. These values are arbitrary so x_r is set to a value of one. Equation B.6 below shows the relationship between these two variables and works on the principle of equal triangles.

$$\frac{x_c}{l_c} = \frac{x_r}{l_r} \tag{B.6}$$

$$x_c = \frac{l_c}{l_r} \tag{B.7}$$

When Equation B.7 is substituted into Equation B.5 the final equation to find the new spring stiffnesses is given, Equation 8.

$$k_c = \frac{{l_r}^2}{{l_c}^2} \cdot k_r \tag{8}$$

APPENDIX C – MATLAB SCRIPTS

Nuki Joint Script

```
Bd=0.25;      %Beam depth (mm)
Bw=0.25;      %Beam width (mm)
Cw=0.4;      %column width (mm)
Ep=9*10^6;   %MoE parallel to grain (KPa)
Et=Ep/20;    %MoE tangential to grain (Pa) assumed 1/20th of MoE parallel to grain
Gap=0.005;      %gap between top of beam and column (m)
stress_y=4.8*10^3; %in KPa of wood in compression perpindicular to grain
x=0;        %the length of beam that is in yield during rotation
strain=0;   %strain of wood at edge of beam-column connection
strain_y=0; %strain at which beam will yield

for i=1:101
    theta=(i-1)/(100*5);  %rotaion of beam in relation to column
    beta=20/((20*(cos(theta))^3.1)+(sin(theta)^3.1)); %variable affecting
rotaitional E of timber, based on Hankinsons formula
    alpha1=Bd/(2*Cw*sin(theta));
    alpha2=(Bd+Gap)/(2*Cw*tan(theta));
    alpha=0.5+alpha1-alpha2; %ratio of comressive zone length to column width

    if alpha<0      %alpha is less than zero beam is in rigid body motion, no beam
column contact yet
        alpha=0;
    end

    gamma=((3-2*alpha)/6)*(alpha^2)*beta*sin(theta);
    stress=((Et*Cw)/Bd)*alpha*beta*sin(theta); % stress at outer edge of beam
column connection

    if stress>=stress_y     %check for yielding of beam

    strain=Cw*alpha*sin(theta)/Bd;      %strain at edge of the beam column
connection assuming linear strain profile
    strain_y=stress_y/(Et*beta);        %strain at the point where stress is at
yielding stress
    x=Cw*alpha*((strain-strain_y)/strain);  %length of compressive zone that is
yielding
    f1=x*Bw*stress_y;                   % force due to this compressive zone at
yielding
    f2=0.5*(Cw*alpha-x)*stress_y*Bw;    %force due to compressive zone not yet at
yielding
    M(i)=f1*(Cw-x)+f2*(Cw-2*x-(2/3)*(Cw*alpha-x));  %moment created by the the
above comressive zone forces

    else

    M(i)=((Cw^3)*Bw*Et*gamma)/Bd; %moment created if beam has not started yielding

    end

    thetaplot(i)=theta;
    stressplot(i)=stress;
    strainplot(i)=strain;

end
```

APPENDIX D – SAP2000 INPUT DATA

Table D.1: Horyu-ji Pagoda SAP2000 input curves for the base isolation joints.

Displacement (mm)	Inner Frame - Force (kN)	Outer Frame – Force (kN)
-20	-20 000	-20 000
-15	-278	-223
-1	-278	-223
0	0	0
1	278	223
15	278	223
20	20 000	20 000

Table D.2: Horyu-ji Pagoda SAP2000 input curves for the sliding friction joints.

Displacement (mm)	Level 1 - Force (kN)	Level 2 – Force (kN)	Level 3 – Force (kN)	Level 4 – Force (kN)	Level 5 Inner Frame – Force (kN)	Level 5 Outer Frame – Force (kN)
-20	-20 000	-20 000	-20 000	-20 000	-20 000	-20 000
-15	-227	-154	-102	-59.9	-17.7	-26.5
-1	-227	-154	-102	-59.9	-17.7	-26.5
0	0	0	0	0	0	0
1	227	154	102	59.9	17.7	26.5
15	227	154	102	59.9	17.7	26.5
20	2 0000	20 000	20 000	20 000	20 000	20 000

Table D.3: Horyu-ji Pagoda SAP2000 input curves for the combined rocking column and nuki joints.

Level 2		Level 3		Level 4		Level 5 Inner Column		Level 5 Outer Column	
Rotation (rads)	Moment (kNm)	Rotation (rads)	Moment (kNm)	Rotation (rads)	Moment (kNm)	Rotation (rads)	Moment (kNm)	Rotation (rads)	Moment (kNm)
-0.2	-192	-0.217	-192	-0.243	-192	-0.277	-95.8	-0.277	-144
-0.196	-191	-0.0651	-257	-0.073	-228	-0.0831	-106	-0.0831	-158
-0.0587	-289	-0.039	-229	-0.0438	-200	-0.0499	-93.6	-0.0499	-140
-0.0352	-264	-0.0086	-65.6	-0.0097	-39	-0.0111	-11.9	-0.0111	-17.9
-0.0078	-98.2	0	0	0	0	0	0	0	0
0	0	0.0086	65.6	0.0097	39	0.0111	11.9	0.0111	17.9
0.00782	98.2	0.039	229	0.0438	200	0.0499	93.6	0.0499	140
0.0352	264	0.0651	257	0.073	228	0.0831	106	0.0831	158
0.0587	289	0.217	192	0.243	192	0.277	95.8	0.277	144
0.196	191								
0.2	192								

Table D.4: Generic model SAP2000 input curves for the base isolation joints.

Displacement (mm)	Inner Frame - Force (kN)	Outer Frame – Force (kN)
-20	-20 000	-20 000
-15	-167	-84.3
-1	-167	-84.3
0	0	0
1	167	84.3
15	167	84.3
20	20 000	20 000

Table D.5: Generic model SAP2000 input curves for the sliding friction joints.

	Level 1		Level 2		Level 3	
Displacement (mm)	Inner Frame (kN)	Outer Frame (kN)	Inner Frame (kN)	Outer Frame (kN)	Inner Frame (kN)	Outer Frame (kN)
-20	-20 000	-20 000	-20 000	-20 000	-20 000	-20 000
-15	-167	-154	-102	-59.9	-17.7	-26.5
-1	-167	-154	-102	-59.9	-17.7	-26.5
0	0	0	0	0	0	0
1	167	154	102	59.9	17.7	26.5
15	167	154	102	59.9	17.7	26.5
20	2 0000	20 000	20 000	20 000	20 000	20 000

Table D.6: Generic model SAP2000 input curves for the combined rocking column and nuki joints.

	Level 2 Inner Frame	Level 2 Outer Frame	Level 3 Inner Frame	Level 3 Outer Frame
Rotation (rads)	Moment (kNm)	Moment (kNm)	Moment (kNm)	Moment (kNm)
-0.2	-144	-144	-144	-144
-0.1	-138	-138	-138	-138
-0.03	-129	-103	-86	-82
-0.018	-80.4	-53.4	-34.5	-30.3
-0.004	-40.9	-20.7	-6.53	-3.36
0	0	0	0	0
0.004	40.9	20.7	6.53	3.36
0.018	80.4	53.4	34.5	30.3
0.03	129	103	86	82
0.1	138	138	138	138
0.2	144	144	144	144